Westfälische
Wilhelms-Universität
Münster

Master's Thesis

QCD Corrections to SUSY Dark Matter Coannihilation Processes

Johannes Branahl

December 11, 2019

Institut für Theoretische Physik Münster

First examiner: Prof. Dr. Michael Klasen

Second examiner: PD Dr. Karol Kovařík

Declaration of Academic Integrity

I hereby confirm that this thesis on ”*QCD Corrections to SUSY Dark Matter Coannihilation Processes*” is solely my own work and that I have used no sources or aids other than the ones stated. All passages in my thesis for which other sources, including electronic media, have been used, be it direct quotes or content references, have been acknowledged as such and the sources cited.

(date, signature)

I agree to have my thesis checked in order to rule out potential similarities with other works and to have my thesis stored in a database for this purpose.

(date, signature)

Abstract

The main part of the community of physicists assumes today that the so-called dark matter is essentially responsible for the mass in our Universe. Currently, its nature and properties are in fact entirely unkown - several different theories compete against each other. Supersymmetry yields a potential candidate, the lightest neutralino; this assumption is the basis of our work. This thesis deals with annihilation processes of supersymmetric particles that had an impact on the dark matter relic density by neutralino coannihilations. The underlying project is hereby the *DM@NLO* collaboration having the goal to calculate a hopefully complete set of such SUSY processes at next-to-leading order in QCD. The thesis contains first the Born cross section calculation. Afterwards, the virtual corrections are discussed - they are UV finite after successful renormalisation. It remains the treatment of real corrections. For these calculations, a formalism is developed that is based on the dipol subtraction method. Additionally, the project of stau annihilation (a previous thesis) comes to an end via Sommerfeld corrections (resummation) for the ingoing scalar taus. We perform a detailed numerical analysis, apply our corrected cross section results to gravitino physics and investigate theoretical uncertainties arising from a variation of the renormalisation scheme and scale.

Kurzfassung

Vom größten Teil der Wissenschaftsgemeinde wird heute angenommen, dass die sogenannte Dunkle Materie einen wesentlichen Anteil der Masse des Universums ausmacht. Deren tatsächliche Natur ist jedoch derzeit noch gänzlich unbekannt - verschiedenste Theorien konkurrieren miteinander. Die Supersymmetrie liefert einen potenziellen Kandidaten, das leichteste Neutralino; eine Annahme, die die Grundlage dieser Arbeit ist. Sie befasst sich mit Annihilationsprozessen supersymmetrischer Teilchen, welche durch Neutralino-Koannihilation im sehr frühen Universum die Reliktdichte Dunkler Materie beeinflusst haben können. Übergeordnetes Projekt ist hierbei die *DM@NLO*-Kollaboration, welche das Ziel hat, einen möglichst vollständigen Satz solcher SUSY-Prozesse auf NLO-Level in der QCD zu berechnen. In der Arbeit wird zunächst die Stop-Annihilation auf Born-Niveau berechnet, anschließend die virtuellen Korrekturen, sodass nach Renormierung ein UV-konvergentes Ergebnis vorliegt. Es verbleiben reelle Abstrahlungen. Hierfür wird ein Formalismus entwickelt (auf Dipol-Subtraktion basierend), welcher bislang bei NLO-Rechnungen noch nicht aufgetreten ist. Außerdem wird das Projekt der Stau-Annihilation aus einer vorangegangenen Arbeit beendet durch Sommerfeld-Korrekturen (Resummation) auf Seite der eingehenden skalaren Taus. Die Ergebnisse werden detailliert numerisch ausgewertet, ferner wird der korrigierte Wirkungsquerschnitt auf Gravitino-Physik angewandt. Wir gehen der theoretischen Unsicherheit der Ergebnisse nach, welche aus der Variation von Renormierungsschema und -skala erwächst.

Contents

1. Introduction

The coexistence of astonishingly precise predictions - in remarkable accordance with the experiments - of the Standard Model of particle physics and its inadequacies concerning meaningful questions in modern physics is surely a peculiar fact. It describes three fundamental forces with great exactness and is still unable to give answers e.g. to gravity at microscopic scales, to baryon asymmetry and the nature of dark matter. Due to these riddles, theorists tried to expand the Standard Model in several ways within the last decades. The modifications start with minimal extensions and end in the highly speculative world of strings.

This thesis will deal with supersymmetry (SUSY) yielding us a promising candidate - the neutralino - which has exactly those properties we expect from our current picture of dark matter. Its big mass and insensitivity to electromagnetic interaction gave birth to several projects assuming that at least a main part of dark matter is made of neutralinos. We will start with a brief summary about dark matter: evidence, possible candidates and other theories explaining the observations as well as the present state of research. Furthermore, we present the *DM@NLO* (*dark matter at next-to-leading order*) collaboration - the underlying project of this thesis - in Chapter 2. We explain how our processes can be integrated in the whole picture of this kind of research.

The following chapter deals with some theoretical introductions. For the discussion of supersymmetry, but also for the treatment of colours and the colour decomposition, a group theoretical overview is inevitable. Our process also requires an understanding of Faddeev-Popov ghosts, so we give short remarks regarding the quantisation procedure in QCD.

Diverse contents of Chapter 3 find an application in Chapter 4, dedicated to supersymmetry. Although the theory cannot be explained in all its facets, we will have a look at the gradation of the Poincaré algebra and how to break SUSY, too. The chapter also provides some quantitative information about the new particle zoo arising from the minimal SUSY extension of the SM. With all this background knowledge, we are prepared to perform the calculation of the Born cross section and virtual NLO corrections of stop annihilation (Chapter 5) under the assumption that the technical details (regularisation, tensor reduction, ...) are already known (to be found in the appendix). The next chapter will deal with the development of a dipole subtraction formalism for initial massive scalar bosons. We give a suggestion how to perform the calculations explicitly.

The second big process - stau-antistau annihilation into top quarks - comes to an end in

Chapter 7. We introduce the concept of Sommerfeld enhancement and comment on the remaining QCD-corrections. A detailed numerical analysis of this process follows: Chapter 8 discusses the annihilation cross section with respect to neutralino and gravitino physics and theoretical uncertainties from renormalisation scale and scheme variation. Finally, we conclude and leave some remarks on future projects of the collaboration.

For a transfer of knowledge, a detailed appendix had to be written. We give results of virtual corrections and the used algebraic techniques.

2. The Dark Universe

Several convincing observations suggest that we actually know only five percent of the components our Universe is made of. Even after several decades of research in cosmology and particle physics, we have no concrete idea what the unknown 95 percent could be. There is, on the one hand, the strange nature of dark energy being responsible for an accelerated expansion of the Universe. On the other hand, we have to solve the problem of dark matter giving stability to galaxies and galaxy clusters (23 percent). The concept of supersymmetry gives birth to a candidate the dark matter could possibly made of. In this section we will give a short overview of the current level of research in the area of dark matter and show in which way SUSY could give an answer to its nature and how the *DM@NLO* project, especially the content of this thesis, is connected to that field of research.

2.1. The Hidden Nature of Dark Matter

2.1.1. Evidence

Probably, Fritz Zwicky was rather surprised that rotational curves of galaxies do not obey the irrefutable law describing the centripetal force, under the assumption that only visible matter contributes to the gravitational potential [1]. And perhaps, he would be even more astounded that almost ninety years later physicists could not find a convincing answer to the composition of the so-called dark matter which presumably holds the galaxies together. After observing the Coma cluster and determining the mass of its luminous matter, he used the virial theorem to obtain an averaged velocity of the rotating stars. The great disagreement with his redshift measurements led to the conclusion that dark matter has to be much heavier than the luminous one - a conclusion that was also found by V. Rubin and W. Kent Ford [2]: By observing the rotation velocities of stars around the galactic centers, these astronomers wanted to reproduce the behaviour we know from the planets rotating around the sun (proportional to $\frac{1}{\sqrt{R}}$, distance R). However, a constant rotation velocity, independent of the distance to the galaxy center, was observed. In their opinion, this discrepancy is naturally explainable by assuming a dark matter halo surrounding every galaxy and being responsible for their structure. The most doubts regarding the presence of dark matter in the Universe vanished after observing the bullet cluster (1E 0657-558) shown in the Fig. 2.1. The picture shows two galaxies that collided 100 million years ago, now diverging from each other. During this collision, the intergalactic medium (the major baryonic matter component) interacted, so it slowed down, whereas the galaxies itself moved further. The astonishing conse-

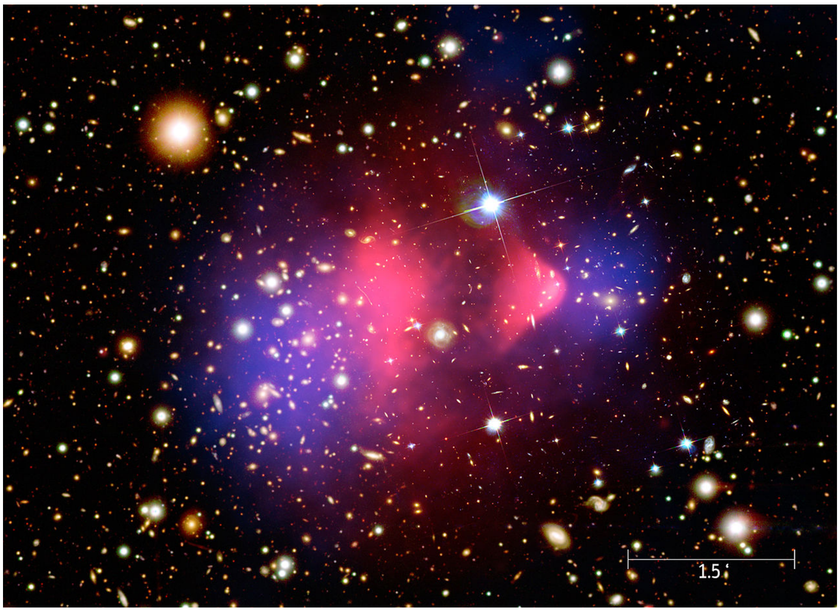

Figure 2.1.: Superposition of the visible spectrum of the bullet cluster together with the pink-coloured X-ray emission of the intergalactic plasma and the blue gravitational potential arising from lens effects [3].

quence of the picture is that the lens effects occur mostly at the galaxies and, therefore, they have to contain a huge amount of dark matter to explain the big curvature. Dark matter would not interact during a collision, so the halos around the galaxies would be left untouched. Other theories that deny the existence of dark matter cannot explain this phenomenon. Thus, the bullet cluster is seen by many astrophysicists as an experimental proof of dark matter.

The evaluation of the WMAP and Planck satellite measurements made it furthermore possible to go beyond qualitative statements about dark matter since the actual density of dark matter would be hard to determine only by observing galaxies. Today, we are indeed capable to perform quantitative analyses - we will encounter the dark matter relic density later.

2.1.2. Candidates

The natural approach to possible dark matter candidates is, of course, to demand that they must not interact electromagnetically as the definition tells us. Jocularly, one divides them up into **MACHOs** and **WIMPs** (*massive astrophysical compact halo objects* and *weakly interacting massive particles*). The first category, consisting only of baryonic matter, was excluded to be a relevant in percentage terms quite early, these objects like e.g. **brown dwarfs** (not luminous at visible wavelength since no fusion occurs) are rare and do not coincide with observations.

More interesting is the list of possible WIMPs, often starting with **neutrinos**. However, making neutrinos responsible for the aforementioned observations is rather contradictory if one has a look upon the evolution of the large structures in the cosmos: In fact, this development happened hierarchically meaning that single stars came into being before galaxies and galaxy clusters were formed (bottom-up scenario). But the influence of dark matter on these structures would cause the complete opposite in the case of fast hot dark matter particles like neutrinos (top-down scenario). The so-called **axion** might be an interesting candidate as field theorists would expect an additional symmetry explaining that no CP violation was observed in QCD processes, although the current theory would not forbid such a violation. This globally broken symmetry (Peccei-Quinn mechanism, see [4]) causes the appearance of pseudo-Goldstone bosons, the axions. They could be proper dark matter particles [5], but an observation was not possible until now.

A contemporary and fruitful area of research is the construction and analysis of **Minimal Models**. Extending the Standard Model as little as possible is often assessed to be a natural approach. Today, a wide spectrum of Minimal Models exists, containing diverse strategies to enlarge the particle content with modified gauge groups, additional Higgs doublets, further Higgs couplings etc. They often try to solve the dark matter problem and a second simultaneously: Radiative see-saw models [6] shall explain non-vanishing neutrino masses, too, whereas a new Higgs coupling aims to explain the $(g-2)_\mu$ anomaly [7]. We do the opposite and postulate a veritable zoo of new particles.

Around 1970, the theory of supersymmetry was born with the ability to solve several (even today) actual problems of particle physics and cosmology (detailed in Chapter 4) yielding us the **neutralino** that we want to discuss now. At first sight, the basic idea of SUSY seems quite easy. The crucial component of this SM-extension is an operator $\hat{Q}$ transforming a boson to a fermion and vice versa:

$$\hat{Q}|B\rangle = |F\rangle \qquad \hat{Q}|F\rangle = |B\rangle \tag{2.1}$$

As we will see in Chapter 4, there is a highly complicated mathematical structure behind this idea which of course can only be outlined in an abridged way. At this point, we just need to know that there is a rather promising candidate within the SM-extension using the concept of SUSY. Working out the SUSY algebra in order to obtain the smallest consistent model (the MSSM, the *Minimal Supersymmetric Standard Model*), a whole catalogue of particles is the outflow of this procedure (Fig. 2.2). What made the neutralino (there are obviously four of them, the object of interest is the lightest - the χ_1^0 or $\tilde{N}_1$) that promising is the introduction of an additional quantum number called R-parity. It is necessary as SUSY sometimes allows the proton decay, seeming quite unlikely after the measurements at Kamiokande (lifetime bigger than 10^{35} years [8]). The R-parity is defined via

$$P_R = (-1)^{3B+L+2s} \tag{2.2}$$

where B and L are baryon and lepton number and s the spin of the respective particle. It leads to the value 1 (SM) or -1 (SUSY). This quantum number implies the

Names	Spin	P_R	Mass Eigenstates	Gauge Eigenstates
Higgs bosons	0	+1	h^0 H^0 A^0 $H^\pm$	H_u^0 H_d^0 H_u^+ H_d^-
squarks	0	−1	$\widetilde{u}_L$ $\widetilde{u}_R$ $\widetilde{d}_L$ $\widetilde{d}_R$ $\widetilde{s}_L$ $\widetilde{s}_R$ $\widetilde{c}_L$ $\widetilde{c}_R$ $\widetilde{t}_1$ $\widetilde{t}_2$ $\widetilde{b}_1$ $\widetilde{b}_2$	" " " " $\widetilde{t}_L$ $\widetilde{t}_R$ $\widetilde{b}_L$ $\widetilde{b}_R$
sleptons	0	−1	$\widetilde{e}_L$ $\widetilde{e}_R$ $\widetilde{\nu}_e$ $\widetilde{\mu}_L$ $\widetilde{\mu}_R$ $\widetilde{\nu}_\mu$ $\widetilde{\tau}_1$ $\widetilde{\tau}_2$ $\widetilde{\nu}_\tau$	" " " " $\widetilde{\tau}_L$ $\widetilde{\tau}_R$ $\widetilde{\nu}_\tau$
neutralinos	1/2	−1	$\widetilde{N}_1$ $\widetilde{N}_2$ $\widetilde{N}_3$ $\widetilde{N}_4$	$\widetilde{B}^0$ $\widetilde{W}^0$ $\widetilde{H}_u^0$ $\widetilde{H}_d^0$
charginos	1/2	−1	$\widetilde{C}_1^\pm$ $\widetilde{C}_2^\pm$	$\widetilde{W}^\pm$ $\widetilde{H}_u^+$ $\widetilde{H}_d^-$
gluino	1/2	−1	$\widetilde{g}$	" "
gravitino/ goldstino	3/2	−1	$\widetilde{G}$	" "

Figure 2.2.: The MSSM contains a wide range of new particles, the superpartners of known SM-particles [3].

existence of a lightest supersymmetric particle (LSP) that cannot decay in further steps. R-parity is currently hard to motivate - there is simply no doubt that a conserved quantum number has to exist. An underlying symmetry is not known, yet. In many models the lightest neutralino ($\tilde{N}_1$ or $\tilde{\chi}_0^1$) is the LSP. Due to its big mass in several scenarios and its property not to interact electromagnetically, the research in this area is an actual, hot topic and, moreover, the underlying assumption of the *DM@NLO* project - the subject of this thesis - claims the neutralino to be the (or at least a) dark matter particle.

As a side-project, *DM@NLO* included also the **gravitino** as LSP and possible dark matter candidate - the superpartner of the spin-2 tensor boson mediating a quantised gravitational interaction, namely the graviton. Section 8.1.4 is completely dedicated to this spin-3/2 Rarita-Schwinger fermion. Viable, but not treated in this thesis, is the superpartner of the right-handed neutrino, called sneutrino. After measuring the Z boson decay width at the LEP, the lighter left-handed brother could be excluded [9]. According to the **sterile/right-handed neutrino** (with its high mass due to e.g. the see-saw mechanism, it is also a candidate for at least *warm dark matter*, therefore highly restricted - see [10]), this particles are often called **sterile sneutrinos**.

Before this section comes to an end, we want to discuss briefly the remainder of relevant ideas in the history of dark matter. In 1983, M. Milgrom decided to follow a completely different path to solve the dark matter problem - that there is no additional matter we have to search for. Instead, our understanding of gravity is no sufficient theory on cosmological scales. Therefore, he introduced the hypothesis of **MOND** [11], standing for *Modified Newtonian Dynamics*, which modifies the Newtonian equation of motion with a multiplicative function $\mu(x)$

$$F = ma\mu\left(\frac{a}{a_0}\right) \qquad \mu(x) = \frac{x}{\sqrt{1+x^2}} \tag{2.3}$$

leading to another understanding of velocity (here, a_0 has to be seen as a new constant of Nature):

$$\frac{GmM}{r^2} = m^2\frac{a^2}{a_0} \Leftrightarrow v = (a_0GM)^{1/4} \tag{2.4}$$

In the limit of large accelerations, the Newtonian dynamics as we know them can be reproduced. Over and above, the constant rotation velocity for stars in outer regions are congruent with the observed rotation curves. This theory was expanded to a relativistic one as an improvement of general relativity, but the Bullet cluster results are interpreted as a convincing counter-argument. In the scientific community, these theories are often excluded from the current area of research.

Last, but not least, we keep in mind that the assumption that dark matter does not interact electromagnetically, but at least weakly, might be a wrong one: There is no reason to exclude that dark matter could interact just gravitationally as it was explained in [12]. In this case, direct detection efforts would be in vain.

2.1.3. Experimental Search for Dark Matter Particles

Within the last decades, several techniques were invented to verify the existence of dark matter experimentally. In general, one can divide these techniques into three types of research that can be drawn schematically (Fig. 2.3). At this point, we should mention that only a handful of experiments can be treated in this section whose detailed background is explained in the references. The dark matter chapter does not demand completeness. Maybe the most natural way to find dark matter (in the following, we concentrate on finding WIMPs) is to assume that these unknown particles are somehow able to interact with SM particles on Earth. This of course requires that the Earth is passing through a dark matter halo in order to detect a measurable flux. The detection can be performed by e.g. a cooled germanium crystal having an excellent radio purity (like the CoGeNT project, US [13]). Another project is the detection with xenon as target material. Well-known experiments are, for instance, the XENON Dark Matter Project in the Gran Sasso underground laboratories, Italy [14], or PandaX in Sichuan, China [15].

The great colliders in the world may also enlighten the field of dark matter: Dark matter signatures in collision experiments could occur, if particle collisions produce dark matter particles directly and also if heavy SM particles created by collisions decay into dark matter particles. Since 2015, proton collisions at energies of 13 TeV are technically possible at the LHC. Although two LHC experiments, namely CMS and ATLAS [16,17],

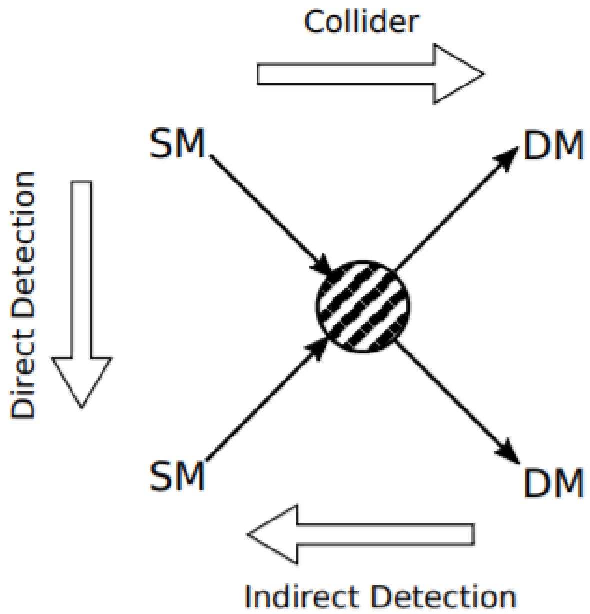

Figure 2.3.: Three types of experimental dark matter research dominate the current work on this topic [31].

include the searches for particles beyond the SM and, therefore, the search for dark matter, there is still no data containing evidence. Furthermore, the detection of SUSY particles does not automatically imply that neutralinos are really the main component dark matter consists of. Some particle physicists criticise the principle of collider physics to enlarge the collision energies further and further. Shifting the SUSY mass spectrum ever higher to explain why no superpartners were found leads to a theory, that cannot be falsified (an unscientific theory, [18]). One should also take into consideration that the dark matter problem might be a misunderstanding and a wrong interpretation of measurements at a deeper level.

It remains a third way of investigating the strange nature of dark matter - the indirect one, that we do not treat in detail. Our strategy is independent of the diagram in Fig. 2.3. To scrutinise dark matter with its relic density is the experimental background of this thesis and, furthermore, the foundation of a wide range of publications arising from the *DM@NLO* collaboration and other projects.

2.2. The *DM@NLO* Project

Let us now assume that the WIMPs are indeed the main constituent of dark matter. Fig. 2.3 shows us that this kind of research is just the opposite of collider experiments - the object of desire hereby is the (thermally averaged) annihilation cross section of dark matter or rather the resulting relic density. We need to find a way to calculate the remaining dark matter after annihilation processes to obtain theoretical results that can be compared with the actual, remarkably precise measurement (1σ interval)

$$\Omega_{CDM}h^2 = 0.1200 \pm 0.0012 \tag{2.5}$$

from the Planck collaboration [19] (see Fig. 2.4). The determination of this value was supported with polarisation data from the WMAP project. h represents the current Hubble expansion rate described as H_0 67,8 km/(s MPc) in units of 100 km/(s MPc). Statistical physics gives us a suitable model to perform the theoretical prediction: The Boltzmann equation describing in this case the time evolution of the neutralino number density n_χ (n_χ^{eq} denotes the number density in equilibrium)

$$\boxed{\frac{dn_\chi}{dt} = -3Hn_\chi - \langle\sigma_{ann}v\rangle[n_\chi^2 - (n_\chi^{eq})^2]\,.} \tag{2.6}$$

The term proportional to the (time-dependent) Hubble rate H is just a cosmological one respecting the expansion of our cosmos and therefore the dilution of matter. Particle physics enters the stage through the thermally averaged annihilation cross section $\langle\sigma_{ann}v\rangle$ that contains how many neutralinos are created and annihilated. The challenging task to calculate every process including neutralinos (and other sparticles that coannihilate with neutralinos, details in Chapter 8) to SM particles with an acceptable precision was created. In the very early Universe a thermal equilibrium of the number

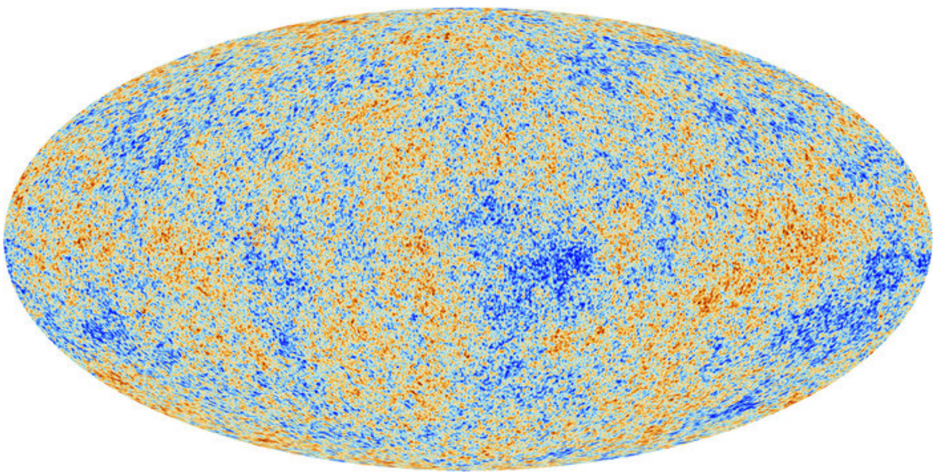

Figure 2.4.: Today, the Planck satellite measurements provide the best investigation of the cosmic microwave background (CMB). Using the results, several quantities appearing in cosmology and astroparticle physics were determined quite precisely [20].

density is assumed; however, this equilibrium is shifted by the cooling of the Universe since it expands: More neutralinos are annihilated than generated. After a certain time, the moment comes where the expansion rate triumphs over the annihilation rate. The particles leave each other so fast that the possibility to annihilate is suppressed. The relic density becomes constant (value of Eq. 2.6), there are no appreciable annihilation processes in the present Universe. This value is reached with the so-called freeze-out mechanism, shown in the Fig. 2.5 below. Apparently, a high cross section value causes a lower level of the final number density. Also notice that the x-axis includes the particle mass. Applying SUSY to dark matter physics is therefore practicable due to the high masses of the new particles. There are naturally three scenarios that can happen after

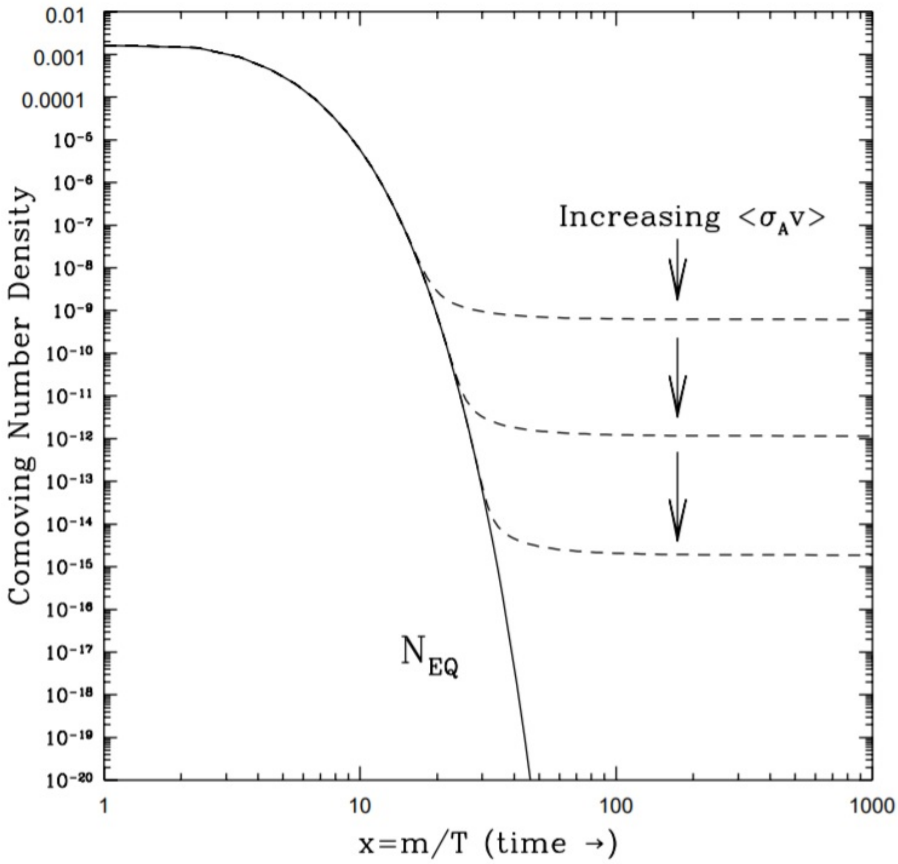

Figure 2.5.: The freeze-out mechanism of the neutralino number density depending on the thermally averaged cross section of annihilation processes [21].

the neutralino relic density was obtained via

$$\Omega_\chi = \frac{n_\chi m_\chi}{\rho_c} \tag{2.7}$$

with the critical density ρ_c of the Universe and the particle's mass m_χ. The result may exceed the value from measurements which is, of course, an incompatiblity of supersymmetric WIMPs as our underlying assumption. But the calculations would not have been worthless since we would have falsified our model; and falsification is the way how modern science works. We could have more luck - the value totally agrees with the experimental research. If our calculations instead fall below these measurements we had at least the possibility that SUSY explains dark matter partially, but no evidence. This is the scientifically unsatisfactory scenario. In order to get these theoretical results, Björn

Herrmann, Michael Klasen and Karol Kovařík initiated the *DM@NLO* project around 2006, with the goal to implement every relevant process for the neutralino relic density calculations (solving the Boltzmann equation) respectively to get a value of all cross sections at NLO. Further NLO corrections are suppressed because of smaller coupling constants. Currently, there exist public packages calculating Born cross sections in the MSSM with some effective couplings (e.g. *DarkSusy* [22]) - however: The QCD corrections are necessary for reliable values as they occasionally shift them up to 40 percent. With these precise predictions one can perform meaningful comparisons with experimental results. Hence, several subprojects were started and the *DM@NLO* collaboration increased. They can be divided up into the following subunits:

- **gaugino pair-annihilation into quark pairs**

  At the beginning, there were just the SUSY-QCD corrections at one-loop level for the neutralino annihilation into quarks, exchanging an A^0. Within the following years, the generalisation was worked out, namely the neutralino and chargino annihilations for every single possible combination - a quite extensive calculation [23,24,25,26].

- **gaugino-squark coannihilation into a quark and a gauge/Higgs boson**

  As described before, also the coannihilation processes obviously reduce the amount of neutralinos as dark matter in the Universe. Their impact was calculated in several processes including the most important stop coannihilations with every Higgs boson, the electroweak bosons and gluons in the final state as well as a quark [27,28].

- **squark-antisquark annihilation into electroweak final states**

  The smaller the mass difference between squarks (especially the scalar top) and the dark matter particle, the more likely is the relevance of pure squark annihilation for the relic density. This contains Higgs and electroweak bosons in the final state and, furthermore, combinations of them [29].

- **squark-antisquark annihilation into coloured final states**

  Perhaps the most time-consuming NLO calculations in SUSY-QCD occur in the case of coloured final states. Again, we have just pure squark annihilations, now with quarks in the final state, performed by S. Schmiemann, or gluons treated by the author of this thesis.

- **stau annihilation into coloured final states**

  Note that there are also other coannihilations with relevance like a heavy slepton annihilation. For stau masses in the near of the neutralino mass, they also could have an impact on the dark matter density [30]. The staus also give rise to an application of the cross section for gravitino dark matter physics [31].

We mentioned that one goal of *DM@NLO* is calculating cross sections for indirect detection of dark matter particles. We emphasize, however, that the code can also be used for direct detection precision predictions: These processes are obtained diagrammatically by rotating the scheme in Fig. 2.3. But also mathematically, we do not need much effort to apply the existent code to direct detection processes. So how does the *DM@NLO* code actually work? It can be divided into several parts, also containing free, already existing programs (Fig. 2.6). Basic requirement for fruitful calculations is the choice of scenarios

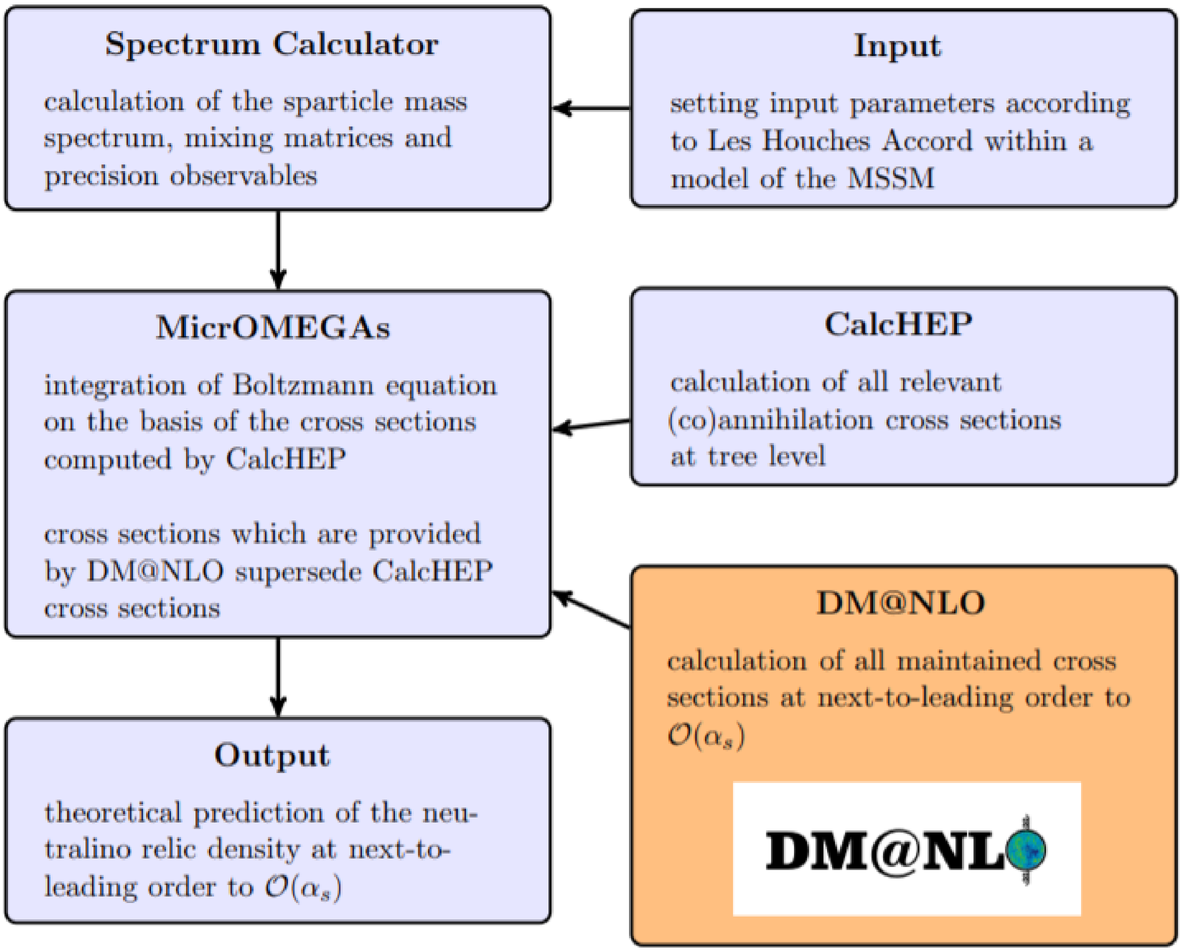

Figure 2.6.: The flow chart illustrates the computation of the neutralino relic density enhanced by *DM@NLO* results [32].

having SUSY particle mass spectra where the investigated (co-)annihilation processes are relevant for the entire relic density. By giving an input file, provided by an SLHA (SUSY Les Houches Accord) file [33,34], to a spectrum calculator like *SPheno* [35,36] or *SoftSUSY*, we can extract a quantitative background of our calculations (the SUSY particle masses are not known yet. Instead, they highly depend on the chosen scenario, see Chapter 4.). We will come back to details when specific scenarios for the processes of this thesis have to be found. Based on these spectra as well as mixing angles and further quantities, *MicrOMEGAs* is able to perform the Boltzmann integration after the NLO corrections were implemented and the tree level cross section calculated by *CalcHep*. It was written by A. Pukhkov et al. in order to obtain cross section at LO directly from the Lagrangian [37].

The *DM@NLO* package appears at the next-highest level - its goal is to yield NLO corrections to the value given by *CalcHep*. Due to its low level of automatisation, this can be a quite involving challenge. SUSY leads to an abundance of possible corrections that have to be treated analytically. *MicrOMEGAs*, written by G. Bélanger et al. [38], is a rather general code for the investigation of dark matter properties and can be applied to many SUSY models and other models of new physics, too. Its calculations include both relic densities, indirect detection rates and direct ones. Hence, we end up with predictions of the neutralino relic density at NLO. If one is not interested in calculational details, one might jump to Chapter 8, where the predictions for our processes are presented and analysed graphically.

3. Selected Topics in Quantum Chromodynamics

Although we have already discussed the general background of this thesis, some specific theoretical tools beyond the scope of the common lectures in quantum field theory have to be introduced. Assuming that the reader is already familiar with the way of calculating cross sections in leading and next-to-leading order (otherwise an introduction can be found in [30]), we will rather concentrate on QCD-related techniques arising from group theory and simplifying the coming calculations.

Three quarks for Muster Mark!
Sure he hasn't got much of a bark
And sure any he has it's all beside the mark.

- James Joyce, *Finnegan's Wake* [39]

The theory of quantum chromodynamics provided an important component of the Standard Model, namely a precise description of the strong interaction. Deep insights into the structure of nuclei led to a couple of Nobel prizes. Today, QED is understood quite well, whereas there are still some meaningful open questions in the QCD. Its complicated mathematical structure arises from its non-Abelian nature - the elements of the $SU(3)_C$ Lie group do not commute. This is a keyword leading us to a group theoretical access to the QCD that will be presented in the following section. It is not only written as an intermezzo before the practical calculations start, and not only to enjoy the beauty of the connections of group theory and physics, but for real applications in the calculations of our processes. Over and above that, we need the group theoretical overview to understand the key idea of SUSY.

3.1. Group Theoretical Foundations

We will start with highly abstract thoughts about group theory, then state them more precisely within their occurrence in QCD until we end up with our explicit process. Especially regarding the SM, the concept of Lie groups is the starting point for further discussions.

Definition 1 (Lie group): A Lie group G is a differentiable smooth manifold with a group structure.

Using those groups is a way to describe continuous symmetries. The Lie algebra belonging to G is defined as follows:

Definition 2 (Lie algebra): A Lie algebra is a vector space $\mathfrak{g}$ for which an antisymmetric bilinear form $[,] : \mathfrak{g} \times \mathfrak{g} \to \mathfrak{g}$ (the Lie bracket), satisfying the Jacobi identity, is defined. (Jacobi identity: $[[A, B], C] + [[B, C], A] + [[C, A], B] = 0$).

Without a suitable representation, the Lie algebra would be worthless for any applied calculation. For a general group, we define:

Definition 3 (representation): A n-dimensional representation of G is an homomorphism $D : G \to GL(n, \mathbb{C})$.

In other words, we take an abstract group element g and give an explicit appearance to it by representing the element via a matrix of the general linear group $GL(n, \mathbb{C})$ of dimension n and with complex entries. Under this mapping (homomorphism, to be precise), the group structure $D(g_1 g_2) = D(g_1)D(g_2)$ is preserved. Perhaps one of the most important ingredients of group theory in physics is the concept of

Definition 4 (reducibility): Let $P_{\{m\times m\}}$, $Q_{\{n\times n\}}$ and $R_{\{m\times n\}}$ be submatrices of a $n+m$-dimensional representation $D(g)$. If D takes the form

$$D(g) = \begin{pmatrix} P(g) & R(g) \\ 0 & Q(g) \end{pmatrix} \tag{3.1}$$

$\forall g \in G$ the representation is called reducible.

Under certain circumstances, this process of reduction can be continued in the way that $R(g)$ is taken to be a null matrix. Hence, $D(g)$ takes now a block-diagonal form and a complete reduction was performed (it remains an irreducible representation). There exists a famous group theoretical theorem by Heinrich Maschke concerning finite groups that guarantees a successful decomposition into irreducible pieces:

Theorem (Maschke) : *Every reducible representation of a finite group is completely decomposable into irreducible representations.*

Keeping in mind the concept of reducibility, let us have a look at

Schur's Lemma: *Any matrix commuting with those of an irreducible representation $D(g)$ is a multiple of the unitary matrix $\forall g$.*

Note, that this Lemma can be expressed in the language of linear operators on Hilbert spaces, too. During the application of group theory on QCD, the deeper meaning will become clear. At this point, we are ready to deal with objects consisting of combinations of elements from more vector spaces than one, for instance a product function of $\mathbf{v}$ and

$\mathbf{w}$, with the notation $\Gamma_{ac}(x) = \mathbf{v}_a(x)\mathbf{w}_c(x)$ transforming under the irreducible representations $D^{(\mu)}$ and $D^{(\nu)}$. The transformation of Γ is under matrices of the tensor product $D^{(\mu)} \otimes D^{(\nu)}$ of the single representations, which means concretely:

$$\Gamma'_{ac}(x) = D^{(\mu)}_{ba}(g) D^{(\nu)}_{dc}(g) \Gamma_{bd}(x) = D^{(\mu\times\nu)}_{bd;ac}(g)\Gamma_{bd}(x) \tag{3.2}$$

The tensor product can be decomposed into irreducible components in analogy to a single representation: We obtain a direct sum of completely decomposed representations, called *Clebsch-Gordan series*:

$$\boxed{D^{(\mu)} \otimes D^{(\nu)} = \bigoplus a_\sigma D^{(\sigma)}} \tag{3.3}$$

It remains the question regarding an elegant way to determine the Clebsch-Gordan series for non-trivial tensor products. In group theory one often uses the well-established method of the *Young tableau* (plural: tableaux). Such a tableau represents (at least for our usage) the (anti-)symmetrisation of a tensor with n indices.
To apply the method, we briefly comment on the evaluation of dimensionality as well as of tensor products leading to a direct sum. Finding the dimension is a simple procedure: Fill the boxes with numbers like it was done in the tableau below (later in QCD: N=3) [40]:

N	$N+1$	$N+2$	$N+3$	$N+4$
$N-1$	N	$N+1$	$N+2$	
$N-2$	$N-1$	N		
$N-3$	$N-2$			
$N-4$				

Afterwards, take a copy of the tableau and enter the number of boxes to the right of it in its row for every box, add one for itself as well as the number of boxes below it in the same column. Finally, take the product of all entries for each tableau and take the quotient of the first with the second tableau. For a Clebsch-Gordan series, follow the below-mentioned rules:

(I): *Fill the boxes* of the second tableau in the tensor product $T_1 \otimes T_2$ with a in the first row, b in the second and so on.
(II): *Add the boxes* with a, b, ... to T_1 that every augmented tableau is still a Young tableau. If boxes have the same label, they must not appear twice or more in the same column. Furthermore, for any given box position the equation $n_a \geq n_b \geq ...$ is valid (with n as the number of same labels to the right and above).
(III): *Cross diagrams* with the same shape off the tableaux except of one.
(IV): *Cancel columns* with N boxes.

After these steps, the direct sum of irreducible representations is the output of the process. Dependent on the tableau, it is occasionally a quite time-consuming procedure. Altogether, it initially seems a bit vague, but we will make use of the advantages in the future cross section calculations. Next, we will concretize the vague concepts by keeping our eyes on QCD.

3.2. Colour Decomposition

With our knowledge about group theory, let us have a look at the QCD as an application of the general concepts of the previous section. The group theoretical point of view on the QCD starts with the $SU(3)_C$ gauge invariance of this theory. Aforesaid $SU(3)$ group is the N=3 case of the special unitary group $SU(N)$ fulfilling the properties (for a group element U):

1. **Determinant:** $\det U = 1$
2. **Unitarity:** $U^\dagger U = UU^\dagger = 1$

In terms of Lie groups, we deal with a $(N^2 - 1)$-dimensional differentiable manifold, in QCD we have $N = 3$ (for each colour). This colour group is generated by the hermitian and traceless generators T^a which are also the generators of the fundamental representation as $N \times N$ matrices. For the case of $N = 3$, there is the following correspondence to the Gell-Mann matrices: $T^a = \frac{\lambda^a}{2}$. With the commutator as a Lie bracket, we can construct a Lie algebra:

$$[T^a, T^b] = if^{abc}T^c \tag{3.4}$$

The structure constants f^{abc} generate the adjoint representation since we can write $f^{abc} = i(T^a)_{bc}$. One can derive a multitude of useful identities in order to calculate colour factors for Feynman diagrams. A few of them are given in App. A, their components will also appear in the vertex factors. Now, we should say a word about Schur's Lemma. The often *quadratic Casimir* called term $T^2 = \sum_{a=1}^{N^2-1} T^a T^a = C_2(T)E_N$ is exactly a simple example of the Lemma from above where the coefficients depend on the representation. In SU(3) symmetry, we have $C_2(T) = 4/3$; a value we will need a couple of times in the calculations.

How can we interpret the aforementioned facts from a physical point of view? The structure constants do not vanish in general, so we have a non-Abelian group. Therefore, the $(N^2 - 1) \to 8$ generators, the gluons, can interact with themselves in contrast to the photons in the Abelian QED. The generators of $SU(3)_C$ can furthermore be seen as rotation matrices in colour space. For an illustration, we define the wave function

$$\begin{pmatrix} \psi_r \\ \psi_g \\ \psi_b \end{pmatrix} = \psi \qquad \text{invariance}: \quad \psi' = \hat{U}\psi \tag{3.5}$$

The whole QCD-Lagrangian (3.6) is invariant under local rotations in colour space.

$$\mathcal{L}_{QCD} = -\frac{1}{4}(F^a_{\mu\nu})^2 - \frac{1}{2\xi}(\partial^\mu A^a_\mu)^2 + \bar{\psi}(i\not{D} - m)\psi + \bar{c}^a(-\partial^\mu D^{ac}_\mu)c^c \tag{3.6}$$

The formulae contains the gauge covariant derivative $D_\mu = \partial_\mu - ig_s \sum_a A_{\mu,a}T^a$ and the field strength tensor $F^a_{\mu\nu} = \partial_\mu A^a_\nu - \partial_\nu A^a_\mu + g_s f^{abc} A^b_\mu A^c_\nu$. Perhaps, the ghost term $c^a(-\partial^\mu D^{ac}_\mu)c^c$ catches someone's eye - ghosts will be a later topic of this chapter.
The Clebsch-Gordan decomposition was formally introduced before - this technique might be well-known from the addition of angular momenta in quantum mechanics. However, we are dealing with colour, not with spin, so we have to decompose tensor products of colours of (s)quarks (3) and gluons (8). Thanks to H. Maschke - or rather to the fact that the object of desire is a finite subgroup of $SU(N)$ - we have the certainty to carry out the decomposition into irreducible representations successfully. In order to use the results later, we work it out with two squarks as well as with two gluons. We follow the general procedure from the previous section using the Young tableaux. For a general process in QCD, one performs the decomposition into irreducible representations of the tensor product of our initial (r) and final state (R):

$$r \otimes \bar{r} = \bigoplus_\alpha r_\alpha \qquad R \otimes \bar{R} = \bigoplus_\alpha R_\alpha \tag{3.7}$$

The Clebsch-Gordan coefficients appear within the unitary basis transformation from the tensor product space $R \otimes \bar{R}$ to the vector space (direct sums of single vector spaces, respectively) of the irreducible representation:

$$\vec{e}_{a_1 a_2} = \sum_{R_\alpha} C^{R_\alpha}_{\alpha a_1 a_2} \vec{e}^{R_\alpha}_\alpha \tag{3.8}$$

Therefore, we can write a vector like $\vec{V} = V_{a_1a_2}\vec{e}_{a_1a_2} = \sum_{R_\alpha} V_\alpha \vec{e}_\alpha$. The main step is just to form pairs $P_i = (r_\alpha, R_\beta)$ of equivalent representations from the initial and the final states which means the subset of irreducible representations occurring in both the direct sums $\bigoplus_\alpha r_\alpha$ and $\bigoplus_\beta R_\beta$. We are now able to rewrite the scattering amplitude via

$$\boxed{\mathcal{M}_{a_1a_2a_3a_4} = \sum_i c^{(i)}_{a_1\ldots a_4}\mathcal{M}^{(i)} \qquad c^{(i)}_{a_1a_2a_3a_4} = \frac{1}{\sqrt{\dim(r_\alpha)}} C^{r_\alpha}_{\alpha a_1 a_2}(C^{R_\beta}_{\beta a_3 a_4})^* .} \tag{3.9}$$

The remaining task is only to carry out the decomposition with the usage of the Young tableaux. We retrace the application of this method for the explicit initial state $r \otimes \bar{r} = 3 \otimes \bar{3}$ (here: squarks, but also valid for quarks, of course) and the final state $R \otimes \bar{R} = 8 \otimes 8$. Obviously, the initial state is much easier, so that we start with $r \otimes \bar{r} = 3 \otimes \bar{3}$, expressed as:

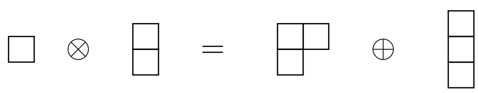

Our Clebsch-Gordan series of $\tilde{q}\tilde{q}^*$ can be written as $8 \oplus 1$. Furthermore, if we express the wave function like $\psi = (u, d, s)$ - at the moment the colour is not important, but the quark types - the direct sum gives the observed meson multiplets, by the way. For the tensor product $8 \otimes 8$, the decomposition starts with the two Young tableaux and we label the second like in (I).

We repeat step (II) thrice for every box at the right:

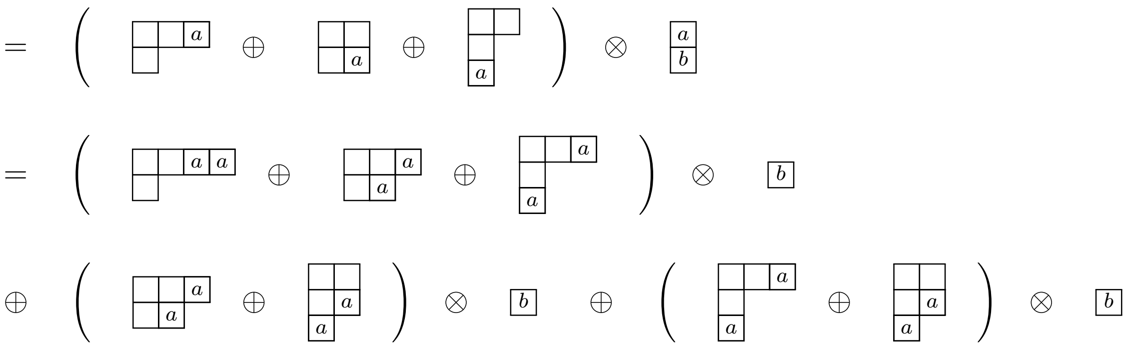

In between, we cross off some diagrams according to (III).

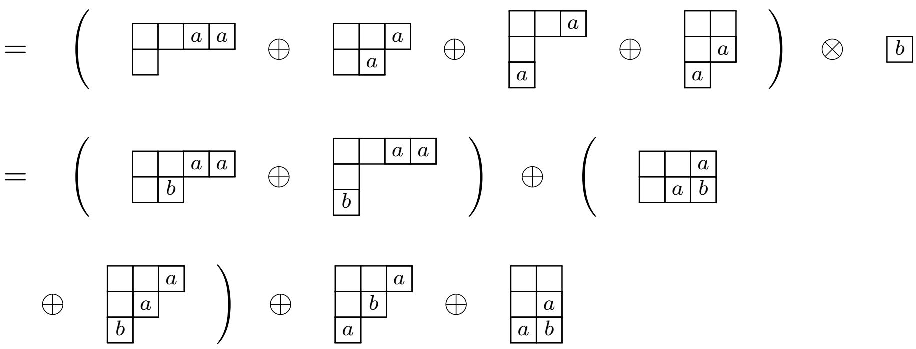

Now, the procedure gradually comes to an end: We do only step (IV)

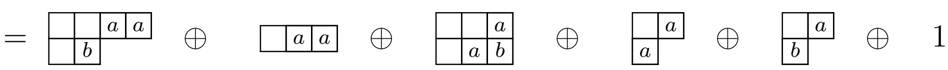

This result can be seen as the irreducible representation of the tensor product of our two gluons after using the rules for the dimensionality of Young tableaux:

$$8 \otimes 8 = 27 \oplus 10 \oplus \bar{10} \oplus 8_A \oplus 8_S \oplus 1 \tag{3.10}$$

Hence, we end up with the pairs (due to colour conservation)

$$P_i \in \{(1,1), (8, 8_S), (8, 8_A)\} \tag{3.11}$$

so we can perform the decomposition in Chapter 5 by using the colour structures $c^{(i)}$ taken as an orthonormal basis satisfying

$$c^{(i)}(c^{(j)})^* = \delta_{ij} \,. \tag{3.12}$$

We can give the colour basis explicitly - having in mind that there are other suitable sets of basis vectors:

$$c^{(1)}_{ijbc} = \frac{1}{\sqrt{N^3 - N}}\delta_{ij}\delta_{bc} \tag{3.13}$$

$$c^{(2)}_{ijbc} = \sqrt{\frac{2N}{(N^2-1)(N^2-4)}}T^a_{ji}d^{abc} \tag{3.14}$$

$$c^{(3)}_{ijbc} = \sqrt{\frac{2}{N^3 - N}}T^a_{ji}if^{abc} \tag{3.15}$$

Here, we see several elements of the above-mentioned colour algebra in different representations. With this knowledge and the relations in App. A, we are able to calculate the colour factors later. Hence, we just ended with easily applicable tools for cross section calculations in QCD starting from abstract concepts and definitions. The only open question is the advantage of the procedure of decomposition: After a successful decomposition, every interference containing an impossible colour flow is automatically excluded from the whole squared amplitude - one directly sees which diagrams do not have to be calculated. For NLO corrections, a more important feature of this technique is the fact that the irreducible parts of the decomposed amplitude are convergent on their own. Especially for a multitude of vertex corrections and/or real emissions, it is convenient to divide the process into smaller parts to check the ultraviolet or infrared convergence.

3.3. Ghosts: A Relic of Quantisation

Two vector bosons in the final state of our $\tilde{t}_1\tilde{t}_1^* \to gg$ process lead us to an obstacle within the quantisation of non-Abelian gauge theories. Initially, we should have a look at the permitted polarisations $\epsilon^T_{i\mu}$ ($i = 1, 2$, transversely polarised) of the two gluons. In QED, there is nothing to fear since the on-shell Ward identity $\mathcal{M}^\mu k_\mu = 0$ forbids unphysical polarisation states of the photon. Unfortunately, in some cases this does not hold in the non-Abelian QCD anymore. By evaluating the amplitudes at tree level and later applying the Ward identity, we are able to set a precedent for the ostensibly allowed production of longitudinal polarisations (we call them here $\epsilon^{+/-}_\mu(k)$ for the forward and backward lightlike polarisation vectors) - this unphysical phenomenon that we will easily see cannot just be ignored. Furthermore, the violation of the optical theorem is as unattractive as ignoring the appearance of $\epsilon^{+/-}_\mu(k)$. Where does this violation come from? In the figure below we see the imaginary part of an internal loop related to the tree level process that can be constructed by cutting the loop diagram. A look at the completeness relation

$$g_{\mu\nu} = \epsilon^+_\mu\epsilon^{*-}_\nu + \epsilon^-_\mu\epsilon^{*+}_\nu + \sum_i \epsilon^T_{i\mu}\epsilon^{*T}_{i\nu} \tag{3.16}$$

betrays that the optical theorem claims to take every polarisation state (even the unphysical) into consideration for the outgoing gluons, as the metric tensors appears within the gluon loop (vector propagator). Apparently, there is something missing before a

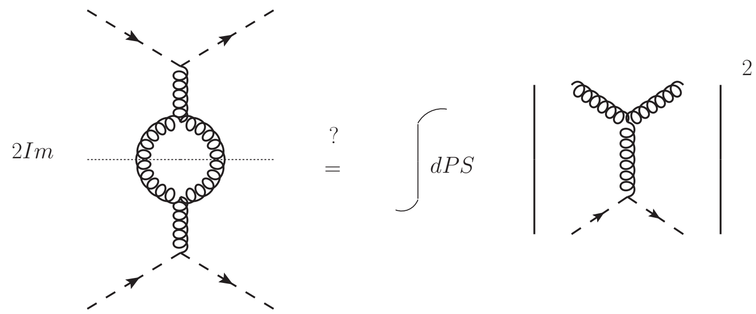

Figure 3.1.: The optical theorem seems to be contradictory in non-Abelian gauge theories.

non-Abelian gauge theory works consistently. The most elegant way of deriving the additional Lagrangian to make the unphysical degrees of freedom disappear is, perhaps, the method of path integrals. To do this, we must require the background knowledge in the field quantisation procedure with the help of functional methods (introduction in [41]). We simplify the QCD to a pure gauge theory (no fermions) leading us to the easier functional integral

$$\int \mathcal{D}A \exp\left[i \int d^4x \left(-\frac{1}{4}(F^a_{\mu\nu})^2\right)\right] \tag{3.17}$$

for the gauge field A that can be transformed like $(A^\alpha)^a_\mu = A^a_\mu + \frac{1}{g} D_\mu \alpha^a$ with the covariant derivative D_μ. The path integral measure hereby does not change, the integration over gauge motions α can be factored out. We follow the procedure of Fadeev and Popov [42] who inserted an effective 1 into (3.17):

$$1 = \int \mathcal{D}\alpha(x) \delta(G(A^\alpha)) \det\left(\frac{\delta G(A^\alpha)}{\delta\alpha}\right) \tag{3.18}$$

Within the determinant, we find a functional derivative. The idea behind this identity is to bring the gauge fixing condition $G(A) = \partial^\mu A^a_\mu(x) - \omega^a(x) = 0$ (generalised Lorenz gauge condition) into the field theory - the evaluation of the functional determinant can be done, if one remembers the quantisation of spinor fields θ_i where a helpful identity appeared:

$$\left(\prod_i \int d\theta_i^* d\theta_i\right) \exp(-\theta_i B_{ij} \theta_j^*) = \det B \tag{3.19}$$

This identity gave birth to the idea to express the determinant from above as a functional integral over anticommuting fields c, later called FP ghosts (where the equation can only be fulfilled if they are scalars under Lorentz transformation - they cannot be physical particles due to spin statistics):

$$\det\left(\frac{1}{g}\partial^\mu D_\mu\right) = \int \mathcal{D}c\mathcal{D}\bar{c}\exp\left[i\int d^4x\bar{c}(-\partial^\mu D_\mu)c\right] \tag{3.20}$$

The optical theorem is preserved by adding this ghost contribution to processes with to non-Abelian gauge bosons in the final state (Fig. 3.2)

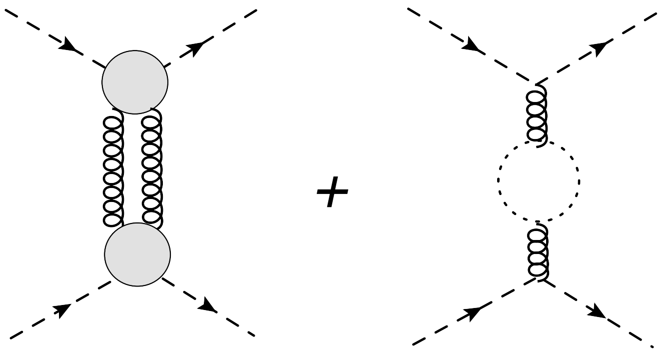

Figure 3.2.: The additional ghost contribution causes that the optical theorem holds again.

4. An Approach Towards Supersymmetry

Based only on a proper respect for the power of Nature to surprise us, it seems nearly as obvious that new physics exists in the 16 orders of magnitude in energy between the presently explored territory near the electroweak scale and the Planck scale

-Stephen P. Martin, *A Supersymmetry Primer* [43]

4.1. Underlying Ideas

To get a sense what SUSY is about, let us start with a quite simple model in Fock space (generally following [44]). We only place the demand on this model that it should contain bosons as well as fermions (more precise: n_B bosons and n_F fermions). Consider two operators $Q_\pm$ that we want to call SUSY operators, with the following impact on states in our Fock space:

$$Q_+|n_B, n_F\rangle \propto |n_B - 1, n_F + 1\rangle \qquad Q_-|n_B, n_F\rangle \propto |n_B + 1, n_F - 1\rangle \tag{4.1}$$

They obviously create a fermion/boson and destroy a boson/fermion simultaneously - what we can interpret as a transformation of fermions into bosons and v.v. We would like to demand energy conservation, as known expressed via $[H_S, Q_\pm] = 0$ for an arbitrary SUSY-Hamiltonian H_S. It is helpful to construct the hermitian operators $Q_1 = Q_+ + Q_-$ and $Q_2 = -i(Q_+ - Q_-)$ because the ansatz $H_S = Q_i^2$ fulfils the energy conservation. Hence, we end up with a quite easy SUSY algebra:

$$\boxed{[H_S, Q_i] = 0 \qquad \{Q_i, Q_j\} = 2H_S\delta_{ij}} \tag{4.2}$$

Luckily, we encounter the mathematical definitions of the previous chapter in SUSY - we see that Lie algebras and representation theory occur in a multitude of theories. With our background knowledge, we see that this simple SUSY algebra is no Lie algebra as we know it from quantum field theories within the SM since an anticommutator relation appears. The usage of an anticommutator in the new algebra extending the prior QFT is exactly the way to maximise the symmetry of a QFT. It was proven by Haag, Łopuszański and Sohnius [45]:

Theorem (1975): *The possible symmetry of a consistent four-dimensional quantum field theory becomes maximal, if it contains a supersymmetry as a non-trivial extension of the Poincaré symmetry.*

We will come later to details about the Poincaré algebra. Thanks to this proof, the correctness of a SUSY algebra as a generator of physically existent symmetries in a QFT was mathematically well-defined. Only eight years earlier, Coleman and Mandula presented a proof that every generator of relevant symmetries should be Poincaré-invariant (so every bigger symmetry is a product group of the Poincaré group and a group which has nothing to do with spacetime.) [46]. The conditions of this work seemed to be general enough, but one realised that also fermionic generators (see anticommutator from above) of symmetries exist. The aforementioned SUSY algebra was just an introductory one and should not be seen as a supersymmetric extension of the Poincaré group. The simplest extension was constructed by Wess and Zumino [47] in 1974. We will now study more in detail how an extension of an algebra could work.

4.2. Mathematical Background

4.2.1. Gradation: The Poincaré Superalgebra

While looking upon Figure 2.2 one probably asks where all these new particles shall come from. What is the origin of this highly keen conjecture that every elementary particle should have a (currently undetected) superpartner? As one perhaps knows, elementary particles in Nature can be described as irreducible representations of the Poincaré group including the Lorentz transformation as well as translations in the Minkowski space. Group elements therefore perform a transformation of coordinates like $x^\mu \to \tilde{x}^\mu = \Lambda^\mu_\nu x^\nu + a^\mu$. The algebra behind the Lorentz transformations is generated by the tensors $M^{\mu\nu} = L^{\mu\nu} + \Sigma^{\mu\nu}$, where $M^{\mu\nu}$ as a generator of rotations in the Minkowski space is decomposed into inner and external rotations like angular momenta in quantum theory ($\hat{J} = \hat{L} + \hat{S}$). We can write the them like

$$M^{\mu\nu} = x^\mu P^\nu - x^\nu P^\mu + \frac{i}{4}\begin{pmatrix} \sigma^\mu\tilde{\sigma}^\nu - \tilde{\sigma}^\mu\sigma^\nu & 0 \\ 0 & \tilde{\sigma}^\mu\sigma^\nu - \sigma^\mu\tilde{\sigma}^\nu \end{pmatrix} \qquad \tilde{\sigma}^\mu = (E_2, -\vec{\sigma}) \tag{4.3}$$

or in the short-hand notation $\Sigma^{\mu\nu} = \mathrm{diag}(\sigma^{\mu\nu}, \tilde{\sigma}^{\mu\nu})$ with the Pauli matrices $\sigma^\mu = (E_2, \vec{\sigma})$ and the four-momentum P^μ which also stands for the four generators of translations. Altogether, the Poincaré group underlies a 10-dimensional Lie algebra with the following commutator relations:

$$\boxed{\begin{gathered} [P^\mu, P^\nu] = 0 \qquad [P^\nu, M^{\rho\sigma}] = i(g^{\mu\rho}P^\sigma - g^{\mu\sigma}P^\rho) \\ [M^{\mu\nu}, M^{\rho\sigma}] = -i(g^{\mu\rho}M^{\nu\sigma} - g^{\mu\sigma}M^{\nu\rho} - g^{\nu\rho}M^{\mu\sigma} + g^{\nu\sigma}M^{\mu\rho}) \end{gathered}}$$

By finding the Casimir operators $P^2 = P_\mu P^\mu$ and W^2 with the Pauli-Lubański vector $W^\mu = \frac{1}{2}\epsilon^{\mu\nu\rho\sigma}P_\nu M_{\rho\sigma}$ (relativistic description of the spin vector) - commuting with all 10 generators -, we get our irreducible representations, characterised by (m, s) being the fundamental properties of elementary particles: mass and spin. Back to our question from the beginning: The enlarged particle zoo (augmented by taking SUSY into consideration) can be obtained by evaluating a suitable Poincaré superalgebra and finding the accompanying Casimir operators, too. The proceeding to widen a given algebra is a well-defined concept in mathematics. The construction of a SUSY algebra from which the supermultiplets result as a new sort of elementary particles, a mathematician would call a gradation of the Poincaré algebra. Grading an algebra works as follows:

Definition 5 (graded algebra): A $\mathbb{Z}_n$-graded algebra is a direct sum of vector spaces $\mathbb{L} = \bigoplus_{i=0}^{n-1} \mathbb{L}_i$ with a product $\circ$ defined as $u_j \circ u_k \in \mathbb{L}_{j+k \mod n}$, $u_i \in \mathbb{L}_i$.

Our next step is to construct a graded Lie algebra for the case $n = 2$ made of the Poincaré algebra and the above-introduced generators of SUSY transformations Q_a. It has a deviant quality in comparison to a normal Lie algebra:

Definition 6 (graded Lie algebra): A $\mathbb{Z}_2$-graded Lie algebra is defined by the following three properties:

1. **Gradation:** $x_i \circ x_j \in \mathbb{L}_{i+j \mod 2}$
2. **Supersymmetry:** $x_i \circ x_j = -(-1)^{i \cdot j} x_j \circ x_i$
3. **Expanded Jacobi identity:** $x_k \circ (x_l \circ x_m)(-1)^{k \cdot m} + x_m \circ (x_k \circ x_l)(-1)^{m \cdot l} + x_l \circ (x_m \circ x_k)(-1)^{l \cdot k}$

For the product $\mathbb{L}_0 \times \mathbb{L}_0 \to \mathbb{L}_0$, we still have the Poincaré algebra since the SUSY generators do not appear in this map. A bit more challenging is the case of $\mathbb{L}_0 \times \mathbb{L}_1 \to \mathbb{L}_1$. Of course, we should have a result factorised with Q_a - the SUSY generators define the $\mathbb{L}_1$-space. For generic generators Z^i of a Lie algebra, we expect the structure $[Z^i, Q_a] \propto z^i_{ab} Q_b$. The new Jacobi identity from above should of course be fulfilled - inserting this ansatz yields directly that z^i_{ab} has to be a $N \times N$-representation of our $\mathbb{L}_0$-generators. We see that we are dealing with four SUSY generators, for the Lorentz group we choose the inner rotations in Minkowski space, for translation we use the trivial transformation, so we obtain the Lie brackets

$$[P^\mu, Q_a] = 0 \qquad [M^{\mu\nu}, Q_a] = -\Sigma^{\mu\nu}_{ab} Q_b \,. \tag{4.4}$$

It remains the map $\mathbb{L}_1 \times \mathbb{L}_1 \to \mathbb{L}_0$ for which one often uses the ansatz $\{Q_a, Q_b\} \propto (\gamma^\mu C)_{ab}$ with the charge conjugation operator C. The calculation is too time-consuming to work it out here (see [44]). What remains is, together with the recently derived properties, a Latin index-free version of the SUSY algebra:

$$\boxed{\begin{array}{c} [Q, P^\mu] = [\bar{Q}, P^\mu] = \{Q, Q\} = \{\bar{Q}, \bar{Q}\} = 0 \\ [Q, M^{\mu\nu}] = \sigma^{\mu\nu} Q \qquad [\bar{Q}, M^{\mu\nu}] = \tilde{\sigma}^{\mu\nu} \bar{Q} \\ \{Q, \bar{Q}\} = 2\sigma_\mu P^\mu \qquad \{\bar{Q}, Q\} = 2\tilde{\sigma}_\mu P^\mu \end{array}} \tag{4.5}$$

4.2.2. Irreducible Representations of the SUSY Algebra

In order to obtain our new particles, we follow the same procedure as mentioned in the former section - with the only difference that we have to construct another Casimir operator representing the superspin, whereas P^2 still stands for the particle mass. The operator C^2, defined by $C^{\mu\nu} = Y^\mu P^\nu - Y^\nu P^\mu$, commutes with all 14 generators of our superalgebra where Y^μ is an SUSY-extension of the Pauli-Lubański vector - namely $W^\mu - \frac{1}{4} Q\sigma^\mu \bar{Q}$. This vector fulfils the well-known angular momentum algebra. First of all, we are interested in the massive representation, so we can write:

$$C^2 = 2m^2 Y^2 - 2(Y_\mu P^\mu)^2 = -2m^2 \vec{Y}^2 = -2m^4 y(y+1) \tag{4.6}$$

In the last steps, we worked in the rest system of the particle and wrote its eigenvalues with $y = (0, 1/2, 1, ...)$, not containing the mass as a prefactor anymore. Therefore, a massive representation is characterised by (m, y) in analogy to our irreducible representations of the Poincaré group. Let us now create generation and annihilation operators acting on a so-called Clifford vacuum $|\Omega\rangle$ in order to see the action of the SUSY generators Q on a state $|Z\rangle$:

$$f_A^- := \frac{1}{\sqrt{2m}} Q_A \qquad f_A^+ := \frac{1}{\sqrt{2m}} \bar{Q}_{\dot{A}} \tag{4.7}$$

These operators act on $|\Omega\rangle := (f_1^-)^{n_1}(f_2^-)^{n_2})|Z\rangle$ with $n_1, n_2 = 0, 1$ (we let the annihilation operator act on a state until no particle is in it - a vacuum) since it is natural to assume the properties

$$f_1^-|\Omega\rangle = 0 \qquad f_2^-|\Omega\rangle = 0\,. \tag{4.8}$$

Obviously, we can construct four states with the operators $\{1, f_1^+, f_2^+, \frac{1}{\sqrt{2}} f_1^+ f_2^+\}$. Using the definitions from above, one directly finds $\vec{Y}|\Omega\rangle = \vec{W}|\Omega\rangle$ having the interesting consequence: spin = superspin (also valid for the component s^3). Just the other three actions on the Clifford vacuum are remaining questions to achieve a complete supermultiplet. With some spinor algebra (which we cannot perform in detail; we refer to [44] where a big part of this chapter is explained more precisely), one gets the following eigenvalue equations:

$$W^3 f_1^+|\Omega\rangle = m(y^3 + \frac{1}{2}) f_1^+|\Omega\rangle \tag{4.9}$$

$$W^3 f_2^+|\Omega\rangle = m(y^3 - \frac{1}{2}) f_2^+|\Omega\rangle \tag{4.10}$$

$$W^3 \frac{1}{\sqrt{2}} f_1^+ f_2^+|\Omega\rangle = m y^3 \frac{1}{\sqrt{2}} f_1^+ f_2^+|\Omega\rangle \tag{4.11}$$

These equations are crucial to read off the important supermultiplets for $y = 0, 1/2$. The chiral supermultiplet $(m, 0)$ describes matter - the quarks and leptons belong to this multiplet as well as their superpartners we know from Chapter 2, Table 2.2. Additionally, one also includes the Higgs particles and their superpartners (we will discuss later why there is more than one Higgs boson). The chiral supermultiplet consists of fermions ($s_3 = \pm\frac{1}{2}$), of scalars (no SUSY operator acting on $|\Omega\rangle$) and pseudoscalar particles, when we construct the fourth state. The next-complicated representation is used to describe interaction - we start with $y = 1/2$ and therefore a fermionic Clifford vacuum and end up with a vector supermultiplet with the gauge bosons and their superpartners (photino, wino, zino/bino before electroweak symmetry breaking, gluino). The pair $(m, 1/2)$ leads to particles with spin 1/2 (2x), 1 (2x) and 0 (1x) by using the $f^{\pm}$ for both superspins $y_3 = \pm 1/2$.

We see that we reached our goal to understand why an extended algebra produces a huge number of new particles only using algebraic techniques. Again, we have an astonishing example that in particle physics the theoretical prediction comes before the experimental detection in the most cases, and not vice versa as it happens in several disciplines of science. It is not surprising that SUSY does not exist nowadays, it is no exact symmetry in our Universe. We therefore have the necessity to construct a symmetry breaking mechanism.

4.2.3. Breaking the Symmetry

So far, we have only seen how particles appear by constructing a new algebra. This overview was quite general and we have not talked about the expected ingredients of a quantum field theory, e.g. Lagrangians, yet. We will now become more precise and present briefly the way how the broken SUSY is currently understood. Apparently, we are not able to equate the masses of the superpartners with the SM particle masses since we would have detected them otherwise decades ago. During introducing a SUSY Lagrangian (an elaborate procedure with several new elements that cannot be presented here, we refer to [43]) for the easiest supersymmetric model, the MSSM with the number $\mathcal{N} = 1$ of SUSY generators Q, symmetry breaking terms are needed to explain the observed situation in a suitable way:

$$\mathcal{L}_{MSSM} = \mathcal{L}_{SUSY} + \mathcal{L}_{soft} \tag{4.12}$$

The SUSY-conserving part is responsible for gauge and Yukawa interactions. Since we have no concrete idea how the symmetry breaking mechanism works in detail, one introduced an approach called soft SUSY breaking - the additional terms in the Lagrangian include SUSY-violating mass terms and trilinear couplings. The mass hierarchy can only be maintained for a positive mass dimension. These terms can be expressed in the following way:

$$\boxed{\begin{aligned}\mathcal{L}_{soft} = &-\frac{1}{2}(M_1\tilde{B}\tilde{B} + M_2\tilde{W}\tilde{W} + M_3\tilde{g}\tilde{g} + h.c.)\\ &-(M^2_{\tilde{Q}})_{ij}\tilde{Q}^\dagger_i\tilde{Q}_j - (M^2_{\tilde{\bar{u}}})_{ij}\tilde{\bar{u}}^\dagger_i\tilde{\bar{u}}_j - (M^2_{\tilde{\bar{d}}})_{ij}\tilde{\bar{d}}^\dagger_i\tilde{\bar{d}}_j\\ &-(M^2_{\tilde{L}})_{ij}\tilde{L}^\dagger_i\tilde{L}_j - (M^2_{\tilde{\bar{e}}})_{ij}\tilde{\bar{e}}^\dagger_i\tilde{\bar{e}}_j\\ &-m^2_{H_u}H^\dagger_uH_u - m^2_{H_d}H^\dagger_dH_d - (b_\mu H^\dagger_dH_u + h.c.)\\ &+(A_u)_{ij}H_u\tilde{Q}_i\tilde{\bar{u}}_j + (A_d)_{ij}H_d\tilde{Q}_i\tilde{\bar{d}}_j + (A_e)_{ij}H_d\tilde{L}_i\tilde{\bar{e}}_j + h.c.\end{aligned}} \tag{4.13}$$

A multitude of new elements to be determined appear within this expression, which makes this model problematic seen from the philosophy of science and also in general, as we will see. The M_i are mass parameters of wino, bino and gluino, whereas the $M^2_{...}$ terms are hermitian 3×3 matrices of the soft SUSY breaking mass terms of sfermions. We will discuss the Higgs sector, including $H_{u/d}$, whose mass terms after soft symmetry breaking are given in the third line. b_μ is hereby defined via the off-diagonal squared Higgs mass term m^2_{12}. At last, we encounter the aforementioned trilinear couplings in every possible way. Hence, we end up with 105 new parameters by the mechanism of soft SUSY breaking - an unsatisfactory, however essential and necessary part of SUSY. Fortunately, one can immensely reduce the number of parameters by using phenomenological models. For instance, the constrained MSSM (cMSSM) assumes squared scalar masses and trilinear couplings to be flavour diagonal and universal - shrinking the parameter space to five dimensions. But normally, one wishes a model with not too many constraints - the pMSSM (phenomenological) with 19 parameters is often used [48].

This section shall come to an end with mentioning more detailed approaches to the symmetry breaking that have been worked out in the last decades. The underlying principle is the idea of a hidden sector where the origin of spontaneously broken SUSY is conjectured. It should be transferred by so-called messenger interaction to the visible (measurable) sector. The hidden sector acts at incredibly high energies $\lambda_{soft} \gg \lambda_{electroweak}$, so no particles from this sector appear in the visible sector. Nonetheless, they have effects on this scale by the messenger sector expressed via the soft breaking terms from the upper Lagrangian, that transfer the breaking to the visible sector. This messenger interaction might be gravity (gravity-mediated SUSY breaking) or gauge forces/gaugino mediation. [49,50].

4.3. Motivation

The beauty of SUSY is for many physicists a handwavy argument for the truth of the theory. Although there were several convincing cases in history of science, where a great new model had got a ravishing shortness, this cannot be the main reason to believe in SUSY. Nevertheless, there are other reasons making this theory promising and making shortcomings of the SM disappear. Although we have already encountered the neutralino as a candidate for dark matter, two other interesting problems and how to solve them with SUSY shall be explained.

4.3.1. Hierarchy Problem

The SM is just an effective theory, valid up to a certain mass scale Λ that is entered e.g. for the Higgs mass corrections in NLO. The fermionic contribution carries a quadratic divergence with a cutoff scale lying immensely higher than the electroweak scale. It seems unnatural to cancel this divergence by a fine-tuned procedure due to the fact that the gauge boson masses are protected by symmetries. The symmetry protecting m_h might be SUSY as the scalar loop correction arising from sfermions of the MSSM (Fig. 4.1) cancels the quadractic divergence in the following illustrative way (under the

Figure 4.1.: The cutoff parameter Λ might disappear, if the NLO contributions to the Higgs mass consist of fermionic (left) and sfermionic (right) loops.

assumption of equal couplings $\lambda_{\tilde{f}} = \lambda_f$):

$$\delta m_h^2(f) + \delta m_h^2(\tilde{f}) = \frac{1}{8\pi^2}\left(-\lambda_f^2\Lambda^2 + m_f^2 \ln\left(\frac{\Lambda^2}{m_f^2}\right) + \lambda_{\tilde{f}}\Lambda^2 - m_{\tilde{f}}^2 \ln\left(\frac{\Lambda^2}{m_{\tilde{f}}^2}\right)\right) \tag{4.14}$$

This is a purely statistical result, as the negative sign has its origin in Fermi-Dirac statistics of closed fermion loops. The hierarchy problem could be solved in a natural way. Note, that logarithmic divergences $\ln(\Lambda^2)$ are still existent but weaker. One should be aware of the fact that this cancellation seems only that stunning using the cut-off method to regularise the divergence with the parameter Λ. In other frameworks for the evaluation of loops the effect of including additional scalars is less obvious.

4.3.2. Grand Unified Theories

Unifying every fundamental gauge interaction is the big dream of many physicists believing that in the beginning the Universe was ruled just by a single force. This dream may be supported by the unification of electro- and magnetostatics in the 19th century as well as by the theory of the electroweak force around 1970. The symmetry breaking mechanism of the latter one acts at the electroweak scale. One assumes the energy of the unification $SU(3)_C \times SU(2)_L \times U(1)_Y$ of all gauge forces to be around 10^{16} GeV, but unfortunately the coupling constants do not meet at a single point within the SM. As we can see in Fig. 4.2, SUSY cancels also this problem, so a grand unified theory (GUT) is allowed: Additional contributions to the running of the coupling constants allows for

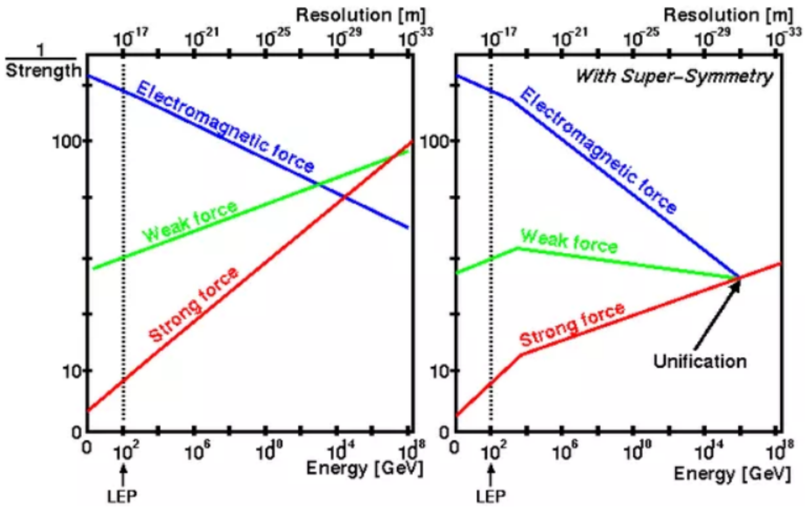

Figure 4.2.: A grand unification at a single point should be possible using SUSY [51].

their meeting at the GUT scale. We keep in mind that gravity is totally excluded from these thoughts; a QFT of gravity is a problem of a frightening size. Nevertheless, SUSY enters again the stage: Including gravity in string theories demands SUSY as well. Such a theory can only be defined using supergravity. The assumption of a GUT yields a pMSSM - rather a toy model -, by the way. We hereby equate the soft SUSY breaking mass terms: $M_i(Q_{GUT}) = m_{1/2}$.

4.4. Specific Aspects

After this overview giving us an understanding of SUSY to a certain degree, we can concentrate on specific components of the Minimal Supersymmetric Standard Model that we will explicitly need in future calculations.

4.4.1. Ingredients: The New Particle Zoo

Despite having discussed a lot of aspects of SUSY, we are still unsuspecting regarding the properties of our new particles within the MSSM, shown in Fig. 2.2. Apparently, the MSSM yields 12 squarks arising from 6 left- and right-handed superpartners, the same holds for the selectron, the smuon and the stau (the explicitly needed particles will be treated in the coming subsection). One should note that these left- and right-handed superpartners could mix non-trivially. More interesting, however, are the Higgs, the neutralino and chargino sectors. Hereby, we have to distinguish carefully between the (measurable) mass eigenstates of this sector and the gauge eigenstates. The Higgs sector comes into being since the electroweak symmetry breaking absorbs only three degrees of freedom, but the MSSM extension enlarges the number of degrees up to eight by an additional Higgs doublet. Today, we therefore should find five Higgs bosons, namely the neutral SM-like boson h^0, a much heavier H^0, a pseudoscalar, CP-odd A^0 and two charged Higgses $H^\pm$ (obtained by mixing the gauge eigenstates $(\tilde{H}_u^+, \tilde{H}_u^0)$ and $(\tilde{H}_d^0, \tilde{H}_d^-)$). Their fermionic partners are called Higgsinos. During symmetry breaking, Goldstone bosons appear - they have the Goldstinos as superpartners.

The gauge symmetries in the MSSM are the same like in the SM ($SU(3)_C \times SU(2)_L \times U(1)_Y$), so it is unsurprising to find gluinos, winos ($\tilde{W}^0$, $\tilde{W}^\pm$) and a bino $\tilde{B}^0$ forming a photino, zino and charged winos via the Weinberg angle θ_W as it happens in the SM after symmetry breaking at the electroweak scale:

$$|\gamma\rangle = \cos\theta_W|B^0\rangle + \sin\theta_W|W^0\rangle \qquad |Z^0\rangle = -\sin\theta_W|B^0\rangle + \cos\theta_W|W^0\rangle \tag{4.15}$$

$$|W^\pm\rangle = \frac{1}{\sqrt{2}}(|W^1\rangle \mp i|W^2\rangle) \tag{4.16}$$

The uncharged particles we recently explained are the ingredients of the neutralino sector, responsible for four neutralinos $\tilde{\chi}_i$ (Majorana fermions) with different masses. They are obtained from the Lagrangian below:

$$\mathcal{L} = -\frac{1}{2}(\Psi^0)^T \mathbf{M}_{\tilde{\chi}} \Psi^0 + h.c. \qquad \Psi^0 = (\tilde{B}^0, \tilde{W}^0, \tilde{H}_d^0, \tilde{H}_u^0) \tag{4.17}$$

$$\mathbf{M}_{\tilde{\chi}} = \begin{pmatrix} M_1 & 0 & -\cos\beta\sin\theta_W m_Z & \sin\beta\sin\theta_W m_Z \\ 0 & M_2 & \cos\beta\cos\theta_W m_Z & -\sin\beta\cos\theta_W m_Z \\ -\cos\beta\sin\theta_W m_Z & \cos\beta\cos\theta_W m_Z & 0 & -\mu \\ \sin\beta\sin\theta_W m_Z & -\sin\beta\cos\theta_W m_Z & -\mu & 0 \end{pmatrix}$$

β is given by $\arctan(\frac{v_u}{v_d})$ with the VEVs $v_{u,d} = \langle H_{u,d}^0 \rangle$. $M_{1,2}$, the *soft parameters*, arise from the electroweak sector in the SUSY breaking Lagrangian (4.13), μ from the Higgsino mass Lagrangian, see also [3]. In a similar way, the so-called charginos $\tilde{C}_{1,2}^\pm$ (mass eigenstates) consist of the charged gauge eigenstates, constructed with the Lagrangian

$$\mathcal{L} = -\frac{1}{2}(\Psi^+, \Psi^-)^T \mathbf{M}_{\tilde{C}} (\Psi^+, \Psi^-) + h.c. \qquad \Psi^\pm = (\tilde{W}^+, \tilde{H}_u^+, \tilde{W}^-, \tilde{H}_d^-) \tag{4.18}$$

$$\mathbf{M}_{\tilde{C}} = \begin{pmatrix} 0 & 0 & M_2 & \sqrt{2}\cos\beta m_W \\ 0 & 0 & \sqrt{2}\sin\beta m_W & \mu \\ M_2 & \sqrt{2}\sin\beta m_W & 0 & 0 \\ \sqrt{2}\cos\beta m_W & \mu & 0 & 0 \end{pmatrix}$$

4.4.2. Special SUSY Particles: Staus and Stops

Now, we comment more precisely on the SUSY particles of which the coannihilation processes are calculated within this thesis. The left- and right-handed gauge eigenstates of the staus and stops mix in a non-trivial way to mass eigenstates with indices 1,2. The Lagrangian is constructed by mixing the sfermion sector via a mass matrix $\mathbf{M}_{\tilde{f}}^2$:

$$\mathcal{L}_{m(\tilde{f})} = \sum_{\tilde{f}} \tilde{f}^\dagger \mathbf{M}_{\tilde{f}}^2 \tilde{f} \qquad \mathbf{M}_{\tilde{f}}^2 = \begin{pmatrix} M_{\tilde{f}_{LL}}^2 & M_{\tilde{f}_{LR}}^2 \\ M_{\tilde{f}_{LR}}^2 & M_{\tilde{f}_{RR}}^2 \end{pmatrix} \tag{4.19}$$

We specify the ingredients of the mass matrix:

$$M^2_{\tilde{f}_{LL}} = M^2_{\{\tilde{Q},\tilde{L}\}} + (I_f^{3L} - e_f \sin^2(\theta_W)) \cos(2\beta) m_Z^2 + m_f^2 \tag{4.20}$$

$$M^2_{\tilde{f}_{LR}} = m_f (A_f - \mu (\tan\beta)^{-2I_f^{3L}}) \tag{4.21}$$

$$M^2_{\tilde{f}_{RR}} = M^2_{\{\tilde{U},\tilde{D},\tilde{E}\}} + e_f \sin^2(\theta_W) \cos(2\beta) m_Z^2 + m_f^2 \tag{4.22}$$

Again, we encounter the soft SUSY-breaking masses $M^2_{\{...\}}$ and the trilinear couplings A_f. Over and above, the third component of the weak isospin, I_f^{3L}, appears. e_f denotes the electric charge of the fermion, expressed in the quantity of the elementary charge e. Our off-diagonal mass matrix becomes important in the third generation. In lower generations the mass eigenstates can be neglected without any problems. But having a look at the off-diagonal entries, we find the fermion mass (increasing with the generation). With the top quark mass in the off-diagonal entry, a considerable mixing is expectable. The actual value is determined by the chosen scenario - we still have free parameters.

Diagonalising yields mixing matrices. For staus, we find the following rotation in the vector space of gauge eigenstates:

$$\mathbf{M}^2_{\tilde{\tau}} = \begin{pmatrix} m^2_{\tilde{\tau}_{LL}} & m^2_{\tilde{\tau}_{LR}} \\ m^2_{\tilde{\tau}_{LR}} & m^2_{\tilde{\tau}_{RR}} \end{pmatrix} = (\mathbf{D}^{\tilde{\tau}})^\dagger \begin{pmatrix} m^2_{\tilde{\tau}_1} & 0 \\ 0 & m^2_{\tilde{\tau}_2} \end{pmatrix} \mathbf{D}^{\tilde{\tau}} \tag{4.23}$$

$$\mathbf{M}^2_{\tilde{\tau}} = \begin{pmatrix} m^2_{\tilde{l}_3} - (\frac{1}{2} - \sin^2\theta_W) M_Z^2 \cos 2\beta + m_\tau^2 & -m_\tau (A^{\tau^*} + \mu \tan\beta) \\ -m_\tau (A^\tau + \mu^* \tan\beta) & m^2_{\tilde{\tau}} - M_Z^2 \cos 2\beta \sin^2\theta_W) + m_\tau^2 \end{pmatrix} \tag{4.24}$$

The rotation operator is called mixing matrix, $\mathbf{D}^{\tilde{\tau}}$, and contains a mixing angle. In a later scenario the mixing is almost maximal and should never be forgotten.

$$\begin{pmatrix} \tilde{\tau}_1 \\ \tilde{\tau}_2 \end{pmatrix} = \mathbf{D}^{\tilde{\tau}} \begin{pmatrix} \tilde{\tau}_L \\ \tilde{\tau}_R \end{pmatrix} = \begin{pmatrix} \cos\theta_{\tilde{\tau}} & \sin\theta_{\tilde{\tau}} \\ -\sin\theta_{\tilde{\tau}} & \cos\theta_{\tilde{\tau}} \end{pmatrix} \begin{pmatrix} \tilde{\tau}_L \\ \tilde{\tau}_R \end{pmatrix} \tag{4.25}$$

From the diagonalisation process, we obtain:

$$m^2_{\tilde{\tau}_{1,2}} = \frac{1}{2} \left(m^2_{\tilde{\tau}_{LL}} + m^2_{\tilde{\tau}_{RR}} \mp \sqrt{(m^2_{\tilde{\tau}_{LL}} - m^2_{\tilde{\tau}_{RR}})^2 + 4 m^4_{\tilde{\tau}_{LR}}} \right) \tag{4.26}$$

Moreover, we can express the mixing angle as follows:

$$\cos\theta_{\tilde{\tau}} = \frac{-m^2_{\tilde{\tau}_{LR}}}{\sqrt{m^4_{\tilde{\tau}_{LR}} + (m^2_{\tilde{\tau}_2} - m^2_{\tilde{\tau}_1})^2}} \qquad (0 \leq \theta_{\tilde{\tau}} < \pi) \tag{4.27}$$

The same holds for the heavy squark sector. For brevity, we simply give the mass matrix from which everything earls can be derived.

$$\mathbf{M}^2_{\tilde{t}} = \begin{pmatrix} m^2_{\tilde{q}_3} + (\frac{1}{2} - \frac{2}{3}\sin^2\theta_W)M_Z^2\cos 2\beta + m_t^2 & -m_t(A^{t^*} + \mu\cot\beta) \\ -m_t(A^t + \mu^*\cot\beta) & m^2_{\tilde{t}} - \frac{2}{3}M_Z^2\cos 2\beta\sin^2\theta_W) + m_t^2 \end{pmatrix} \tag{4.28}$$

$$\mathbf{M}^2_{\tilde{b}} = \begin{pmatrix} m^2_{\tilde{q}_3} - (\frac{1}{2} - \frac{1}{3}\sin^2\theta_W)M_Z^2\cos 2\beta + m_b^2 & -m_b(A^{b^*} + \mu\tan\beta) \\ -m_b(A^b + \mu^*\tan\beta) & m^2_{\tilde{b}} - \frac{1}{3}M_Z^2\cos 2\beta\sin^2\theta_W) + m_b^2 \end{pmatrix} \tag{4.29}$$

The bottom mixing is given since it occurs in virtual corrections in the stau annihilation process on the side of outgoing heavy quarks (generically implemented).

5. Cross Section of the Stop Annihilation

Stop-antistop annihilation into gluon pairs gives birth to uncountable Feynman diagrams at next-to-leading order. We introduce the process by evaluating the colour decomposition and calculation at Born level and continue with self-energies of the propagators. These are also needed for the renormalisation procedure of propagator and vertex diagrams. We leave comments on special difficulties like non-trivial symmetry factors and give at least an overview of the real gluon emissions. Finally, a description of interference terms with the virtual diagrams is given.

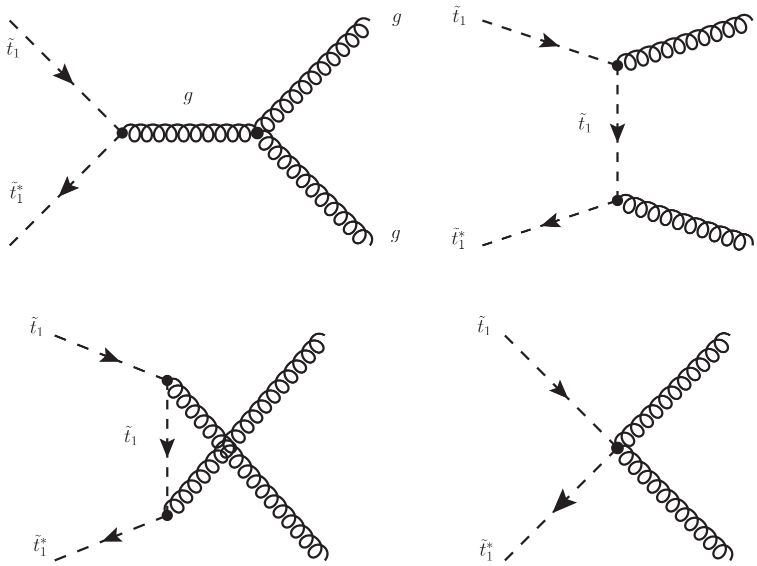

Figure 5.1.: The process $\tilde{t}_1\tilde{t}_1^* \to gg$ contains s-, t- and u-channel. Due to indistinguishable final states, the t- and u-channel are strongly related. A trivial channel is given by the 2-squark-2-gluon vertex that does not include a propagator. All dashed lines indicate the lighter stop.

5.1. Calculation at Tree Level

The process of annihilating stop-antistop pairs into gluon pairs allows for several amplitudes. By taking every possible MSSM interaction into consideration, we end up with the Feynman diagrams in Fig. 5.1. As we know from previous discussions, we are not allowed to ignore the ghost contribution in Figure 5.2 coming from the final state of two gluons in the s-channel (same indices). It was shown by S. Schmiemann that the light-

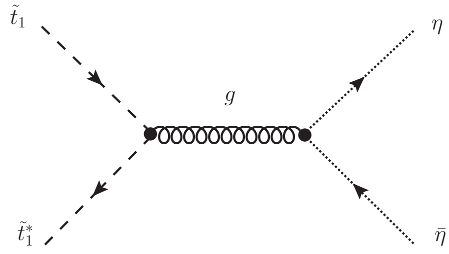

Figure 5.2.: As described in Section 3.3, gauge fixing requires Fadeev-Popov ghosts. Alternatively, the light-cone gauge can be taken into consideration. The inverted flow of the final ghost is a different diagram and has to be calculated separately.

cone gauge leads to the same numerical results. Later on, we naturally have to correct also the ghost vertices that would not appear in a different gauge. But first things first.

5.1.1. Decomposing the Amplitude

Before we calculate the amplitudes explicitly, we should use the technique of colour decomposition to split the total amplitude into the direct sum arising from the Clebsch-Gordan decomposition. In order to conserve the colour, the following pairs from the direct sum in Section 3.2 are allowed: $(1,1),(8,8_S),(8,8_A)$. A short look at the colour structure of the s-channel diagram tells us the direct proportionality to (3.15), so this channel (also including the same colour factor of the ghost contribution) only appears in the antisymmetric octet. For the remaining channels we have to work a bit more and make use of the relations of the colour algebra in App. A.3. We extract the parts of the amplitude equation contributing to the singlet and the octets by multiplying the $c^{(i)}_{ijbc}$ with the colour factors. We obtain (after some steps of colour algebra) the irreducible representations of our amplitude. Luckily, the squared total amplitude fulfils the following relation (orthonormality basis):

$$\boxed{\mathcal{M}_{total} = \mathcal{M}_1 + \mathcal{M}_{8S} + \mathcal{M}_{8A} \rightarrow |\mathcal{M}_{total}|^2 = |\mathcal{M}_1|^2 + |\mathcal{M}_{8S}|^2 + |\mathcal{M}_{8A}|^2} \tag{5.1}$$

We present the final result - the colour decomposition of our squared scattering amplitude:

$$|\mathcal{M}_1|^2 = \frac{N^2-1}{4N}(|\mathcal{M}_t|^2 + |\mathcal{M}_u|^2 + 2|\mathcal{M}_t\mathcal{M}_u| + 4|\mathcal{M}_4|^2 + 4|\mathcal{M}_4\mathcal{M}_t| + 4|\mathcal{M}_4\mathcal{M}_u|) \tag{5.2}$$

$$|\mathcal{M}_{8S}|^2 = \frac{C_F(N^3-4N)}{4}(|\mathcal{M}_t|^2 + |\mathcal{M}_u|^2 + 2|\mathcal{M}_t\mathcal{M}_u| + 4|\mathcal{M}_4|^2 + 4|\mathcal{M}_4\mathcal{M}_t| + 4|\mathcal{M}_4\mathcal{M}_u|) \tag{5.3}$$

$$|\mathcal{M}_{8A}|^2 = \frac{(N^3-N)}{8}(|\mathcal{M}_t|^2+|\mathcal{M}_u|^2-2|\mathcal{M}_t\mathcal{M}_u|+4|\mathcal{M}_s|^2+4|\mathcal{M}_s\mathcal{M}_t|-4|\mathcal{M}_s\mathcal{M}_u|) \quad (5.4)$$

This technique shows us directly the allowed interferences and gives colour factors for every cross section automatically. Next, one has to calculate the squared amplitudes explicitly.

5.1.2. Evaluating the Possible Feynman Diagrams

In this subsection we will give the amplitudes of our five Feynman diagrams, whereas the Born cross section expressed in Mandelstam variables for all squared amplitudes is given in Appendix C. The procedure of calculating cross sections might be well-known - it follows always the same easy steps of writing down the amplitude $\mathcal{M}$, squaring and contracting it and expressing it via s, t and u. At this moment we just obtain the differential cross section $\frac{d\sigma}{d\Omega}$ - conventionally in a spherical coordinate system to tell us the distribution of the final particles, dependent on the space angle element $d\Omega$. The procedure of integration works as follows:

$$\int d\sigma = \frac{1}{F}\int |\bar{\mathcal{M}}|^2 dPS^{(n)} \quad (5.5)$$

Here we find the flux factor F, given by

$$F = 4\sqrt{(p_1p_2)^2-(m_1m_2)^2} = sv \quad (5.6)$$

with the relative velocity v of the incoming particles with masses and momenta m_i and p_i as well as the phase space element $dPS^{(n)}$ for n outgoing particles (here: 2, for real emissions 3):

$$dPS^{(n)} = \left(\prod_{j=1}^{n}\frac{d^3\vec{k}_j}{2E_j(2\pi)^3}\right)(2\pi)^4\delta^{(4)}\left(p_1+p_2-\sum_{j=1}^{n}k_j\right) \quad (5.7)$$

The Dirac distribution guarantees the conservation of momenta and contains the momenta k_j of outgoing particles, too. With this knowledge we are prepared for the cross section at leading order.

s-channel: This is perhaps the most cumbersome calculation due to the three interacting gluons. All following vertex factors as well as propagators can be found in Appendix C. The choice of the momenta is the intuitive one, which means that the momenta go in the direction of time (p_1 and p_2 in the initial state, k_1 and k_2 in the final state). Taking into account every needed factor except of the colour structure of the s-channel yields:

$$\mathcal{M}_s = \frac{-ig_s^2}{s}(p_2-p_1)^\alpha g_{\alpha\rho}[g^{\rho\nu}(k_1+2k_2)^\mu + g^{\mu\nu}(k_1-k_2)^\rho - g^{\mu\rho}(2k_1+k_2)^\nu]\epsilon^*_\mu(k_1)\epsilon^*_\nu(k_2) \quad (5.8)$$

s is the Mandelstam variable (see C.1 kinematics), g_s is the coupling strength of strong interactions, furthermore the outgoing gluons are described with polarisation vectors ϵ^*. For the squared amplitude, one just has to rename the indices and to conjugate $\epsilon^*(k_i)$, the contraction will be done via the relation $\sum \epsilon_\alpha(p_i)\epsilon^*_\beta(p_i) = -g_{\alpha\beta}$ appearing within the summation over all possible polarisations of a vector-like particle in the final state. Hence, we easily obtain:

$$|\mathcal{M}_s|^2 = \frac{g_s^4}{s^2}(p_2-p_1)_\rho(p_2-p_1)_\beta[g^{\rho\nu}(k_1+2k_2)^\mu + g^{\mu\nu}(k_1-k_2)^\rho - g^{\mu\rho}(2k_1+k_2)^\nu] \quad \times \\ [g^{\beta\delta}(k_1+2k_2)^\gamma + g^{\gamma\delta}(k_1-k_2)^\beta - g^{\gamma\beta}(2k_1+k_2)^\delta]g_{\mu\gamma}g_{\nu\delta} \tag{5.9}$$

But with the knowledge about ghosts, we are aware of the incompleteness of the s-channel calculation: The outgoing Fadeev-Popov ghosts split up into two diagrams since the particle with momentum k_1 can be a ghost or an anti-ghost and vice versa for k_2. As the vertex factor carries only the momentum of the particle, we add two similar, but not equal diagrams:

$$\mathcal{M}_{s_{gh}} = \frac{-ig_s^2}{s}(p_2-p_1)^\alpha g_{\alpha\rho}(k_1)_\rho - \frac{ig_s^2}{s}(p_2-p_1)^\alpha g_{\alpha\rho}(k_2)_\rho \tag{5.10}$$

Squaring the amplitude is in this case a trivial procedure. Immensely easier is the treatment of the...

...four-vertex:. Without colours we merely get:

$$\mathcal{M}_4 = ig_s^2 g^{\mu\nu}\epsilon^*_\mu(k_1)\epsilon^*_\nu(k_2) \to |\mathcal{M}_4|^2 = 4g_s^4 \tag{5.11}$$

t- and u-channel: Finally, we can calculate the remaining diagrams simultaneously by interchanging k_1 and k_2.

$$\mathcal{M}_t = (2p_1-k_1)^\mu \frac{ig_s^2}{t-m^2_{\tilde{t}_1}}(2p_2-k_2)^\nu \epsilon^*_\mu(k_1)\epsilon^*_\nu(k_2) \tag{5.12}$$

$$\mathcal{M}_u = (2p_1-k_2)^\mu \frac{ig_s^2}{u-m^2_{\tilde{t}_1}}(2p_2-k_1)^\nu \epsilon^*_\mu(k_2)\epsilon^*_\nu(k_1) \tag{5.13}$$

After the integration, the whole Born cross section is already calculated. This is of course not sufficient for a convincing result - it follows a much more time-consuming part of the next order in the perturbative series.

5.2. NLO Corrections

In this section we assume that the reader is familiar with the technical procedure of loop calculations and give just a quick overview of the coming calculations. Techniques used in this chapter are explained in App. D in detail. Let us first recapitulate the basic ingredients of a full calculation beyond the Born cross section: For an acceptable precision, one normally has to work out the perturbative series up to the second order. At next-to-leading order (NLO), the one-loop corrections appear in the Feynman diagrams. The loop integrals over the internal momenta have the inconvenient property of being divergent in several cases. These divergences turned out to arise from ill-defined Lagrangians (see the coming subsection) that can be made calculable with the procedure of dimensional regularisation/reduction. To eliminate the poles, one must include the counterterms obtained from the self-energy of the particles (renormalisation), subtracting the UV divergences, and in the same way real corrections (e.g. gluon emission), responsible for the IR divergences. Due to the famous theorem of Kinoshita, Lee and Nauenberg [52], the whole Standard Model has IR-convergent cross sections by taking into consideration every *integrated* real emission process (which can be expanded to supersymmetric models):

$$\boxed{\sigma^{NLO} = \int_{2\to 2} d\sigma^{virtual} + \int_{2\to 3} d\sigma^{real}} \tag{5.14}$$

Now, we will retrace the full NLO calculation step by step.

It should be self-explanatory that the description of all NLO calculations would blow up the main part in an irresponsible way. We give the results in the appendix instead, the coming subsections are in fact rather a summary of and a commentary on all permitted diagrams.

5.2.1. Self-Energies and Counterterms

In order to make the loop integrals calculable, we use the common method of dimensional regularisation. Their evaluation is done with Passarino-Veltman integrals, whose theoretical background is described in Appendix D. The following figure gives the set of the four possible squark self-energy diagrams. Treating the gluon is a bit more extensive

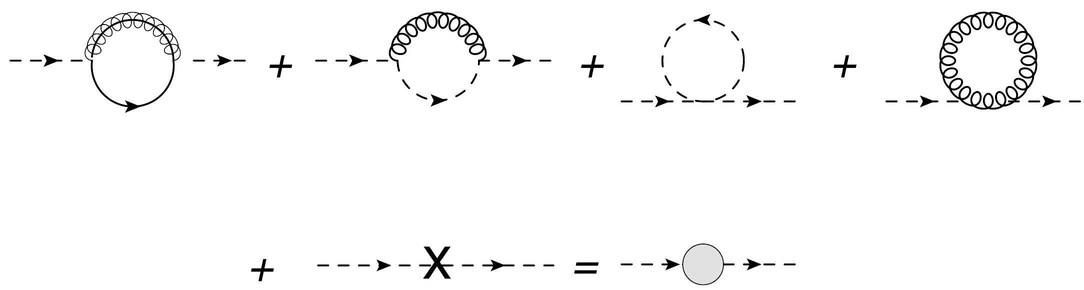

Figure 5.3.: Four loops added to the counterterm yield a UV-convergent squark self-energy.

(seven diagrams, Fig. 5.4). With these diagrams, the propagator corrections are complete. This point is appropriate to mention a handful of facts concerning counterterms

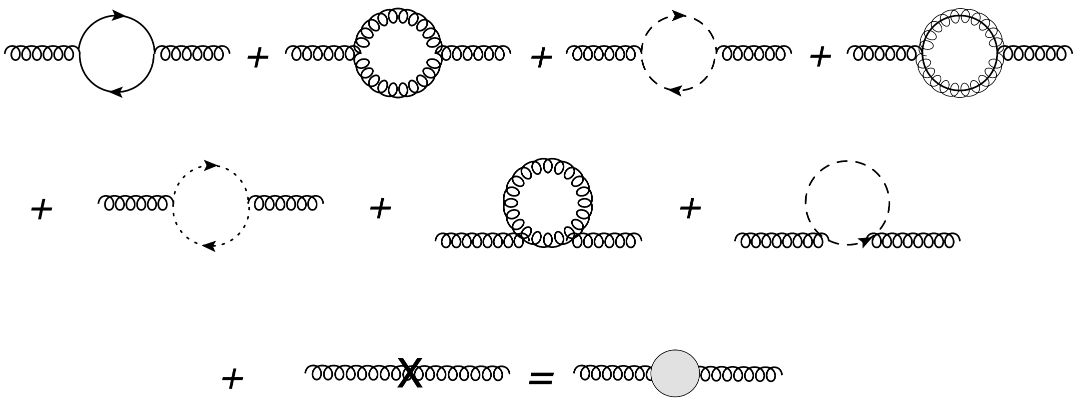

Figure 5.4.: The gluon self-energy known from the Standard Model is extended by squark and gluino loops. Combinatorics with gluino loops is dangerous as they are Majorana fermions. The counterterm can be separated into SM and SUSY.

as the self-energies have to be known to calculate them explicitly. So what is the basic idea behind the procedure of renormalisation? After having identified the inconvenient divergences, the challenging task of absorbing them is still remaining. This problem was solved by the insight that the (so-called bare) Lagrangian we used for calculating the tree level is ill-defined and the bare elements (mass m_0, field ϕ_0 and coupling strength λ_0) have to be rescaled, what is commonly performed by multiplicative renormalisation:

$$\phi_0 = \sqrt{Z_\phi}\phi_R = \left(1 + \frac{1}{2}\delta Z_\phi\right)\phi_R \tag{5.15}$$

$$\lambda_0 = Z_\lambda \lambda_R = (1 + \delta Z_\lambda)\lambda_R \tag{5.16}$$

$$m_0 = Z_m m_R = (1 + \delta Z_m) m_R \tag{5.17}$$

where the NLO expansion $Z_i = 1 + \delta Z_i + \mathcal{O}(\lambda^2)$ was performed. The redefinition yields the renormalised Lagrangian with the structure of our bare one, just with rescaled ingredients, and additional counterterms (drawn with a crossed propagator in the figures from above) containing the δ-terms with a new set of Feynman rules. The occurring diagrams will absorb the UV divergences. Let us have a look at the squarks or rather their bare Lagrangian

$$\mathcal{L}_0^{\tilde{q}} = \partial_\mu \tilde{q}_{0,i}^* \partial^\mu \tilde{q}_{0,i} - m_{\tilde{q}0}^2 \tilde{q}_{0,i}^* \tilde{q}_{0,i} \tag{5.18}$$

that shall be replaced (via rescaling the wave function $\tilde{q}_{0,i}$ and the bare mass $m^2_{\tilde{q}_{0,i}}$ like above) to

$$\begin{aligned}\mathcal{L}_0^{\tilde{q}} = \partial_\mu \tilde{q}_i^* \partial^\mu \tilde{q}_i - m_{\tilde{q}}^2 \tilde{q}_i^* \tilde{q}_i &+ \frac{1}{2}\delta Z_{ij}^{\tilde{q}}(\partial_\mu \tilde{q}_i^* \partial^\mu \tilde{q}_j - m_{\tilde{q}}^2 \tilde{q}_i^* \tilde{q}_j) \\ &+ \frac{1}{2}(\delta Z_{ij}^{\tilde{q}})^*(\partial_\mu \tilde{q}_i^* \partial^\mu \tilde{q}_j - m_{\tilde{q}}^2 \tilde{q}_i^* \tilde{q}_j) \\ &- \delta m_{\tilde{q}_i}^2 \tilde{q}_i^* \tilde{q}_i\end{aligned}$$

$$\rightarrow \mathcal{L}_0^{\tilde{q}} = \mathcal{L}_{ren}^{\tilde{q}} + \delta\mathcal{L}^{\tilde{q}} \tag{5.19}$$

where the δ-terms side absorbs every UV divergence appearing within the squark sector. The indices ij represent the mixing of the squarks which later makes the renormalisation procedure more laborious in contrast to the quarks. In general, one extracts the counterterms from the self-energies $\Pi(p^2)$, what can be carried out in different renormalisation schemes. Probably, the MS scheme (minimal subtraction) is the canonical way to get rid of the divergences, since the counterterm subtracts simply the pure pole without additional terms, so it can be directly read off from the self-energy terms. In the $\overline{MS}$ scheme also the finite term $-\gamma_E + \ln 4\pi$ is subtracted as it appears in every tensor integral (see App. D). This procedure is used for dimensional regularisation without supersymmetry. Its SUSY equivalent is the $\overline{DR}$ scheme - the dimensional reduction namely preserves the supersymmetry (main difference: vector bosons are D-dimensional, not four-dimensional). For directly measurable particles, one introduced the on-shell scheme with the simple idea that the renormalised mass must be equal to the physical one. The counterterms are derived from two renormalisation conditions, setting on the one hand the masses equal and on the other hand asking the residue to be 1:

$$\mathrm{Re}\,\Pi(p^2)|_{p^2=m^2} = 0 \qquad \lim_{p^2\to m^2} \frac{1}{p^2-m^2}\Pi(p^2) = 1 \tag{5.20}$$

If one wishes to derive a vertex counterterm, one simply has to sum over the counterterm components of the vertex, i.e. all appearing wave function counterterms and the renormalised coupling. The propagator counterterm is obtained in the same way: $i[(p^2-m^2)\delta Z_\phi - m_R^2\delta Z_m]$. The gluon and squark renormalisation is explained in detail in App. D. Within our collaboration, a hybrid-scheme consisting of the on-shell and the $\overline{DR}$ scheme is used. Dependent on how many parameters are renormalised on-shell, one may obtain fairly different cross sections that we will analyse in Chapter 8.

5.2.2. Vertex Corrections and Boxes

We consider the vertex corrections for the incoming squarks, the outgoing gluons (not to forget the ghosts) and the 2-quark-2-gluon-vertex: By taking into account every allowed coupling of particles given in App. B, one finds a multitude of corrections presented in the following figures. This set of diagrams has been supported by the *FeynArts* output for our process. Its algorithms yield the wide range of corrections automatically, but in a possibly confusing notation, especially in complex processes. The longest calculation within the vertex corrections affects the 3-vector topology (Fig. 5.5).

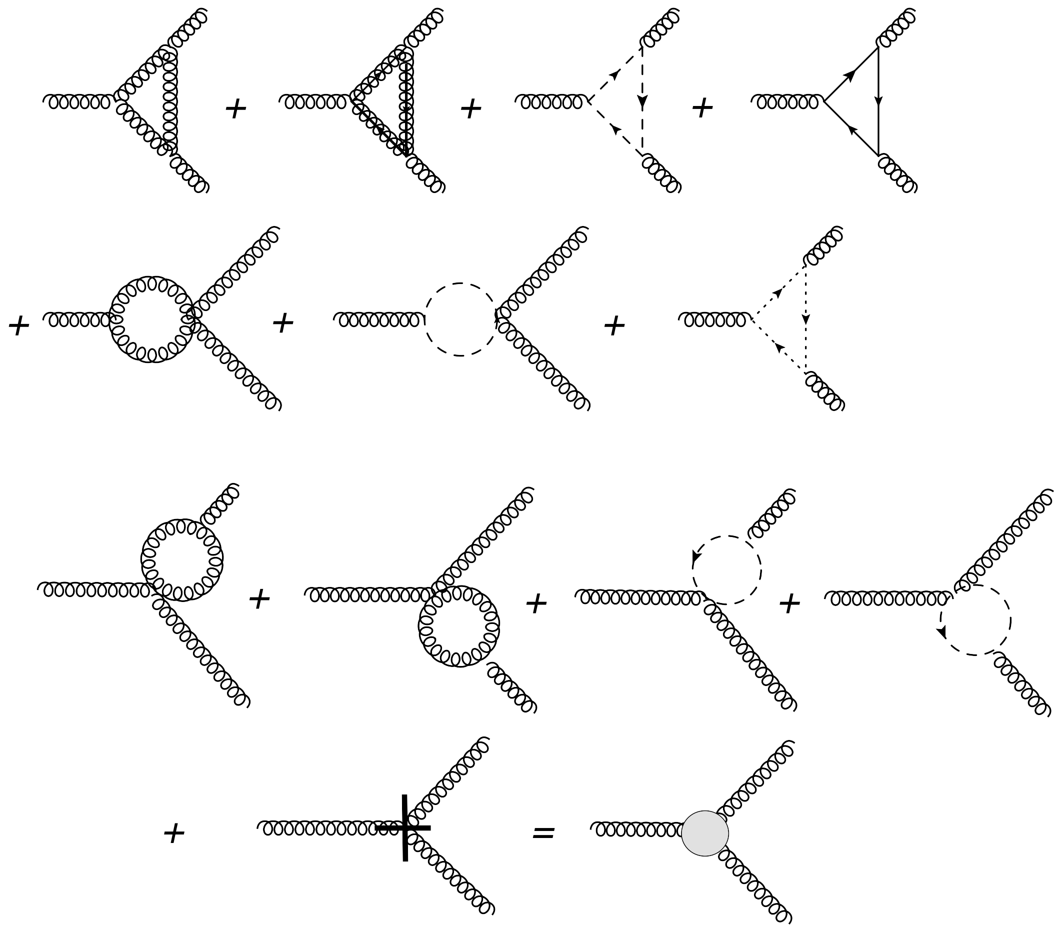

Figure 5.5.: The three-gluon corrections produce thousands of lines of code. However, they build a direct sum of Standard Model and SUSY diagrams that must be separately convergent. The pure gluon loops cancel with the ghost-loop - they are untouched from the counterterm. Some rotational invariances simplify the abundance of diagrams.

We encounter gauge fixing again at next-to-leading order (Fig. 5.6).

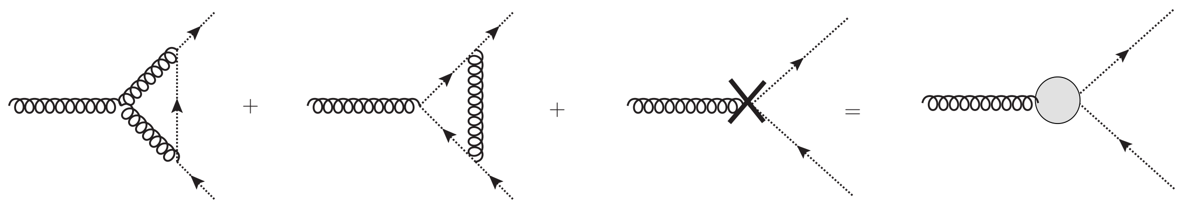

Figure 5.6.: Gauge invariance demands ghost in the final state, exchanging a gluon as well as two virtual gluons decaying into ghosts.

In analogy to the tree level, we have to consider both possibilities of the ghost-anti-ghost creation (antiparticle can be created above and below the virtual gluon). This enlarges the number of diagrams by a factor two. The scalar topology of our incoming squarks is a bit easier to handle. Nonetheless, there is a considerable amount of corrections, shown in Fig. 5.7.

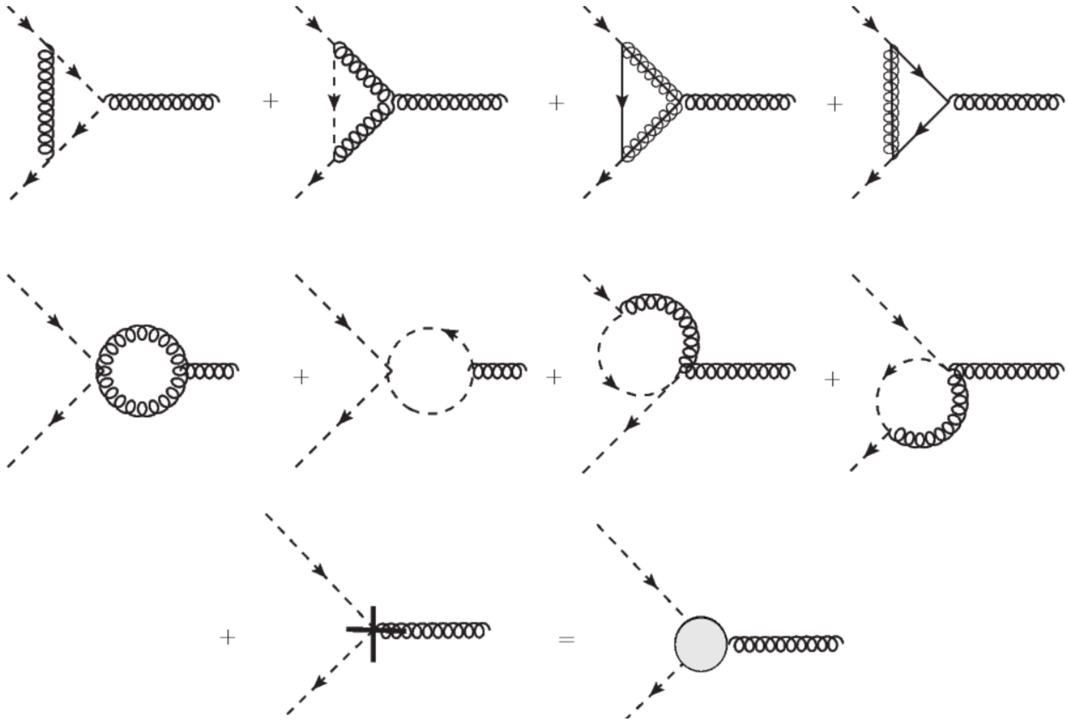

Figure 5.7.: These vertex corrections are of paramount importance as they appear in a fivefold manner within the tree level diagrams. They also appear in the process in [92], the results can be used for a cross-check.

One can easily check that every conceivable correction of the t- and u-channel can be extracted from the above-mentioned ones, where only the momenta and their direction as well as the particle masses have to be adapted. Additionally, the four-vertex involves diverse NLO contributions (Fig. 5.8)

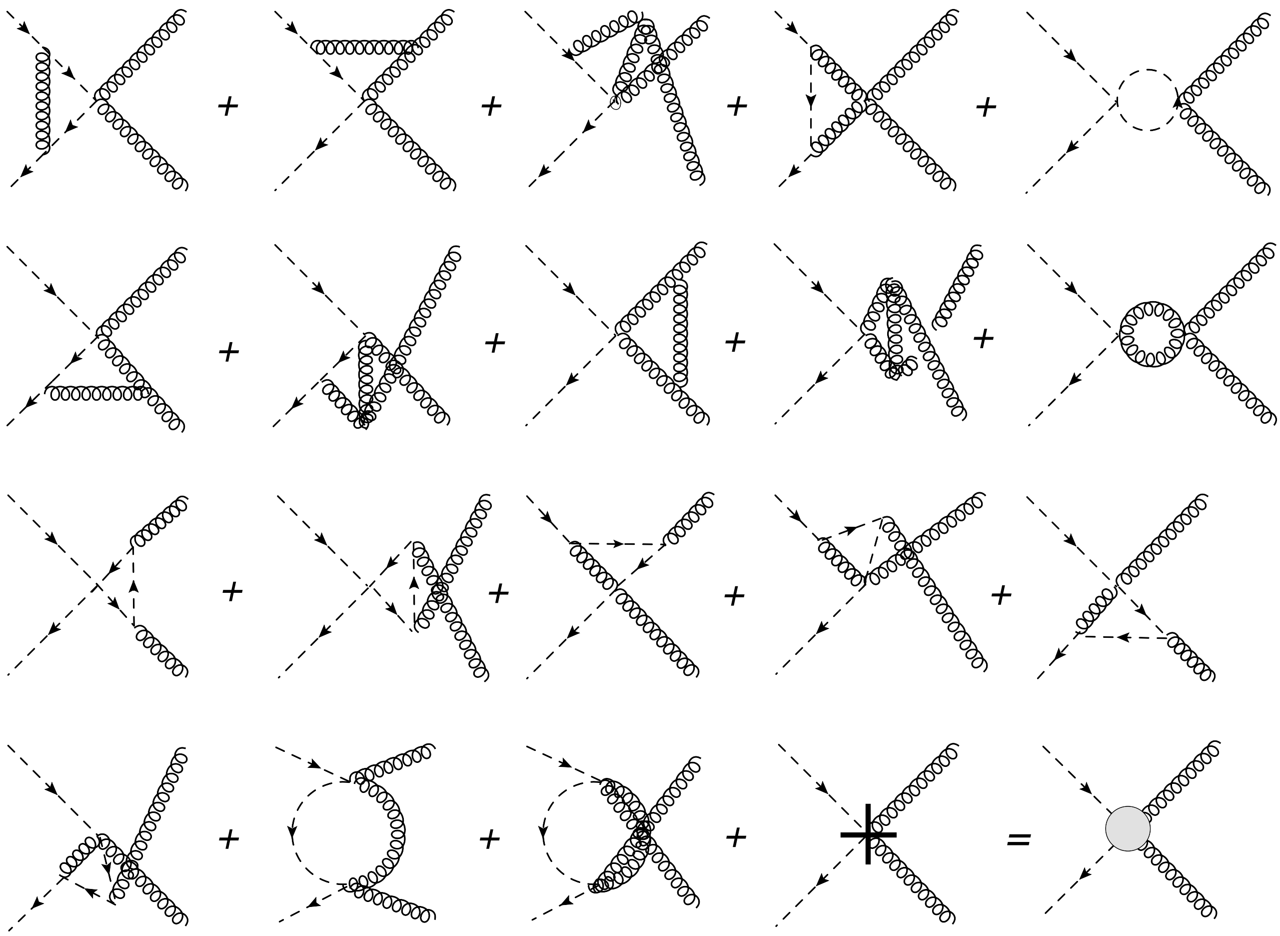

Figure 5.8.: The kinematical structure of all these diagrams is more or less simple. However, combinatorics and colour factors make life harder. Only a handful of diagrams are renormalised by the counterterm. One observes, for instance, that every loop containing two particles of the same kind are cancelled by those that have three particles of this kind (only concerning the poles).

Last, but not least: Box diagrams entail longer calculations due to the four internal particles and vertices. Therefore, every result is given in the appendix in order to keep the main part of the thesis in a limited scale.

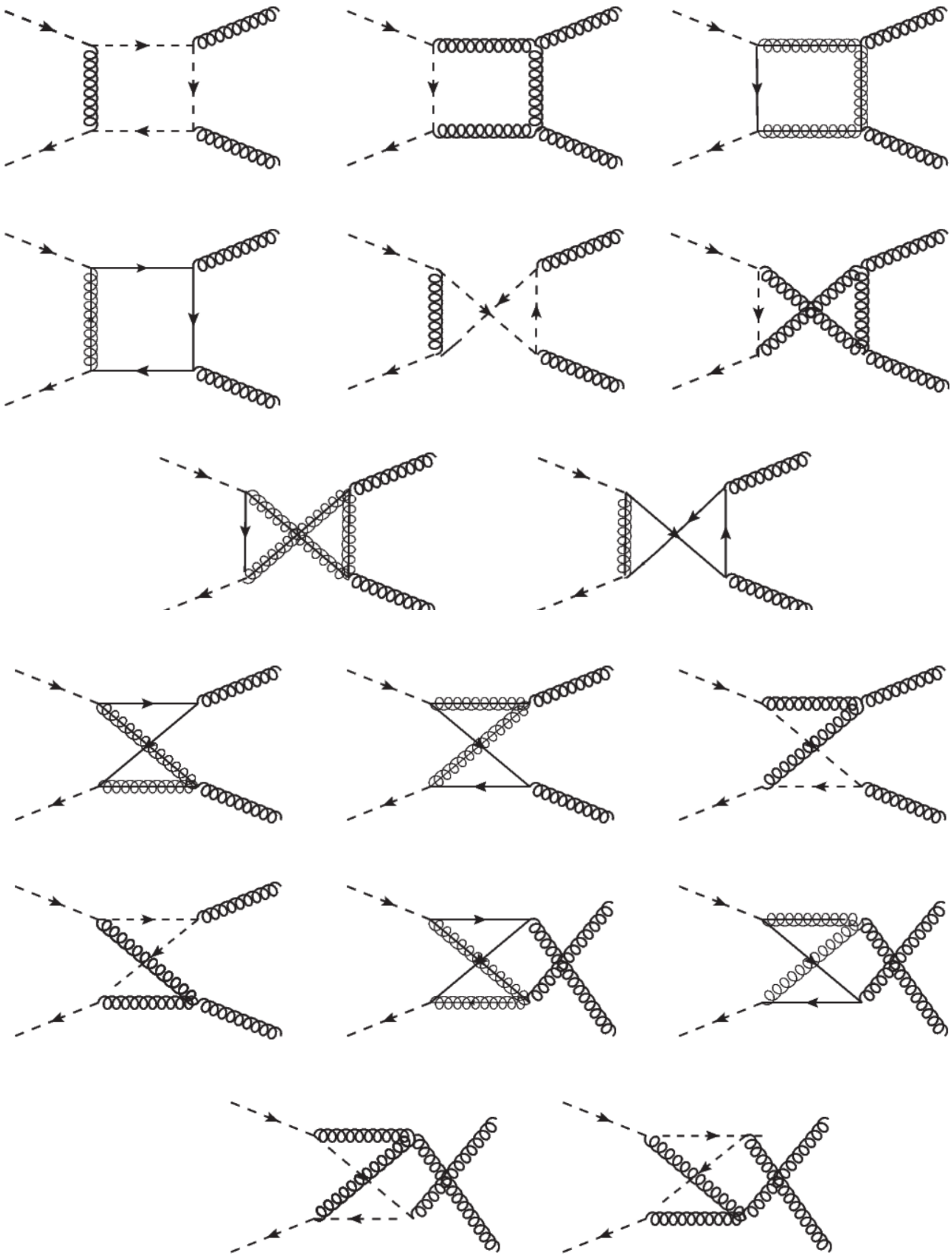

Figure 5.9.: The boxes do not need any counterterm. Power-counting theorems tell us that no pole survives.

The u-channel-like boxes can be evaluated via the simple interchange $k_1 \leftrightarrow k_2$. Luckily, box diagrams are convergent as a whole. There remain two additional NLO corrections due to the Fadeev-Popov ghosts in Fig. 5.10 (of course again containing both flows of the outgoing ghosts, so in fact four boxes):

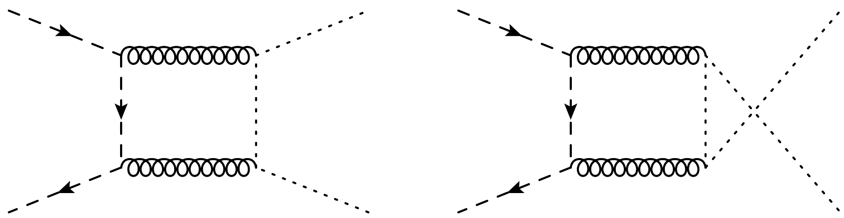

Figure 5.10.: The last virtual corrections are box diagrams with ghosts in the final stat. Both directions have to be calculated.

We will construct the explicit counterterms to renormalise the vertex corrections in the appendix. This subsection needs a further remark as this process contains the following danger: To forget taking into account non-trivial symmetry factors of our NLO diagrams. In a perturbative expansion of correlation functions, one performs in fact a camouflaged evaluation of expressions like

$$T\left\{\exp\left[\int_{\tilde{t}}^{t} H_I(s)ds\right]\right\} \tag{5.21}$$

by Wick contractions. T stands for a time-ordered product of field operators, H_I means the interaction Hamiltonian derived from the Lagrangian of the field theory. Expanding (5.22) explicitly is a quite lengthy and, in the most cases, unnecessary work as the construction of Feynman diagrams like above perfectly works only using Feynman rules. These rules are constructed in a way that, hopefully, no symmetry factor unequal to 1 occurs. This probably holds for 95 percent of cross section calculations. However, this is not the case for the current process, so we have to make use of [53]

Wick's Theorem (1950): *The time-ordered product of arbitrarily many field operators can be expressed as their normal ordering added to all possible contractions of the field operators.*

Normally, this theorem is introduced for scalar field theories and, possibly, fermions. In [54], a way is developed to determine symmetry factors also in QCD and other complicated field theories (the results can be extended to SUSY-QCD). We will now briefly carry out such a procedure for one diagram. All symmetry factors will be given directly in the loop amplitudes in Appendix D. Exemplary, we investigate the gluon loop from the 3-gluon topology:

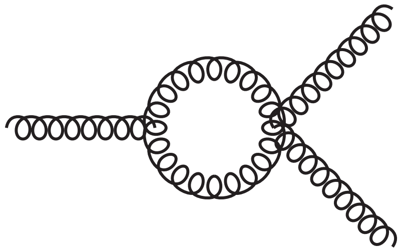

In this case we have to expand $\mathcal{L}_{3g} + \mathcal{L}_{4g}$ up to order $\mathcal{O}(g_s^3)$ and take the mixing term of the binomial in the second order of the Taylor series:

$$\langle 0|2 \cdot A(x)A(y)A(z)\frac{i^2}{2! \cdot 3! \cdot 4!}\int d^4wA^4(w)\int d^4vA^3(v)|0\rangle \tag{5.22}$$

x, y, z denote the on-shell gluons, we integrate over the two gluon fields in the loop. In this equation we used that the Lagrangian densities can be written in such a way, that the vector fields are treated as scalars:

$$\mathcal{L}_{3g} = f^{abc} \times [kinematics] \times \frac{g_s}{3!}[A^a_\mu A^b_\nu A^c_\sigma] \tag{5.23}$$

$$\mathcal{L}_{4g} = [kinematics, colour] \times \frac{g_s^2}{4!}[A^a_\mu A^b_\nu A^c_\sigma A^d_\tau] \tag{5.24}$$

It solely remains to perform the contraction of the gluon fields and to count every combinatorial factor for the contraction of indistinguishable virtual fields. With three ways to contract $A(x)$ and $A(v)$ (two remaining $A(v)$) and four to contract $A(y)$ and $A(w)$, therefore three to contract $A(z)$ and $A(w)$, we end up with the loop contraction of $A^2(v)$ and $A^2(w)$ leading to another factor of 2. Thus, we have $72/144 = 1/2$ as our combinatorial factor. Including (Majorana) fermions is a bit more involved, but the techniques are the same.

5.2.3. Real Emissions

Already at first sight, the structure of our LO diagrams provides an insight into the numerous possibilities of emitting a gluon or gluons decaying into quark pairs. Applying SUSY Feynman rules shows the number of additional diagrams that all have to be interfered with each other:

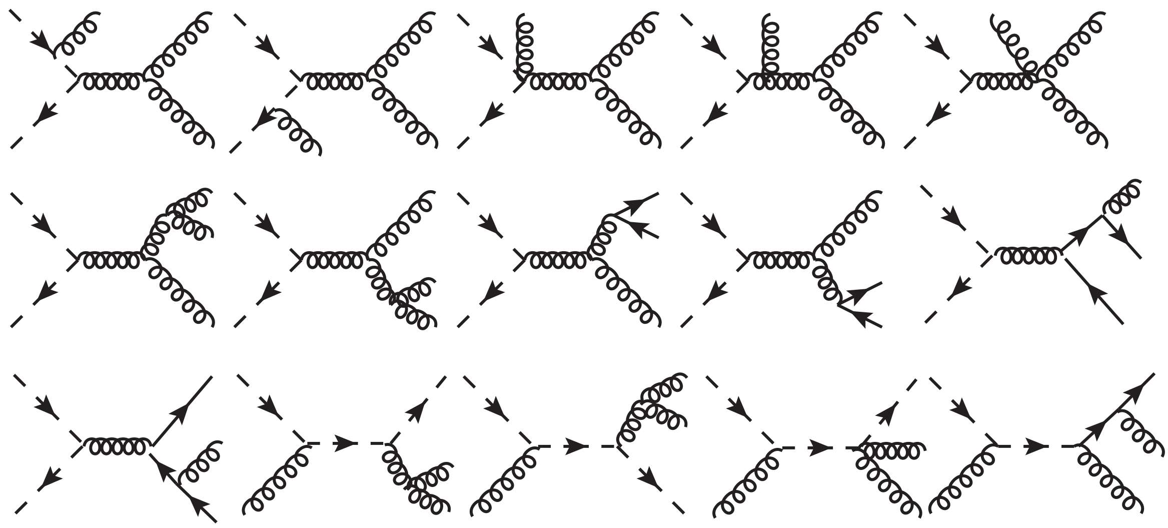

Figure 5.11.: Real corrections to the s-channel (we ignore gauge fixing diagrams).

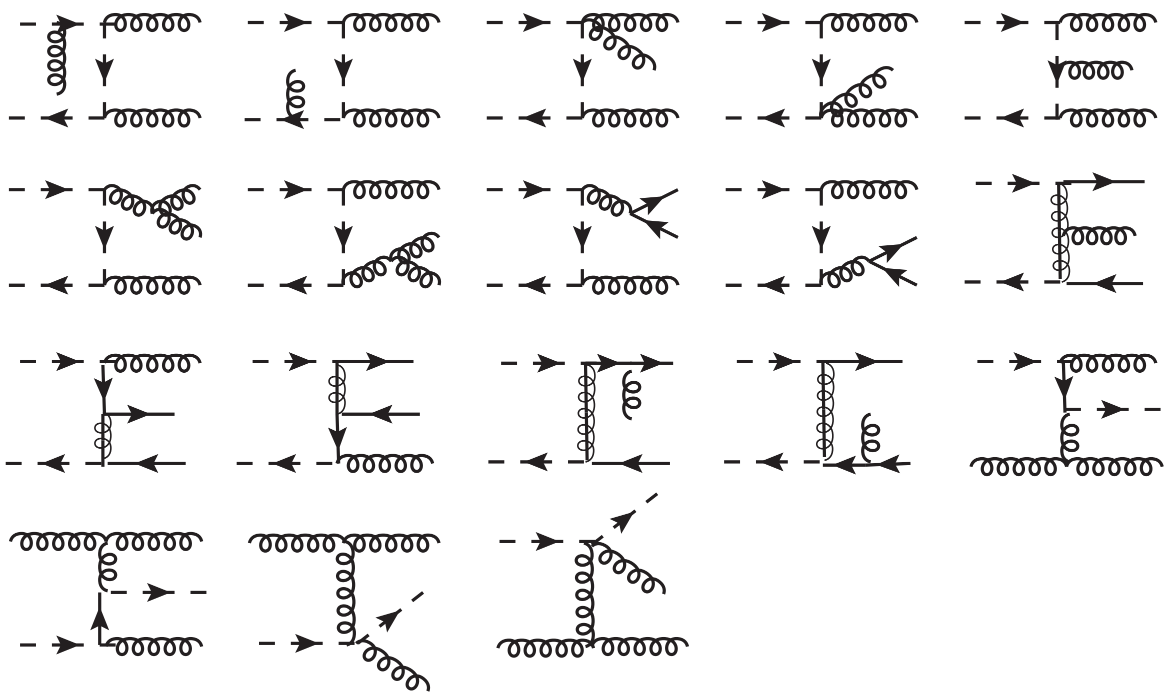

Figure 5.12.: Real corrections to the t-channel, the same structures naturally occur within the u-channel.

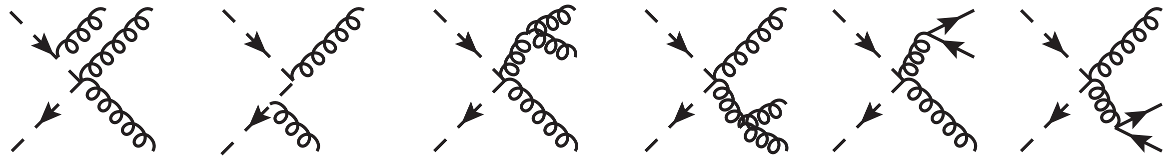

Figure 5.13.: Real corrections to the four vertex.

Once again, we encounter ghosts for gauge fixing reasons. The multitude of additional diagrams is omitted in this section. There are two main difficulties being a hindrance to complete the entire NLO calculation within this thesis. The first one is simply the fact that treating every diagram is too time-consuming for this work. To work out every interference properly, a huge effort of automatisation is needed. The second is more problematic: In general, there exist two ways of performing $2 \to 3$ phase space integrations in order to get an infrared finite result: The *phase space slicing* method as well as the *dipole subtraction* method (s.a. Chapter 6). We will explain, why the latter one is favourable. But currently, the framework for processes with initial scalars is not developed.

5.2.4. Constructing the Total Cross Section

At the moment we just have shown the corrections to the tree level themselves, but not how to deal with them in order to get our object of desire: An UV- and IR-convergent cross section at next-to-leading order. Adding the virtual corrections we showed before means effectively nothing than changing the coupling constants of the vertices: Having in mind the Born cross section contributions

$$|\mathcal{M}_{s+gh} + \mathcal{M}_t + \mathcal{M}_u + \mathcal{M}_4|^2 \tag{5.25}$$

it becomes clear what has to be done at NLO: Every vertex correction carries, in comparison to the tree level vertex factor, an additional factor of g_s^2 or rather α_s, so we get the next contribution of the perturbative series going with α_s^n. To stay at this order - one order higher than the Born cross section - we cannot simply plug in every corrected vertex into the tree level expressions, but for every squared amplitude just one correction. Consider for instance the term $|\mathcal{M}_s^{LO}|^2$: We have now the possibilities of inserting the corrected left or right vertex (2-squark-gluon or 3-gluon vertex) for *one* of the amplitudes. The UV-divergent parts are always proportional to the tree level amplitude, so we are able to use the factorisation $|\mathcal{M}_s^{LO}|^2 \times (\mathcal{A}_{2\tilde{q}g}^{UV-div} + \delta_{2\tilde{q}g} + \mathcal{A}_{3g}^{UV-div} + \delta_{3g})$. We add the counterterms arising from the propagator corrections for the respective vertex that should cancel every divergent Δ-term in the Passarino-Veltman integrals (see App. D). One might ask what happened to the rest of the vertex corrections being ultraviolet safe: Unfortunately, these contributions to the complete NLO calculation have a different kinematical structure compared to the tree level amplitudes. Therefore, every possible structure has to be treated in a separately calculated amplitude.

To get an overview of all vertex corrections inserted into the amplitudes, we first consider the s-channel (the indices l, r denote the corrected left and right vertex):

$$|\mathcal{M}_s^{l,r}\mathcal{M}_s| + |\mathcal{M}_s^{l,r}\mathcal{M}_t| + |\mathcal{M}_s^{l,r}\mathcal{M}_u| \tag{5.26}$$

$$|\mathcal{M}_{gh1}^{l,r}\mathcal{M}_{gh1}| + |\mathcal{M}_{gh2}^{l,r}\mathcal{M}_{gh2}| \tag{5.27}$$

Naturally, the 4-vertex has only one possible correction:

$$|\mathcal{M}_4^{corr.}\mathcal{M}_4| + |\mathcal{M}_4^{corr.}\mathcal{M}_t| + |\mathcal{M}_4^{corr.}\mathcal{M}_u| \tag{5.28}$$

We found during the colour decomposition that no interference with the s-channel is allowed. It becomes more complicated in case of the t- and u-channel (the indices a, b stand for the above and below corrected vertex):

$$|\mathcal{M}_t^{a,b}\mathcal{M}_t| + |\mathcal{M}_t^{a,b}\mathcal{M}_u| + |\mathcal{M}_t^{a,b}\mathcal{M}_4| + |\mathcal{M}_t^{a,b}\mathcal{M}_s| \tag{5.29}$$

$$|\mathcal{M}_u^{a,b}\mathcal{M}_u| + |\mathcal{M}_u^{a,b}\mathcal{M}_t| + |\mathcal{M}_u^{a,b}\mathcal{M}_4| + |\mathcal{M}_u^{a,b}\mathcal{M}_s| \tag{5.30}$$

One should keep in mind that these contributions only contain the virtual corrections at the vertices. Additionally, the propagator corrections have to be filled in, performing the same procedure. The gluon propagator from the s-channel also has factorisable corrections; its divergences are absorbed by the counterterm δZ_g: $|\mathcal{M}_s^{LO}|^2 \times (\Pi_g + \delta Z_g)$. The same has to be done for every possible interference. Furthermore, every box B_i can be interfered with every leading order diagram:

$$|\left(\sum_{i=1}^{6} B_i\right) \cdot \mathcal{M}_{s,t,u,4}| \tag{5.31}$$

Ghosts are interfered separately: $|(B_7 + B_8) \cdot \mathcal{M}_{gh}|$.

Be aware of a global factor 2 in front of the interferences. It remains the treatment of the infrared divergences, absorbed by the real emissions. The Cutcosky rules for cutting Feynman diagrams show the effect of adding the real corrections diagrammatically (s.a. [41]). Afterwards, the whole process is free of divergences, a goal that cannot be achieved within this thesis. To get a sense what the treatment of the real emissions will be about and to describe first results in developing a formalism to treat massive initial scalars, we wrote Chapter 6.

Although conventions and notations are completely different, we emphasize the existence of [55]. Martin and Younkin describe the SUSY-QCD corrections to the stoponium decay into hadrons and photons precisely since they explicitly give every appearing ultraviolet and infrared pole. The corrections to the incoming stops should be comparable and useful for further calculations and checks. This recommendation brings this chapter to an end.

6. Developing the Dipole Subtraction Formalism

After having spent much time in the infinite-momentum regime, we now turn to the low energy (*soft* singularities) and small-angle (*collinear* singularities) regions in phase space. To get rid of these infrared poles (occurring in both the virtual and real corrections), two main methods have been developed over the last decades - *phase space slicing* and *dipole subtraction*. They have in common that the analytical calculations are solely performed in a minimal region in phase space, namely in the vicinity of the IR poles. As these calculations are separated from the whole process, they can be worked out in a generic, process-independent form. Roughly speaking, one carries out the phase space integration once and for all. Phase space slicing is indeed a suitable name for the procedure - one simply truncates the phase space in such a way that all soft regions can be reduced to an integral of the form (consider $2 \to 3$ processes with involved particles a and b and the radiated one carrying the momentum k)

$$I_{ab} = \int_{|\vec{k}|<\Delta E} \frac{d^3k}{2k^0} \frac{2(a.b)}{(k.a)(k.b)} \tag{6.1}$$

with a small cutoff energy of the radiated particle ΔE. The numerical integration is carried out down to the cutoff value needing much CPU time in the singular limit $\Delta E \to 0$. Subsequently, one has to check the global independence of the result from the arbitrarily chosen cutoff value. To avoid such singular numerical integrations, the dipole subtraction formalism seems favourable. The long-standing experience with the implementation of other processes of *DM@NLO* supports this assumption. There exist different formalisms by Catani and Seymour [56,57] for NLO-QCD and for massive fermions by Dittmaier [58] (we follow the latter one). Unfortunately, NLO corrections have been interesting up to now mostly in collider calculations. Initial scalar (massive) particles have not been considered yet as they naturally do not occur in these experiments. We introduce the general approach to eliminate the poles and translate the methods for massive fermions to massive initial scalars afterwards.

6.1. On the General Concept of Dipole Subtraction

Following the notations in [58], we introduce $\mathcal{M}_1$ as the transition matrix element of a process involving a radiated photon/gluon. Without radiation, it is reduced to $\mathcal{M}_0$. They have the corresponding phase space measures $d\Phi_{1,0}$. Due to finite, non-zero masses of the initial squarks, we focus on the soft region ($k \to 0$), where logarithmic IR singularities appear. We obtain an asymptotic proportionality of the upper squared matrix element allowing for a factorisation. The additional prefactor of $|\mathcal{M}_0|^2$ is an auxiliary function that we will call $g_{\alpha\beta}^{(sub)}$, containing the belonging splitting function. The first Greek index denotes the particle that will give birth to infrared singularities (*emitter*, initial or final), the second denotes the uninvolved *spectator* (initial or final). The four combinations cover every thinkable emission process. In Fig. 6.1 the processes of interest are shown diagrammatically. The crucial step is now to add a cumbersome zero, called

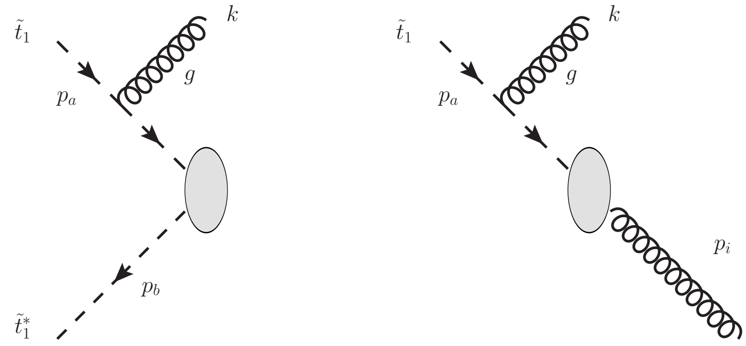

Figure 6.1.: The real corrections to $\tilde{t}_1\tilde{t}_1^* \to gg$ contain initial scalar gluon emitters with initial (left, $g_{ab}^{(sub)}$) and final (right, $g_{ai}^{(sub)}$) spectators. All momenta go from left to the right.

the subtraction function $\mathcal{M}_{sub}$:

$$\int d\Phi_1 \sum_{\lambda_g} |\mathcal{M}_1|^2 = \int d\Phi_1 \Bigg(\sum_{\lambda_g} |\mathcal{M}_1|^2 - |\mathcal{M}_{sub}|^2 \Bigg) + |\mathcal{M}_{sub}|^2 \tag{6.2}$$

It is parametrised by Φ_1 and has the same asymptotic behaviour of the squared $2 \to 3$ matrix, meaning $|\mathcal{M}_{sub}|^2 \propto \sum_{\lambda_g} |\mathcal{M}_1|^2$ for $\lim_{k\to 0}$ or $\lim_{p_a k \to 0}$ (the sum over λ_g denotes the summation over the gluon's polarisation states). Thus, the non-singular difference in the equation from above can be handled numerically. The singular limit, instead, can be integrated analytically, if $\mathcal{M}_{sub}$ is appropriately chosen. We note that the factorisation

$$\int d\Phi_1 = \int d\tilde{\Phi}_0 \otimes \int [dk] \tag{6.3}$$

with the photon/gluon phase space $\int [dk]$ is valid, where $\otimes$ may indicate a non-trivial product (e.g. convolution). As mentioned before, $\int [dk] |\mathcal{M}_{sub}|^2$ can now be calculated generically and is applicable to every process of this kind. Altogether, the expression

$$\boxed{\int d\Phi_1 \sum_{\lambda_g} |\mathcal{M}_1|^2 = \int d\Phi_1 \Bigg(\sum_{\lambda_g} |\mathcal{M}_1|^2 - |\mathcal{M}_{sub}|^2 \Bigg) + \int d\tilde{\Phi}_0 \otimes \left(\int [dk] |\mathcal{M}_{sub}|^2 \right)} \tag{6.4}$$

contains a non-singular Φ_1 space and a single-gluon/photon phase space integration, somehow entangled with the space $\tilde{\Phi}_0$ of the non-radiative process - responsible for the remaining poles within the virtual corrections.

6.2. Real Emissions of Massive Initial Scalars

[57] provides a suitable framework to work out the dipole formulae for massive initial scalars in analogy to the fermionic case. Naturally, a couple of changes have to be considered - we exclude any spin flips, the splitting function differs for scalar emitters, the colour flow must be adapted. The latter one can be factorised from all operations in phase space. Luckily, the convenient phase space parametrisation of [57] does not lose its validity. For completeness, the calculation of the single-gluon and $2 \to 3$ phase space integrals has to be performed for both initial and final spectators leading to lengthy expressions comparable with gluon radiation off fermions. We are convinced that our dipole formulae for the $2 \to 3$ phase space have equivalent, but shorter brothers, but in principal, we present a possible technique how to solve the non-trivial integrals. In case of final spectators, perhaps another strategy has to be developed. We give a warning that this part of the thesis shall rather yield inspirations and hints. It does not contain reliable, checked results - a complete derivation of the dipole formulae is beyond the scope of this work. But the following insights may support the final steps.

6.2.1. Initial Emitter and Spectator

We begin with the left process of Fig. 6.1 by giving the proportionality factor of the matrix elements in the asymptotic limits, namely the auxiliary function

$$\boxed{g_{ab}^{(sub)} = \frac{1}{(p_a k) x_{ab}} \left[\frac{2}{1 - x_{ab}} - 2 - \frac{x_{ab} m_a^2}{p_a k} \right] = \frac{1}{(p_a k) x_{ab}} \left[P_{q\tilde{q}}(x_{ab}) - \frac{x_{ab} m_a^2}{p_a k} \right]} \tag{6.5}$$

with the splitting function $P_{q\tilde{q}}(x_{ab})$. We abbreviate

$$x_{ab} = \frac{p_a p_b - p_a k - p_b k}{p_a p_b} \qquad y_{ab} = \frac{p_a k}{p_a p_b} \tag{6.6}$$

and

$$P_{ab} = p_a + p_b - k \qquad s = (p_a + p_b)^2 \qquad \bar{s} = s - m_a^2 - m_b^2 \tag{6.7}$$

The asymptotic behaviour can be characterised via the following limits:

$$\lim_{p_a k \to 0} x_{ab} = \frac{p_a^0 - k^0}{p_a^0} \qquad \lim_{k \to 0} x_{ab} = 1 \qquad \lim_{p_a k \to 0} y_{ab} = 0 \qquad \lim_{k \to 0} y_{ab} = 0 \tag{6.8}$$

The integrand is therefore determined, we are now interested in the parametrised phase space (derivation: see [58]). With an auxiliary parameter x, we define the convolution with the single-gluon phase space as follows:

$$\int_{x_0}^{x_1} dx \int d\phi(\tilde{P}_{ab}(x); \tilde{p}_a(x) + p_b) \times \left(\frac{1}{4(2\pi)^3} \frac{\bar{s}^2}{\sqrt{\lambda_{ab}}} \int_{y_1(x)}^{y_2(x)} dy_{ab} \int_0^{2\pi} d\varphi \right) \tag{6.9}$$

λ_{ab} denotes the Källen function with the arguments

$$\lambda(s, m_a^2, m_b^2) = s^2 + m_a^4 + m_b^4 - 2m_a^2 m_b^2 - 2m_a^2 s - 2m_b^2 s\,. \tag{6.10}$$

After parametrisation, the original momenta are mapped to $\tilde{p}_a^\mu(x)$ and $\tilde{P}_{ab}^\mu(x)$ still fulfilling the mass-shell relations:

$$\tilde{p}_a^\mu(x) = R_{ab}(x)\left(p_a^\mu - \frac{\bar{s}}{2m_b^2}p_b^\mu\right) + \frac{\bar{s}x + m_g^2}{2m_b^2}p_b^\mu \qquad \tilde{P}_{ab}^\mu(x) = \tilde{p}_a^\mu(x) + p_b^\mu \tag{6.11}$$

with, for the sake of brevity:

$$R_{ab}(x) = \sqrt{\frac{(\bar{s}x + m_g^2)^2 - 4m_a^2 m_b^2}{\lambda_{ab}}} \tag{6.12}$$

Using the definition below, we can perform the first y-integration over the auxiliary function $g_{ab}^{(sub)}$ leading in the end to elementary integrals (the previous angle integration leads to a trivial prefactor of 2π).

$$\mathcal{G}_{ab}^{(sub)}(s,x) = \frac{x\bar{s}^2}{2\sqrt{\lambda_{ab}}}\int_{y_1(x)}^{y_2(x)} g_{ab}^{(sub)}(p_a, p_b, k)dy_{ab} \tag{6.13}$$

$$y_{1,2}(x) = \frac{\bar{s} + 2m_a^2}{2s}(1-x) \mp \frac{\sqrt{\lambda_{ab}}}{2s}\sqrt{(1-x)^2 - \frac{4m_g^2 s}{\bar{s}^2}} \tag{6.14}$$

We multiply the splitting function with $\frac{2p_a p_b}{\bar{s}}$ (first and second term) and with $\frac{\bar{s}^2}{\bar{s}^2}$ for the last and obtain

$$\boxed{\mathcal{G}_{ab}^{(sub)}(s,x) = \frac{\bar{s}}{\sqrt{\lambda_{ab}}}\left[\frac{2x}{1-x}\ln\left(\frac{y_2(x)}{y_1(x)}\right) + \frac{2m_a^2 x}{\bar{s}}\left(\frac{1}{y_2(x)} - \frac{1}{y_1(x)}\right)\right].} \tag{6.15}$$

We completed a main step - the single-gluon phase space integration is already done. $\mathcal{G}_{ab}^{(sub)}(s,x)$ will occur in the treatment of infrared poles in virtual corrections. The +-distribution allows for a harmless treatment of $x \to 1$:

$$\int_0^1 \frac{f(x)}{[1-x]_+}dx = \int_0^1 \frac{f(x) - f(1)}{(1-x)}dx \tag{6.16}$$

The y-integration boundaries yield the maximal value of x:

$$x_0 \geq \frac{2m_a m_b - m_g^2}{\bar{s}} \qquad x_1 = 1 - \frac{2m_g\sqrt{s}}{\bar{s}} \tag{6.17}$$

The kinematical lower bound x_0 is explained in [58]. An artificial gluon mass m_g was introduced in order to regularise the singularities analogously to dimensional regularisation. Under certain circumstances, this regulator is not needed any more: We split the x-integration as presented in [58]

$$\int_{x_0}^{1-\epsilon} dx\, \mathcal{G}_{ab}^{(sub)}(s,x) + \int_{1-\epsilon}^{x_1} dx\, \mathcal{G}_{ab}^{(sub)}(s,x) \tag{6.18}$$

with an infinitesimal ϵ. This trick simplifies the integration enormously: In the vicinity of x_1 we can set every x in non-singular terms to 1, whereas, in the remaining region, $m_g = 0$ is possible without producing singularities. This provides

$$\ln\left(\frac{y_2(x)}{y_1(x)}\right) = \ln\left(\frac{\bar{s} + 2m_a^2 + \sqrt{\lambda_{ab}}}{\bar{s} + 2m_a^2 - \sqrt{\lambda_{ab}}}\right) =: \ln(d_1)\,. \tag{6.19}$$

One can furthermore show that

$$\frac{m_a^2}{\sqrt{\lambda_{ab}}}\left(\frac{2s}{\bar{s} + 2m_a^2 + \sqrt{\lambda_{ab}}} - \frac{2s}{\bar{s} + 2m_a^2 - \sqrt{\lambda_{ab}}}\right) = 1 \tag{6.20}$$

holds. Therefore, some easy substitutions lead to:

$$\int_{x_0}^{1-\epsilon} dx\, \mathcal{G}_{ab}^{(sub)}(s,x) = 2 \cdot \left(\frac{\bar{s}\ln(d_1)}{\sqrt{\lambda_{ab}}} + 1\right)[\ln(\epsilon) - \ln(1-x_0) - \epsilon + (1-x_0)] \tag{6.21}$$

We are now interested in the vicinity of x_1: Inserting this upper boundary will lead to logarithmic mass singularities. Cancelling the roots in $y_{1,2}(x)$ is not self-explanatory any more - the integration becomes fairly non-trivial. We follow another path than in [58] - for the scalar splitting function this ansatz seems reasonable. Nevertheless, the mathematical structure can be reproduced - we obtain polylogarithms, too. The desired transformation of the y boundaries in the logarithm $\ln(au \pm b\sqrt{u^2 - c^2})$, $u = 1 - x$, shall lead to one generic integral

$$\int x^m \ln(\alpha x + \beta) dx \tag{6.22}$$

with $m \in \mathbb{R}$. We found that

$$u = \frac{c\eta}{\sqrt{2\eta - 1}} \qquad \frac{du}{d\eta} = c\frac{\eta - 1}{(2\eta - 1)^{\frac{3}{2}}} \tag{6.23}$$

cancels the roots within the logarithm after a few steps. We work out the transformation to (6.22) explicitly (using $\eta = (z+1)/2$):

$$\frac{\bar{s}}{2\sqrt{\lambda_{ab}}} \int dz \ln\left(\frac{a \pm b}{2} z + \frac{a \mp b}{2}\right) \cdot \left(-\frac{c}{\sqrt{z}} + \frac{c}{\sqrt{z}^3} - \frac{4}{z+1} + \frac{2}{z}\right) \tag{6.24}$$

We solve these four terms with generalised hypergeometric functions

$${}_pF_q(a_1, ..., a_p; b_1, ..., b_q; z) = \sum_{k=0}^{\infty} \prod_{i=1}^{p} \frac{\Gamma(k + a_i)}{\Gamma(a_i)} \prod_{j=1}^{q} \frac{\Gamma(b_j)}{\Gamma(k + b_j)} \frac{z^k}{k!} \tag{6.25}$$

and Eulerian dilogarithms $\mathrm{Li}_2(z)$ (definition to be found in App. D) [59]:

$$\begin{aligned}\frac{\bar{s}}{2\sqrt{\lambda_{ab}}}\sum_{i=1}^{2}(-1)^i\times\Bigg[&2c\sqrt{z}\ln(\xi_i z+\gamma_i)+\frac{4}{3}\frac{z^{3/2}\xi_i}{\gamma_i}c_2F_1\left(1,\frac{1}{2};\frac{3}{2};-\frac{\xi_i z}{\gamma_i}\right)\\&+\frac{2c}{\sqrt{z}}\ln(\xi_i z+\gamma_i)+\frac{4z^{1/2}\xi_i}{\gamma_i}c_2F_1\left(1,-\frac{1}{2};\frac{1}{2};-\frac{\xi_i z}{\gamma_i}\right)\\&+4\ln(\gamma_i-\xi_i)\ln(z+1)+4\mathrm{Li}_2\left(\frac{\xi_i(z+1)}{\xi_i-\gamma_i}\right)+4\mathrm{Li}_2\left(\frac{\xi_i}{\xi_i-\gamma_i}\right)\\&-2\ln|\gamma_i|\ln|z|+2\mathrm{Li}_2\left(\frac{\xi_i z}{\gamma_i}\right)\Bigg]\end{aligned}$$

$$\xi_{1,2}=\frac{\bar{s}+2m_a^2\pm\sqrt{\lambda_{ab}}}{4s}\qquad \gamma_{1,2}=\frac{\bar{s}+2m_a^2\mp\sqrt{\lambda_{ab}}}{4s}\tag{6.26}$$

Their quotients (in the logarithms, induced by the upper sum) yield, by the way, d_1 or $1/d_1$. Plugging in the boundaries $2y(x_1-1)-1$ and $2y(-\epsilon)-1$ simplifies this expression by setting the gluon mass to zero, $m_g=0$, in non-singular terms - a procedure that should be performed carefully. The mathematical structure of the results in [58] can be rediscovered using

$$\mathrm{Li}_2(1-z)+\mathrm{Li}_2\left(1-\frac{1}{z}\right)=-\zeta(2)-\frac{\ln^2(-z)}{2}\,.\tag{6.27}$$

Like in [58], our mass-regularised subtraction formulae shall contain only logarithmic singularities. The translation into dimensional regularisation is performed with (s.a.: App. D)

$$\Delta_{IR}=\ln\left(\frac{\mu^2}{m_g^2}\right)\tag{6.28}$$

A few words dedicated to a simple implementation of special functions: With a lot of algebraic effort, one could transform the hypergeometric functions to dilogarithms in order to obtain a comparable result to [58] for fermions using

$$\mathrm{Li}_2(z)=z_3F_2(1,1,1;2,2;z)\tag{6.29}$$

Instead, we rather recommend an easy, quickly converging implementation of both ${}_2F_1$ functions the series, if needed:

$$\sum_{k=0}^{\infty}\frac{1}{2k+1}\left(\frac{-\xi_i z}{\gamma_i}\right)^k\qquad\sum_{k=-1}^{\infty}\frac{1}{2k+1}\left(\frac{-\xi_i z}{\gamma_i}\right)^{k+1}\tag{6.30}$$

by exploiting several relations of the Γ function. It interpolates the factorial, implying $\Gamma(z+1)=z\Gamma(z)$, and has the special values

$$\Gamma\left(n+\frac{1}{2}\right)=\frac{(2n-1)!!}{2^n}\sqrt{\pi}=\frac{(2n)!}{4^n n!}\sqrt{\pi}\qquad\Gamma\left(\frac{1}{2}\right)=\sqrt{\pi}\qquad\Gamma\left(-\frac{1}{2}\right)=-2\sqrt{\pi}\tag{6.31}$$

Due to different prefactors, the hypergeometric functions unfortunately do not cancel at all, but the series simplifies the upper expression. In App. E we comment on the convergence behaviour as it is of own interest (see coming chapter). The second part of the y-integrated splitting function (6.15), containing the boundaries $au \pm b\sqrt{u^2 - c^2}$, again with $1 - x =: u$, disappears after lengthy, but simple algebra. We make use of

$$\int dx \frac{\sqrt{x^2 - m}}{x^2 - n} \cdot x = \sqrt{x^2 - m} + \frac{(n - m) \arctan\left(\frac{\sqrt{x^2 - m}}{\sqrt{m - n}}\right)}{\sqrt{m - n}} \tag{6.32}$$

$$\int dx \frac{\sqrt{x^2 - m}}{x^2 - n} = \frac{(n - m) \arctan\left(\frac{\sqrt{nx^2 - mn}}{x\sqrt{m - n}}\right)}{\sqrt{mn - n^2}} + \frac{\ln(|\sqrt{x^2 - m} + x|) - \ln(|\sqrt{x^2 - m} - x|)}{2} \,. \tag{6.33}$$

Inserting the substituted boundaries reduces the integration to

$$\frac{\bar{s}}{\sqrt{\lambda_{ab}}} \int_{1-\epsilon}^{x_1} \frac{2m_a^2 x}{\bar{s}} \left(\frac{1}{y_2(x)} - \frac{1}{y_1(x)} \right) = \frac{m_a^2}{(s + 2m_a)^2 - \lambda_{ab}} \ln(|-1|) = 0 \,. \tag{6.34}$$

We refer to [58] how to achieve a numerically accessible form of the convoluted phase space integrals.

6.2.2. Initial Emitter and Final Spectator

Compared to this case, the dipole formulae of the previous section were of dreamlike shortness. Welcome to the jungle of abbreviations - we start with kinematics:

$$P_{ia} = p_i + k - p_a \qquad \bar{P}_{ia}^2 = P_{ia}^2 - m_a^2 - m_i^2 - m_g^2 \qquad \lambda_{ia} = \lambda(P_{ia}^2, m_a^2, m_i^2) \tag{6.35}$$

$$R_{ia}(x) = \frac{\sqrt{(\bar{P}_{ia}^2 + 2m_a^2 x)^2 - 4m_a^2 P_{ia}^2 x^2}}{\sqrt{\lambda_{ia}}} \tag{6.36}$$

$$r_{ia}(x) = 1 + \frac{\bar{P}_{ia}^2(\bar{P}_{ia}^2 + 2m_a^2)}{\lambda_{ia}} \frac{1 - x}{x} \tag{6.37}$$

The momenta in the case of final spectators (or vice versa) shall be expressed as

$$x_{ia} = \frac{p_a p_i + p_a k - p_i k}{p_a p_i + p_a k} \qquad z_{ia} = \frac{p_a p_i}{p_a p_i + p_a k} \,. \tag{6.38}$$

Again, we can give the asymptotic behaviour:

$$\lim_{k \to 0} x_{ia} = 1 \qquad \lim_{p_a k \to 0} x_{ia} = \frac{p_a^0 - k^0}{p_a^0} \qquad \lim_{p_i k \to 0} x_{ia} = 1 \tag{6.39}$$

$$\lim_{k \to 0} z_{ia} = 1 \qquad \lim_{p_a k \to 0} z_{ia} = 1 \qquad \lim_{p_i k \to 0} z_{ia} = \frac{p_i^0}{p_i^0 + k^0} \tag{6.40}$$

The structure of phase space parametrisation is fairly similar to the previous case. The following convolution

$$\int_{x_0}^{x_1} dx \int d\phi(\tilde{p}_i(x), p_b - P_{ia}; \tilde{p}_a(x) + p_b) \frac{1}{4(2\pi)^3} \frac{\bar{P}_{ia}^4 \rho_{ia}(\bar{s})}{\sqrt{\lambda_{ia}} R_{ia}(x) x^2} \int_{z_1(x)}^{z_2(x)} dz_{ia} \int_0^{2\pi} d\varphi_g \quad (6.41)$$

together with redefined momenta

$$\tilde{p}_a^\mu(x) = \frac{1}{R_{ia}(x)} \left(x p_a^\mu + \frac{\bar{P}_{ia}^2 + 2m_a^2 x}{2P_{ia}^2} P_{ia}^\mu \right) - \frac{P_{ia}^2 + m_a^2 - m_i^2}{2P_{ia}^2} P_{ia}^\mu \quad (6.42)$$

$$\tilde{p}_i^\mu(x) = \tilde{p}_a^\mu(x) + P_{ia}^\mu \quad (6.43)$$

and

$$\rho_{ia} = \sqrt{\frac{\lambda(\tilde{s}, m_a^2, m_b^2)}{\lambda(s, m_a^2, m_b^2)}} \qquad \tilde{s} = (\tilde{p}_a + p_b)^2 \quad (6.44)$$

is the basis of the coming integration procedure. A suitable definition for the single-gluon phase space integrated result is, for later purposes:

$$\mathcal{G}_{ai}^{(sub)}(P_{ia}^2, x_{ia}) = \frac{\bar{P}_{ia}^4}{2\sqrt{\lambda_{ia}} R_{ia}(x_{ia})} \int_{z_1(x_{ia})}^{z_2(x_{ia})} g_{ai}^{(sub)}(p_a, p_i, k) dz_{ai} \quad (6.45)$$

The integration boundaries, however, are this time quite lengthy.

$$z_{1,2}(x) = \frac{\bar{P}_{ia}^2[\bar{P}_{ia}^2 - x(\bar{P}_{ia}^2 + 2m_i^2)] \mp \sqrt{\bar{P}_{ia}^4(1-x)^2 - 4m_i^2 m_g^2 x^2} \sqrt{\lambda_{ia}} R_{ia}(x)}{2\bar{P}_{ia}^2[\bar{P}_{ia}^2 - x(\bar{P}_{ia}^2 - m_a^2)]} \quad (6.46)$$

Our last ingredient is of course again the auxiliary function in analogy to 6.5. We inserted the SUSY splitting function and obtained the expression

$$\boxed{g_{ai}^{(sub)}(p_a, p_i, k) = \frac{1}{(p_a k) x_{ia}} \left[\frac{2}{2 - x_{ia} - z_{ia}} - 2R_{ia}(x_{ia}) - \frac{x_{ia} m_a^2}{p_a k} \right]} \quad (6.47)$$

which provides after several elementary integrals:

$$\begin{aligned} \mathcal{G}_{ai}^{(sub)}(P_{ia}^2, x) = - \frac{\bar{P}_{ia}^2}{\sqrt{\lambda_{ia}} R_{ia}(x)} \Bigg\{ & \frac{2}{1-x} \ln\left(\frac{[1 - z_2(x)][2 - x - z_2(x)]}{[1 - z_1(x)][2 - x - z_1(x)]} \right) \\ & + 2R_{ia}(x) \ln\left(\frac{[1 - z_1(x)]}{[1 - z_2(x)]} \right) + \frac{2m_a^2 x^2}{\bar{P}_{ia}^2} \left[\frac{1}{1 - z_2(x)} - \frac{1}{1 - z_1(x)} \right] \Bigg\} \end{aligned} \quad (6.48)$$

The convolution, namely the x integration with the boundaries

$$x_0 > \frac{-\bar{P}_{ia}^2}{2m_a(m_a - \sqrt{P_{ia}^2})} \qquad 0 < \sqrt{P_{ia}^2} < m_a - m_i \quad (6.49)$$

$$x_1 = \frac{\bar{P}_{ia}^2}{\bar{P}_{ia}^2 - 2m_i m_g} = 1 - \frac{2m_i m_g}{|\bar{P}_{ia}^2|} + \mathcal{O}(m_g^2) \tag{6.50}$$

is performed with the same separation technique as in 6.2.1. Applying the methods from this subsection is possible, but would lead to an irresponsibly complicated term. Understanding the calculations of [58] (nonetheless, the fermionic result fills roughly one page) would at least shrink the result a bit. Thus, we cannot recommend using our methods for this case, so we only give the single-gluon phase space integrated dipole formula. A time-consuming retracing of S. Dittmaiers approach seems to be a reasonable way to obtain also a useful expression for scalars.

For the attentive reader, it did not remain a secret that also a gluon radiation directly from the squark-gluon vertex can occur. In this case, the determination of emitter and spectator is in vain. However, such an amplitude cannot produce both soft and collinear divergences - these finite terms will be added without having developed a dipole formula. Colour was a dominating topic during within the thesis. For the dipole formulae, we should not forget the colour flow as well.

6.2.3. On the Colour Flow

The previous subsections dealt with uncoloured initial scalars. In the underlying work, [58], the colour flow is not implemented (QED), but the author recommends the formalism of [56], explicitly worked out for a handful of cases, to formulate the colour flow for further cases analogously. We consider a (SUSY-)QCD process with $m = 1, 2, 3, ...$ final and additional initial (a, b,...) partons, described by an amplitude

$$\mathcal{M}_{m,a...}^{c_1,...,c_m,c_a,...;s_1,...,s_m,s_a...}(p_1, ..., p_m, p_a, ...)\,. \tag{6.51}$$

To explain the indices, let us construct a vector in colour and helicity space

$$\begin{aligned} |1, ..., m; a, ... >_{m,a,...} :=& \frac{1}{\sqrt{n_c(a)...}}(|c_1, ..., c_m; c_a, ... > \otimes |s_1, ..., s_m; s_a, ... >) \\ \times & \quad \mathcal{M}_{m,a...}^{c_1,...,c_m,c_a,...;s_1,...,s_m,s_a...}(p_1, ..., p_m, p_a, ...) \end{aligned} \tag{6.52}$$

with

$$|\mathcal{M}_{m,a...}|^2 = _{m,a,...}< 1, ..., m; a, ...||1, ..., m; a, ... >_{m,a,...} \ . \tag{6.53}$$

The helicity space is spanned by the particle's spin index s, whereas c denotes the colour index of every parton (1...3 for squarks, 1...8 for gluons). Initial coloured particles demand the normalisation factor $\frac{1}{\sqrt{n_c(a)...}}$ that we already included in the tree-level calculation. It is now important to see, how the colour-charge operator $\mathcal{T}_i$ acts on these vectors and which properties are needed for the coming evaluation of the colour flow.

$$\mathcal{T}_i = t_i^c|c> \qquad [\mathcal{T}_i, \mathcal{T}_j]_- = 0 \qquad \mathcal{T}_i^2 = C_i \tag{6.54}$$

The squared operator becomes a Casimir operator $C_i = C_F$ for (s)quarks and $C_i = C_A$ for gluons. In our terminology, we can write the concept of colour conservation in the following way:

$$\left(\sum_{i=1}^{m} \mathcal{T}_i + \mathcal{T}_a + ... \right) |1, ..., m; a, ... >_{m,a...} = 0 \tag{6.55}$$

In order to understand the later calculation, we take a look on operators acting on a squared matrix element:

$$\begin{aligned} |\mathcal{M}^{I,J}_{m,a...}|^2 =& _{m,a,...} < 1, ..., m; a, ... | \mathcal{T}_i \cdot \mathcal{T}_j | 1, ..., m; a, ... >_{m,a,...} \\ =& \frac{1}{n_c(a)...} \left[\mathcal{M}^{a_1...b_I...b_J...}_{m,a...} \right]^* t^c_{b_I a_I} t^c_{b_J a_J} \mathcal{M}^{a_1...a_I...a_J...}_{m,a...} \end{aligned} \tag{6.56}$$

The colour-charge operator of an initial parton a becomes the colour matrix in the adjoint representation in case of gluons, $(\mathcal{T}_a)^c_{bd} = i f_{bcd}$, and in the fundamental representation in case of (s)quarks, $(\mathcal{T}_a)^c_{\alpha\beta} = -T^c_{\beta\alpha}$ (for antiparticles, change sign and Greek indices). Catani and Seymour give the following dipole formula for initial spectator and emitter (notation explained in 7.1 and in [85]):

$$\boxed{\mathcal{D}^{ai,b} = -\frac{1}{2 x_{ab} p_a k} \, _{3,ab} < 1, 2, 3; ai, b | \left(\frac{\mathcal{T}_b \cdot \mathcal{T}_{ai}}{\mathcal{T}^2_{ai}} \mathbf{V}^{ai,b} \right) | 1, 2, 3; ai, b >_{3,ab}} \tag{6.57}$$

using definitions of 6.2.1. The splitting function $g^{(sub)}_{ab}$ is a matrix $\mathbf{V}^{ai,b}$ in the helicity space. One can show that the colour structure cancels exactly to 1. We take a last look at the case of final spectators:

$$\boxed{\mathcal{D}^{ai}_k = -\frac{1}{2 x_{ia} p_a k} \, _{3,ab} < 1, 2, 3; ai, b | \left(\frac{\mathcal{T}_k \cdot \mathcal{T}_{ai}}{\mathcal{T}^2_{ai}} \mathbf{V}^{ai}_k \right) | 1, 2, 3; ai, b >_{3,ab}} \tag{6.58}$$

In this case, a small calculation yields a factorised colour structure $f^{abc} T^c$.

7. Sommerfeld Enhancement of the Annihilation of Staus

In the author's Bachelor thesis [30] the much smaller process of annihilating staus into top quarks was calculated up to NLO corrections (for the Higgs propagator). An additional calculation, often having even greater impact on cross sections than NLO corrections), is the procedure of resummation.

7.1. General Remarks on Previous Work

For any details, we refer to [30], but at least a brief overview of the stau annihilation processes is adequate to mention, before the resummation is performed. The Born cross section contains several propagators, but only in the s-channel (Fig. 7.1). The staus and,

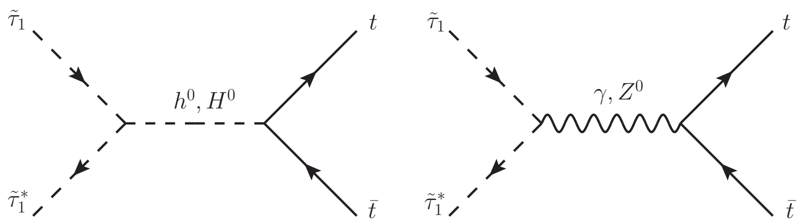

Figure 7.1.: Tree level diagrams of stau-antistau annihilation into top-antitop pairs: Possible propagators are CP-even Higgs bosons h^0, H^0 and photons/Z-bosons.

simultaneously, the final quarks, couple to the CP-even Higgs bosons (to the pseudoscalar only in case of mixing $\tilde{\tau}_{1,2}$) as well as to the uncharged electroweak bosons. The Higgs-vector-interference is extremely small - compared with the other interferences by a factor of 10^{-6}. Some kind of symmetry we do not understand yet suppresses this contribution. As it is valid also for squarks, one QCD (gluon exchange) and one SUSY-QCD (gluino exchange) correction occur on the right hand side of the s-channel diagrams:

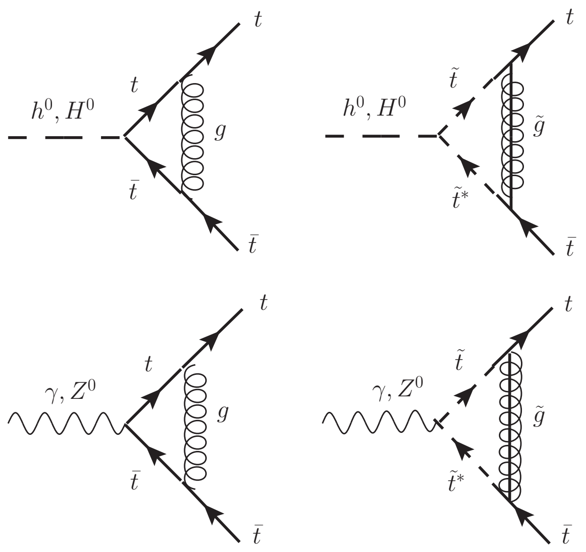

Figure 7.2.: Only the Higgs-top-top/vector-top-top vertices are corrected by SUSY-QCD.

Since we only have coloured final states, the number of gluon emission diagrams is quite small, never containing collinear divergences, by the way.

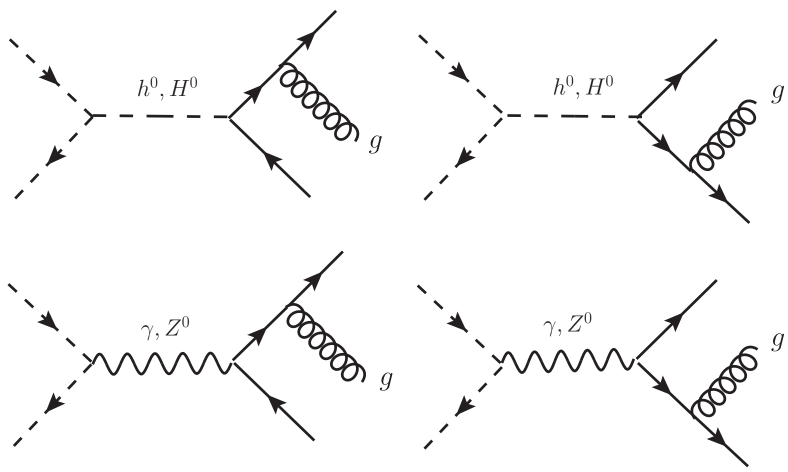

Figure 7.3.: Four possible gluon emissions from the final quark states.

These real corrections only regard the virtual gluon exchange as the exchange of massive gluinos is infrared convergent. The phase space integration is, in the most cases, quite far from trivial and only possible with the help of numerical integration. This rather convenient process, instead, allows for an analytical treatment of the final state phase space since it can be factorised and treated independently from the initial state. In analogy to the aforementioned tensor integrals, a couple of basis phase space integrals were developed by A. Denner [60], containing an artificial gluon mass λ (in the denominator) that gives birth to the infrared divergences:

$$
\begin{aligned}
I^{j_1,\ldots,j_m}_{i_1,\ldots,i_n}(m_0,m_1,m_2) &= \frac{1}{\pi^2}\int \frac{d^3p_1}{2E_1}\frac{d^3p_2}{2E_2}\frac{d^3q}{2E_q} \\
\times \quad \delta(p_0-p_1-p_2-q) &\frac{(\pm 2qp_{j_1})\ldots(\pm 2qp_{j_m})}{(\pm 2qp_{i_1})\ldots(\pm 2qp_{i_n})}
\end{aligned}
\tag{7.1}
$$

In this notation a particle with four-momentum p_0 decays into two particles with momenta p_1 and p_2; one radiates off a gluon with momentum q. For the scalar products with q, one has to choose the negative sign for the index 1,2. The explicit expressions of these integrals are given in App. D. In analogy to the counterterms, the singularities are matched subtractively as it can be seen in the following exemplary expression:

$$
I_{00} = \frac{1}{4m_0^4}\left[\frac{\kappa}{2}\ln\left(\frac{\kappa^2}{\lambda^2 m_0 m_1 m_2}\right) - \kappa - (m_1^2-m_2^2)\ln\left(\frac{\beta_1}{\beta_2}\right) - m_0^2\ln\beta_0\right] \tag{7.2}
$$

The divergence is contained in the pole $\ln(\lambda^2)$, obviously diverging for a vanishing photon mass.

An essential requirement for the application of this method is, of course, the factorisability of the left and the right vertex, as the phase space integrals only contain the momenta of the final states. Since a factorisation could not be find for the vector-Higgs interference, the dipole subtraction method was chosen to treat these real corrections numerically. Furthermore, it gave us the chance to compare the absorption of infrared divergences by the analytical and the numerical method. Unfortunately, the calculation of the cross section is more time-consuming due to the numerical integration of the $2 \to 3$ phase space. One integration has to be carried out over the whole $2 \to 3$ phase space (counterterm for the real emissions), the other one goes simply over the single phase space of the gluon. This integral, occurring in

$$
\int_{2\to 2}(d\sigma^{virt}|_{\epsilon=0} + d\sigma^{tree}\otimes \mathbf{I}|_{\epsilon=0}) \tag{7.3}
$$

is quite lengthy and shall be written with some abbreviations [86]:

$$
\begin{aligned}
\mathbf{I} = -\frac{C_F g_s^2}{8\pi^2}\frac{(4\pi)^\epsilon}{\Gamma(1-\epsilon)}\cdot &\left[\left(\frac{\mu^2}{s_{12}}\right)^\epsilon\left(\mathcal{V}_q(s_{12},m_q,m_q;\epsilon) - \frac{\pi^2}{3}\right)\right. \\
&\left. + \frac{\Gamma_q(m_q,\epsilon)}{C_F} + \frac{3}{2}\ln\left(\frac{\mu^2}{s_{12}}\right) + 5 - \zeta(2)\right]
\end{aligned}
\tag{7.4}
$$

We will give details on the dipole formulae in App. F. Following again [57], we can also use an analytic expression for the squared auxiliary matrix element for the $2 \to 3$ process:

$$
|\mathcal{M}^{2\to 3}|^2 = \mathcal{D}_{31,2} + \mathcal{D}_{32,1} \tag{7.5}
$$

The dipole contributions $\mathcal{D}_{ij,k}$ are functions of k_1, k_2 and k_3 where the index structure denotes the emitter pair ij (i=3) according to the momenta k_i, k_j and the untouched spectator k (App. F). Naturally, these expressions can also be factorised with the tree level contribution.

7.2. Sommerfeld Corrections

After having performed precision calculations in relativistic quantum field theory, we will now follow a completely different path of stating cross section results more precisely: The low-energy regime of small relative velocities of our incoming staus leading us to Schrödinger equations of two-body wave functions Ψ_{ij}. The coannihilation region in the MSSM is probably the most relevant case where these additional corrections are needed. A suitable ansatz to describe this system is the theory of bound states in a quantum field theoretical version. In our case, one may call this state a stauonium, structurally equivalent to e.g. a positronium or exciton state. A general theoretical framework is provided by the Bethe-Salpeter equation [61] that has to be specified for our purposes. It has the generic form of a recursion relation (Dyson equation) $G = S_1 S_2 + S_1 S_2 K_{12} G$ including a two-particle Green's function $G = \langle \Omega | \phi_1 ... \phi_4 | \Omega \rangle$. The S_i stand for the free propagators and K for the interaction kernel. The recursion may become clearer by drawing its diagrammatical interpretation in Fig. 7.4. Repeating this recursion step

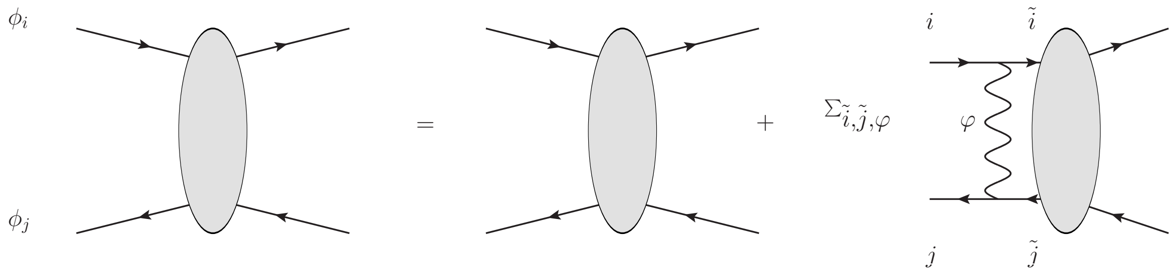

Figure 7.4.: Applying the Dyson equation iteratively, a ladder-like diagram comes into being. Each step adds one exchanged photon.

yields an infinite sum of exchanged virtual particles standing for an arbitrary interaction between the constituents forming the bound state. Apparently, we obtain a corrected vertex up to all orders of the interaction of interest - one chose the name *resummation* to describe it (this word should be handled carefully as it appears in several contexts). This special kind of resummation was named Sommerfeld or Coulomb enhancement. Such calculations have been performed in various ways - we cite the for our purposes most important work [62]. The diagram from above belongs to the two-body Schrödinger equation (with reduced masses m_{ij} and decay width Γ):

$$\left(-\frac{\Delta}{m_{ij}} + \sum_{\tilde{i},\tilde{j},\varphi} V^{\varphi}_{i,j,\tilde{i},\tilde{j}} \right) \Psi_{ij}(\vec{r}) = (E + i\Gamma_{ij}) \Psi_{ij}(\vec{r}) \tag{7.6}$$

The potential of course depends on the current interaction (QED: Coulomb potential, QCD colour-dependent Coulomb-like potential, multiplicative Yukawa term $\exp(-m_\varphi r)$ for massive bosons,...) and can be expanded via the β-function of its quantum field theory. Now it remains to find a Green's function describing the dynamics of the stauonium-like state with the help of the Bethe-Salpeter equation. With this expression, we end up, in our special case, with the ladder approximation of the Bethe-Salpeter amplitude $\tilde{\Gamma}$ including an exchange of infinitely many photons (Fig. 7.5). Let the staus exchange a

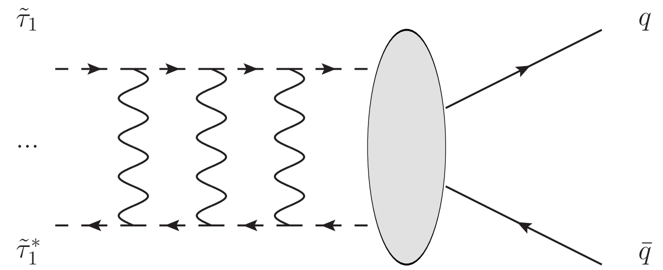

Figure 7.5.: A multiple photon exchange between the initial staus is the key element of the Sommerfeld enhancement in QED.

photon with momentum $p-k$, the momentum q shall be defined via $q^T = (2m_{\tilde{\tau}_1} + E, 0)$ (binding energy E). Then we can write the Bethe-Salpeter equation as [63]

$$\tilde{\Gamma}(\vec{p}, q) = 1 + \int \frac{d^3k}{(2\pi)^3} \frac{\tilde{\Gamma}(\vec{k}, q)\tilde{V}(|\vec{p}-\vec{k}|)}{[E - k^2/m_{\tilde{\tau}_1} + i\Gamma_{\tilde{\tau}_1}]} \,. \tag{7.7}$$

By defining

$$\tilde{G}(\vec{k}, E + i\Gamma_{\tilde{\tau}_1}) = -\frac{\tilde{\Gamma}(\vec{k}, E + i\Gamma_{\tilde{\tau}_1})}{[E - k^2/m_{\tilde{\tau}_1} + i\Gamma_{\tilde{\tau}_1}]} \tag{7.8}$$

and inserting into the upper equation, we see after Fourier transformation that G is a Green's function to the Schrödinger equation from above:

$$(H - E - i\Gamma_{\tilde{\tau}_1})G(\vec{r}, E + i\Gamma_{\tilde{\tau}_1}) = \delta^{(3)}(\vec{r}) \tag{7.9}$$

The choice of the general potential $V^{\varphi}_{i,j,\tilde{i},\tilde{j}}$ will be a NLO-corrected Coulomb potential in case of our QED resummation. We need the QED β-function of the running coupling to express the potential (Fourier-transformed from momentum space) [64,65]:

$$V(\vec{r}) = \frac{\alpha(\mu_C)}{|\vec{r}|}\left\{1 + \frac{\alpha(\mu_C)}{4\pi}\left[2\beta_0\left(\ln(\mu_C\vec{r}) + \gamma_E\right) + a_1\right]\right\} \tag{7.10}$$

$\gamma_E = 0.5772$ indicates the Euler-Mascheroni constant,

$$a_1 = -\frac{20}{9}\sum_f Q_f^2 \qquad \beta_0 = -\frac{4}{3}\sum_f Q_f^2 \tag{7.11}$$

are values where the second is derived from the one-loop β-function containing all fermions f up to the scale of the typical momentum exchange. We will comment on the Coulomb scale μ_C,

$$\mu_C = \max\left\{\mu_B, 2m_{\tilde{\tau}_1} \cdot v_s\right\} \,, \tag{7.12}$$

in the next chapter, when the scale variation is taken into consideration ($\mu_B = 2m_{\tilde{\tau}_1} \cdot \alpha$: inverse Bohr radius). Now, we are ready to give the Sommerfeld-enhanced result, factorisable with our leading order amplitude:

$$\boxed{\sigma^{Som}(\tilde{\tau}_1\tilde{\tau}_1^* \to t\bar{t}) = \frac{4\pi}{vm_{\tilde{\tau}_1}^2}\Im[G(\vec{r}=0;\sqrt{s}+i\Gamma_{\tilde{\tau}})] \times \sigma^{LO}(\tilde{\tau}_1\tilde{\tau}_1^* \to t\bar{t})} \tag{7.13}$$

In fact, only the $\vec{r} = 0$ Green's function is known in an analytic expression

$$G(0;\sqrt{s}+i\Gamma_{\tilde{\tau}_1}) = \frac{\alpha(\mu_C)m_{\tilde{\tau}_1}^2}{4\pi} \times \left[g_{LO} + \frac{\alpha(\mu_C)}{4\pi}g_{NLO} + \mathcal{O}(\alpha^2)\right] \tag{7.14}$$

that will be discussed in App. E.

Finally, we remark that these results are based on the implicit assumption of an s-wave-dominated matrix element. Only this fact guarantees the strikingly simple factorisability. The term *s-wave* has its origin in the partial wave expansion in quantum mechanical scattering theory. This series is usually expanded in powers of the scattering angle, where the exponent l indicates s-, p- and d-waves motivated by the quantum number l for electrons in an atom. As the annihilation process only occurs in the s-channel, the scattering angles do not appear in the matrix elements. Therefore, our chosen computation is justified. The approximation fails, if higher partial waves dominate parts of the leading-order amplitude and the amplitude depends on the momenta of the Sommerfeld-enhanced particles. In this case even the leading-order Coulomb potential has to be modified (we refer to [63]). Nonetheless, higher partial waves are suppressed by orders of the relative velocity v, so processes with t- and u-channels can be treated in the same way after an in-depth look on the performed partial wave decomposition.

Present research deals also with a multiple Higgs exchange leading to similar ladder diagrams [66] under the assumption of light Higgs bosons (compared to the initial particles). The formalism can be transferred easily. Related to the Bethe-Salpeter equation is, furthermore, the formation of bound states emitting photons/gluons. This process was rediscovered from the theory of exotic quarkonium states and is now applied in order to improve the precision of dark matter (co-)annihilation processes. [67]

8. Numerical Results

After all calculations, we will come now to the numerical investigation of our implemented code. First, we briefly introduce to the background of the chosen scenarios in the SUSY parameter space. Then, we discuss the percentage importance of stau annihilations for the dark matter relic density with the help of a mass scan. We analyse the impact of our NLO corrections and the Sommerfeld enhancement on the integrated cross section and the resulting shift of the relic density. Moreover, the gravitino is discussed as LSP. The main results led to the publication [31], in which we also perform an analysis of theoretical uncertainties arising from renormalisation scale and scheme variation.
At least an analysis of the leading order contribution to the stop annihilation into gluons shall be performed.

8.1. Stau Annihilation Into Top Quarks

8.1.1. Phenomenology of the Chosen Scenarios

In SUSY the explicit physical properties of the particle content are - as described in Section 4.2 - entirely undetermined. In fact, there is an endless number of possible points in the 105-dimensional parameter space. In this study we constrain the free parameters and end up with 19+3 values of a special kind of the pMSSM. A huge amount of data was produced after the LHC Run 1, in which the sensitivity to supersymmetry was investigated within the ATLAS project. This analysis is based on proton-proton collisions at $\sqrt{s} = 7$ and 8 TeV and interpreted in the context of the pMSSM with neutralinos as LSP. The points in the parameter space have to be in accordance with certain constraints from LHC searches: Mainly, the Higgs mass of the scenario has to be congruent with the observed one ($m_{h^0} = 125$ GeV) and the parameter point must not be in conflict with rare decays like $b \to s\gamma$ or $B_s \to \mu^+\mu^-$. With the help of these restrictions, the gigantic parameter space can be reduced to specific regions. Possible scenarios are written in so-called SLHA (SUSY Les Houches Accord) files [82,83] we used to implement the needed parameters. They are listed in the table below. We can neglect Scenario II for a while, as it corresponds to the gravitino analysis. This table contains several parameters we encountered in Chapter 4: The M_i mass parameters and μ were already in the context of SUSY-breaking. Now, the spectrum calculator *SPheno 3.3.3* [35] needs a particular value, at which the symmetry breaks - the SUSY-breaking scale Q (can be expressed via the physical stop masses: $Q = \sqrt{m_{\tilde{t}_1} m_{\tilde{t}_2}}$). The trilinear and Yukawa couplings, A_i and y_i, occur regarding the couplings of (s)fermions to Higgs bosons; the mass parameters are self-explanatory (note that they are given in the gauge

	I	II
$M_{\tilde{q}_L}$	1599.9	5000
$M_{\tilde{t}_L}$	3007.0	5000
$M_{\tilde{u}_R}$	3904.4	5000
$M_{\tilde{t}_R}$	3093.0	5000
$M_{\tilde{d}_R}$	3096.7	5000
$M_{\tilde{b}_R}$	581.6	5000
$M_{\tilde{\ell}_L}$	3586.7	5000
$M_{\tilde{\tau}_L}$	563.6	1800
$M_{\tilde{\ell}_R}$	3950.4	5000
$M_{\tilde{\tau}_R}$	585.5	1846
Q	3047.8	5000

	I	II
M_1	546.0	5000
M_2	-3461.7	5000
M_3	3126.7	5000
A_t	5246.7	-3000
A_b	-2530.3	1000
A_τ	1586.4	5000
$\tan\beta$	18.0	22.0
μ	2643.6	5000
m_{A^0}	2962.3	5000
$m_{\tilde{\chi}_1^0}$	540.6	4915.8
$m_{\tilde{\tau}_1}$	540.7	1810.8

Table 8.1.: Scalar soft mass parameters, gaugino mass parameters, trilinear couplings, and parameters related to the Higgs sector at the input scale Q for two reference scenarios I and II within the pMSSM. We also indicate the resulting physical masses of the lightest neutralino and the lighter stau. The values of the remaining physical masses are not displayed here, as they are not relevant for our study. The gravitino mass for the study of Scenario II will be specified in subsection 8.1.4. All dimensionful quantities are given in GeV.

eigenstates, mixing matrices may lead to the observable states). We do not explicitly give the Yukawa couplings as they are defined solely by SM parameters (explaining the notation 19+3 parameters), therefore small deviations appearing in different scenarios arise simply from the running of the renormalisation group equations. $\tan(\beta)$ is equal to the ratio of the VEVs $\langle H_u^0\rangle$ and $\langle H_u^0\rangle$ (see 4.4). A sufficiently small value prefers top quarks in the final state as their coupling to the Higgs is proportional to $\sin^{-1}(\beta)$. We also give the physical stau and neutralino mass calculated by the mixing angles. The physical neutralino is due to vanishing mixing a pure bino in both scenarios. Due to less interactions than a Wino-like neutralino (corresponding to $SU(2)_L$ with more thinkable coannihilations), the relic density of the bino-like LSP is bigger. The lighter stau is strongly mixed, the mixing angle corresponding to $\cos^2\theta_{\tilde{\tau}} \approx 0.42$ and $\sin^2\theta_{\tilde{\tau}} \approx 0.58$ for Scenario I and $\cos^2\theta_{\tilde{\tau}} \approx \sin^2\theta_{\tilde{\tau}} \approx 0.50$ for Scenario II.

For the understanding of the relevance of stau annihilation it is necessary to discuss the mass degeneracies appearing in the table. In Chapter 2 the Boltzmann equation for the neutralino number density contained the averaged annihilation cross section. All the possible interactions of dark matter can be expressed in a generalised version of the annihilation cross section, containing every possible (co-)annihilation process:

$$\langle\sigma_{ann}v\rangle = \sum_{i,j}\langle\sigma_{ij}v_{ij}\rangle\frac{n_i^{eq}}{n_\chi^{eq}}\frac{n_j^{eq}}{n_\chi^{eq}} \qquad v_{ij} = \frac{\sqrt{(p_i\cdot p_j)^2 - m_i^2 m_j^2}}{E_iE_j} \tag{8.1}$$

Processes	I	II
$\tilde{\tau}_1\tilde{\tau}_1^* \to t\bar{t}$	31.5	25.9
$\tilde{\tau}_1\tilde{\tau}_1^* \to \gamma\gamma$	12.9	21.4
$\tilde{\tau}_1\tilde{\tau}_1^* \to h^0h^0$	10.0	2.2
$\tilde{\tau}_1\tilde{\chi}_1^0 \to \ell h^0$	9.2	-
$\tilde{\tau}_1\tilde{\tau}_1^* \to \ell\bar{\ell}, \nu\bar{\nu}$	7.4	8.4
$\tilde{\tau}_1\tilde{\chi}_1^0 \to \ell Z^0$	7.0	-
$\tilde{\tau}_1\tilde{\chi}_1^0 \to \ell\gamma$	6.0	-
$\tilde{\tau}_1\tilde{\tau}_1^* \to W^+W^-$	6.5	11.3

Table 8.2.: Relative contributions in percent of the dominant annihilation channels contributing to the annihilation cross section σ_{ann} in the two reference scenarios I and II defined in Tab. 8.1. Here, ℓ and ν denote arbitrary lepton and neutrino states, $\ell = e, \mu, \tau$ and $\nu = \nu_e, \nu_\mu, \nu_\tau$. Further contributions below 5% are omitted.

In this thermally averaged expression, the ratios of the equilibrium number densities n^{eq} are suppressed via the so-called Boltzmann factor:

$$\frac{n_i^{eq}}{n_\chi^{eq}} \propto \exp[-(m_i - m_\chi)/T] \tag{8.2}$$

This proportionality tells us that only small mass differences between the coannihilating particles are responsible for a reasonable impact on the whole relic density. These approximative degeneracies often occur in the investigated SUSY scenarios (usually LSP+NLSP). For small freeze-out temperatures T, the suppression factor increases - in our case, this value turned out to be 26.6 K. The small mass difference between stau and neutralino can be directly be read off from the table.

Scanning the stau and neutralino mass a few GeV above and below the values of the chosen scenario is a good opportunity to identify regions in the parameter space in which the process of interest has greater importance for the relic density. In Fig. 8.1 we can see how strongly the percentage impact may differ: By varying the two key parameters bino mass M_1 and the left-handed stau mass parameter $M_{\tilde{\tau}_L}$ in the vicinity of our parameter values in the upper table, we find a value for the neutralino relic density for each point in the plane. Taking the experimental value of this quantity, a Planck-compatible ribbon can be drawn in the plane. This is of course in the near of the line with equal masses of LSP and NLSP, in accordance with the Boltzmann suppression. The deep green regions are of particular interest as stau annihilation yields a considerable contribution to the relic density. In general, this scenario possesses a handful of further dominant channels we summarize in Tab. 8.2. Unfortunately, these are insensitive with respect to QCD corrections and, therefore, no other processes implemented in our code can be used to improve the precision.

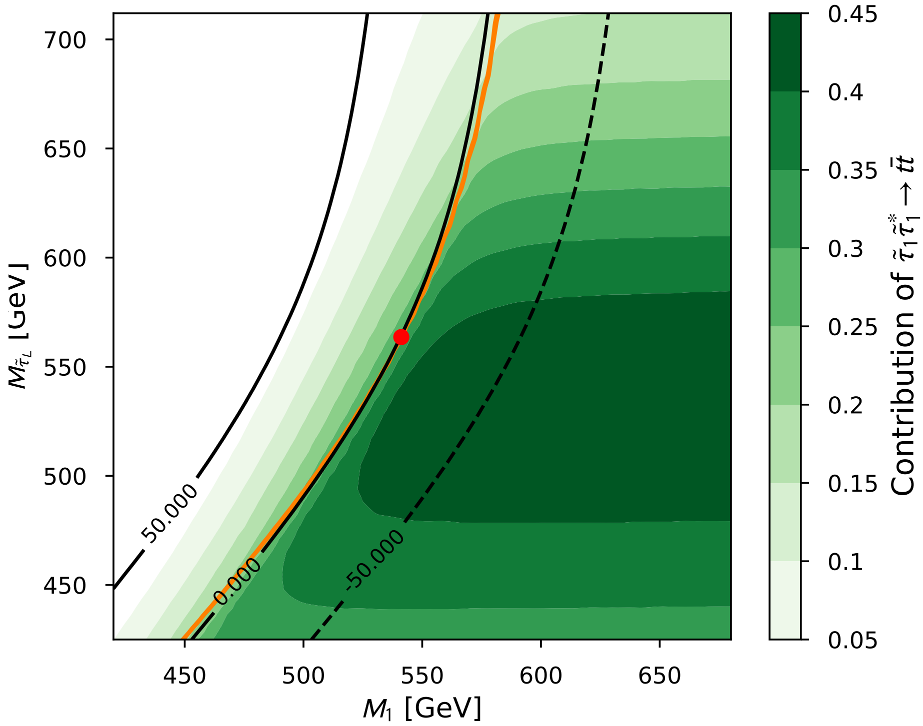

Figure 8.1.: Parameter regions in the M_1–$M_{\tilde{\tau}_L}$ plane that are compatible with the Planck limits given in Eq. 2.5, where the relic density has been computed using *micrOMEGAs*. All other parameters are fixed to those given in Table 8.1. The red dot indicates Scenario I defined in the same table. The green contours correspond to the contribution of the process $\tilde{\tau}_1\tilde{\tau}_1^* \to t\bar{t}$. The black contour lines indicate the difference $m_{\tilde{\tau}_1} - m_{\tilde{\chi}_1^0}$ in GeV between the physical masses of the lighter stau and the lightest neutralino.

8.1.2. Cross Sections and Their Theoretical Uncertainties

In present dark matter research not only the experimental uncertainty is a quantity that has to be dealt with. At next-to-leading order, theoretical predictions may differ, dependent on the renormalisation scale and scheme (a small uncertainty at NLO excludes the necessity of higher-order calculations in order to reduce possibly upcoming uncertainties). In order to estimate their reliability, it is a common method to perform a variation of the scale μ_R for investigating the sensitivity of our NLO results. More precisely, we vary around the central scale of 1 TeV and analyse the ratio of these results and those of 0.5 TeV and 2 TeV, respectively. Due to the aforementioned hybrid-renormalisation scheme, a handful of the parameters in Table 8.1 are renormalised on-shell; therefore, the μ_R variation is only relevant for the masses and couplings which are taken in the $\overline{DR}$ scheme. We postpone the scale variation and discuss the scheme dependence first: Our two renormalisation schemes should be defined.

- ***DM@NLO scheme***: m_b and trilinear couplings shall be renormalised in $\overline{DR}$ scheme, m_t, $m_{\tilde{t}_1}$, $m_{\tilde{b}_1}$ and $m_{\tilde{b}_2}$ are defined on-shell, mixing angles and $m_{\tilde{t}_2}$ are dependent parameters (can be calculated using the remainder)
- ***alternative scheme***: $m_{t,b}$ and trilinear couplings renormalised in $\overline{DR}$ scheme, $m_{\tilde{t}_1}$, $m_{\tilde{b}_1}$ and $m_{\tilde{b}_2}$ defined on-shell, mixing angles and $m_{\tilde{t}_2}$ are dependent parameters

In Fig. 8.2 we show the stau annihilation cross section with parameters from Scenario I and as a function of the centre-of-mass momentum p_{cm}. The corresponding thermal distribution is plotted since the Boltzmann equation contains the thermally averaged cross section. A velocity distribution demonstrates these momenta which are most relevant to calculate the neutralino relic density.

In the figure the black *micrOMEGAs* line does not coincide with our tree level results, due to different Yukawa couplings (the former one uses effective couplings). The Sommerfeld enhancement enters the stage, as expected, for small relative velocities and enlarges the cross section, as the QED interaction is attractive. The annihilation process becomes more likely. The interesting point in our standard renormalisation scheme is the (approximate) cancellation of the NLO results with the Sommerfeld enhancement yielding no visible corrections to the leading-order results. That accident gave the motivation to investigate the sensitivity of the cross section regarding the renormalisation scheme. Turning to our ***alternative scheme*** changes the definition of the top-quark mass. To change consistently, we demand

$$m_t^{OS} + \delta m_t^{OS} = m_t^{DR} + \delta m_t^{DR} \tag{8.3}$$

Hence, the top mass appearing in the tree level calculations changes massively leading to rather different cross sections (the difference is larger than 30 %): In the ***alternative scheme*** the leading order is the lowest line. This implies that NLO and Sommerfeld corrections are not subtractive any more - we see a considerable shift. The impact on the

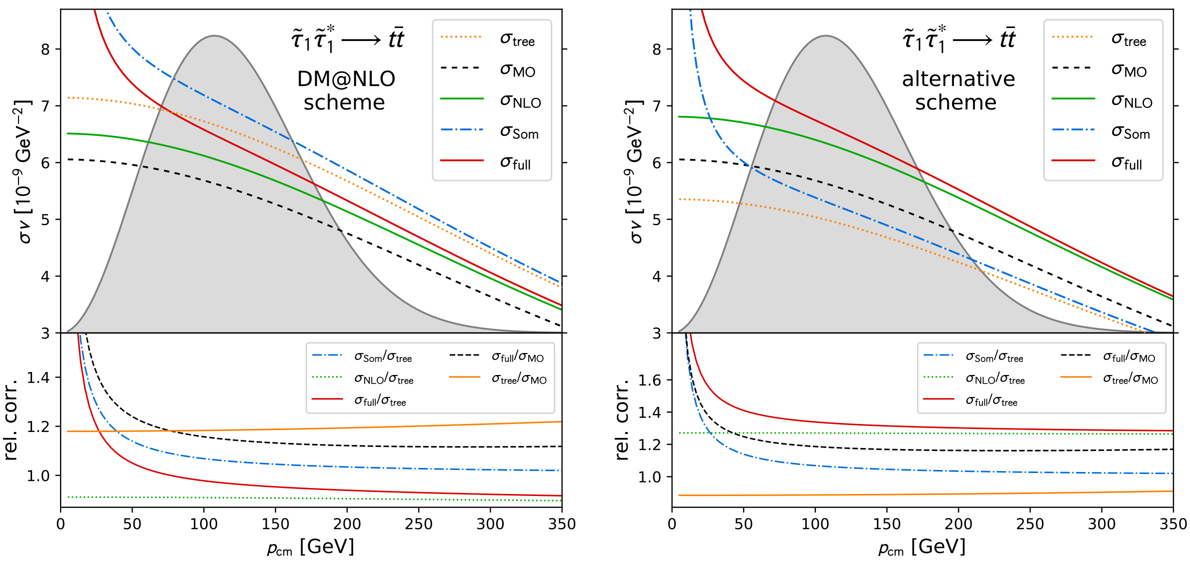

Figure 8.2.: Annihilation cross section of the process $\tilde{\tau}_1\tilde{\tau}_1^* \to t\bar{t}$ as a function of the centre-of-mass momentum p_{cm} for Scenario I of Tab. 8.1 using the standard ***DM@NLO scheme*** (left) and the ***alternative scheme*** (right). The upper panels show tree level results and different levels of corrections that were discussed in Chapter 7. The lower panels show the corresponding relative corrections. The grey areas indicate the thermal distribution in arbitrary units.

NLO results, however, is relatively mild (4 %). This fact guarantees a good reliability of the second order of perturbation theory. Taking into account higher-order corrections will not visibly affect the theoretical uncertainty. We plotted the discussed ratios in Fig. 8.3. Now, we turn back to the mentioned scale variation. Again, it is rather important if the SUSY parameter is renormalised in the $\overline{DR}$ scheme, otherwise it is insensitive with respect to the renormalisation scheme. It is worth mentioning that all other SUSY parameters were read at the central scale, as we are only interested in QCD corrections. In fact, this solely holds for the trilinear coupling A_t and (in the ***alternative scheme***) for the top mass, when we take those parameters into account which appear within the stau annihilation. Note, that the Born cross section is completely electroweak, so the running strong coupling and its contribution to the cross section is a totally new phenomenon appearing at NLO. The variation has an impact on the strong coupling $\alpha_s(\mu_R)$ as well since it is renormalised in the $\overline{DR}$ scheme. This effect is the main reason for the deviations that can be found in the left of Fig. 8.4, because A_t only appears within the gluino vertices, contributing less than the SM corrections. Nonetheless, the deviation is immensely small (around 0.25 %). We did not treat bottom quarks in the final state (dependent on variation) and no mixing matrices occurred in the calculations. Taking the top mass into consideration (***alternative scheme***, right hand side of Fig. 8.4) leads, of course, to a higher dependence on the scale. But luckily, the 3 % deviation at

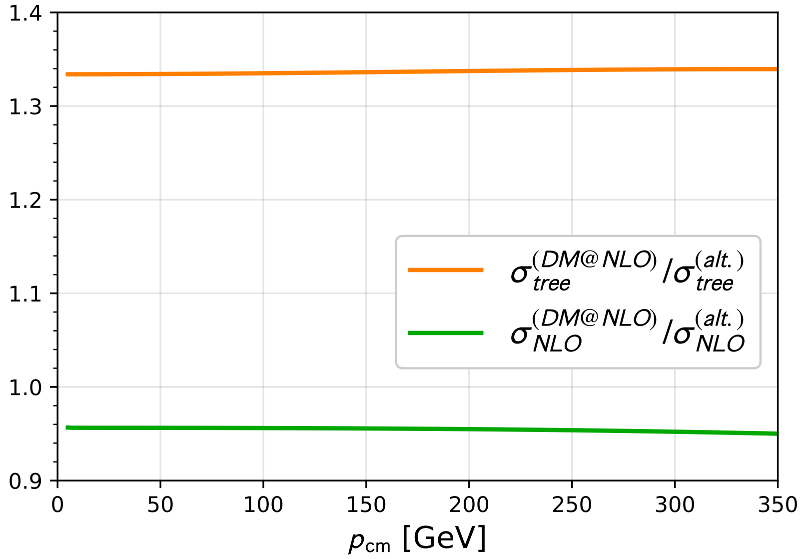

Figure 8.3.: Ratios of the $\tilde{\tau}_1\tilde{\tau}_1^* \to t\bar{t}$ cross section calculated in the ***DM@NLO scheme*** and the ***alternative scheme*** at leading (orange) and at next-to-leading order (green).

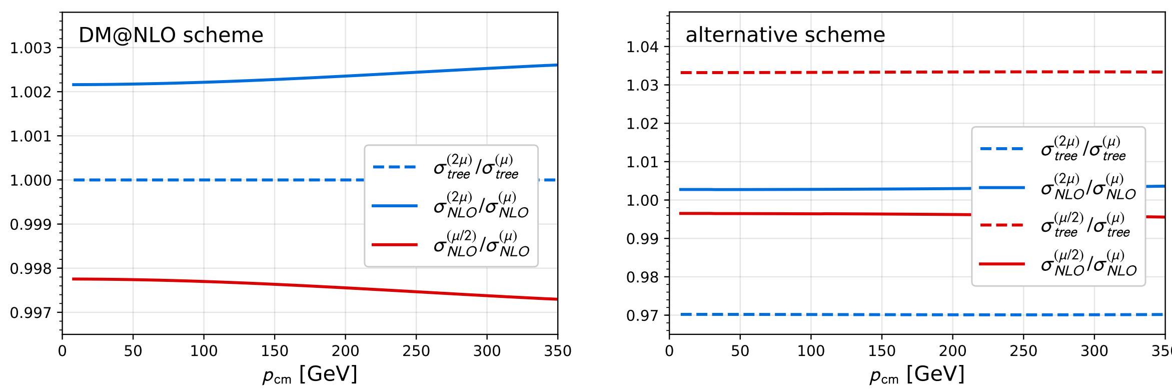

Figure 8.4.: Ratios of the $\tilde{\tau}_1\tilde{\tau}_1^* \to t\bar{t}$ cross section for renormalisation scale μ_R varied around the central scale (μ_R =1 TeV) at leading (dashed line) and next-to-leading order (solid line) for the ***DM@NLO scheme*** (left) and the ***alternative scheme***.

leading order shrinks to a per mille level at NLO - the theoretical uncertainty is reduced in a similar manner like in the scheme variation. The remaining open question might be, if deviations from the resummation scale μ_C may affect our results more visibly. This value was determined via

$$\mu_C = \max\{\mu_B, 2m_{\tilde{\tau}_1} \cdot v\} \tag{8.4}$$

using the relative velocity of the initials and $\mu_B = 2m_{\tilde{\tau}_1} \cdot \alpha$ (corresponding to the inverse Bohr radius). The choice of α as 1/137 (zero-energy, instead of 1/128 at Z^0 energy) and even by taking twice the value of $\mu_C^{central}$ had no visible impact on the results. It furthermore turned out that due to this independence, the β-function of QED yields a negligible NLO contribution. For this reason, our results could have even been investigated using a leading-order Green's function.

Obviously, the main theoretical uncertainties occur within the renormalisation scheme variation. We finally plot the Planck-compatible band in both schemes again in the vicinity of our parameter point from Scenario I at LO and NLO and compare them with a smeared band (yellow), the *micrOMEGAs* result including the 1σ confidence level. The NLO lines nearly overlap and contain therefore much lower uncertainties than those that come from measurements.

8.1.3. Impact on the Neutralino Relic Density

The impact of our corrections on the neutralino relic density was already implicitly investigated in the part of theoretical uncertainties. Nonetheless, we turn back to our standard ***DM@NLO scheme*** as in previous publications about other processes and take a look at both the soft-parameter and the physical mass plane, i.e. M_1–$M_{\tilde{\tau}_L}$ plane (left) and $m_{\tilde{\chi}_1^0}$–$m_{\tilde{\tau}_1}$ plane (right) as shown in Fig. 8.6. We compare *micrOMEGAs* with our NLO+Sommerfeld results and plot the areas which are compatible with Eq. 2.5 in orange/blue. The small corrections (less than 1 GeV) are explained by the aforementioned cancellation of NLO and enhancement corrections in our standard renormalisation scheme and, furthermore, by the small contribution of $\tilde{\tau}_1\tilde{\tau}_1^* \to t\bar{t}$ to the total annihilation cross section we gave in Tab. 8.2. However, the gap between the lines should not be underestimated: In shortcoming of an overlap, the corrections are at least beyond the experimental uncertainty and have to be taken into account. Generally, one should not worry about small corrections. Since in the ***DM@NLO scheme*** the NLO corrections are visibly smaller than in the ***alternative scheme***, we assume a quicker convergence of the perturbative series.

Although a gap was found, the main message of this numerical investigation is rather the strong dependence of leading order results on the renormalisation scheme. One should always keep in mind that even small changes like the on-shell top quark mass massively affect the Born cross section. Adding now higher-order corrections does not only enlarge the precision of the perturbative series - the deviations after changing the

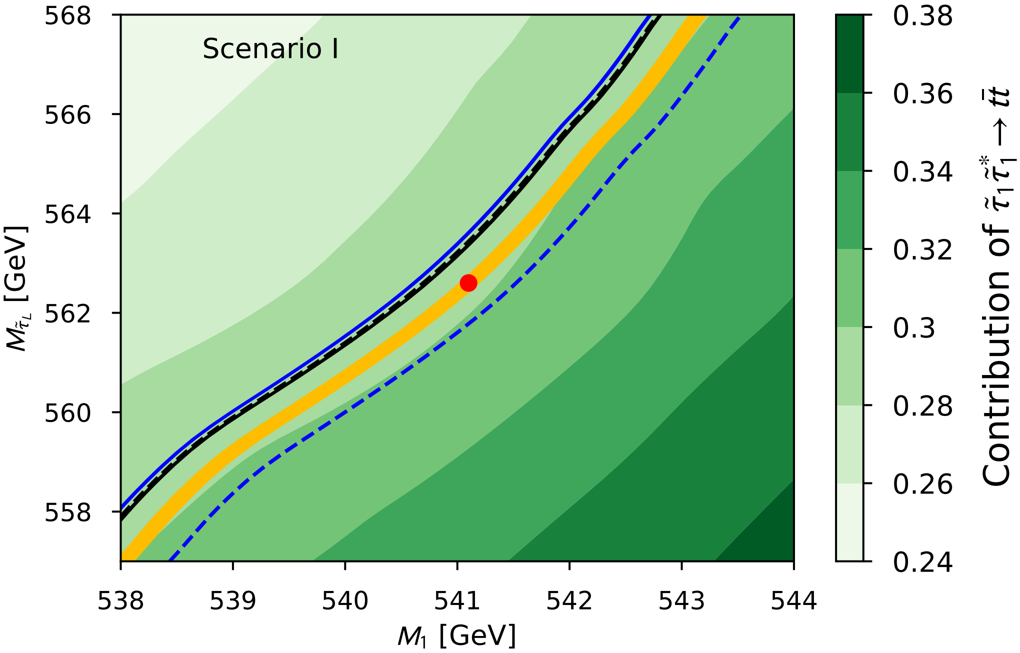

Figure 8.5.: Comparison of experimental and theoretical uncertainties in the M_1–$M_{\tilde{\tau}_L}$ plane around reference Scenario I (indicated by the red dot). The yellow band shows the experimental uncertainties given in Eq. 2.5 as measured by the Planck satellite at the 1σ confidence level. The leading (next-to-leading) order relic density from both our renormalisation schemes is denotes by blue (black) lines. The predictions in the ***DM@NLO (alternative) scheme*** are shown using the solid (dashed) lines. As in Fig. 8.1, the green contours indicate the relative contribution of the process $\tilde{\tau}_1\tilde{\tau}_1^* \to t\bar{t}$ to the total annihilation cross section, based on the *micrOMEGAs* calculation.

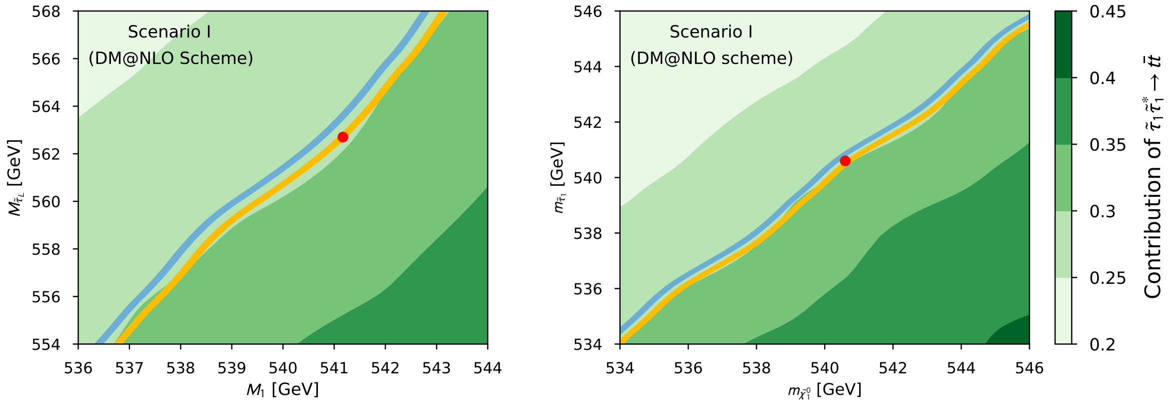

Figure 8.6.: Parameter regions in the M_1–$M_{\tilde{\tau}_L}$ plane (left) and $m_{\tilde{\chi}_1^0}$–$m_{\tilde{\tau}_1}$ plane (right) that are compatible with the Planck limits given in Eq. 2.5, where the stau relic density has been computed using ***micrOMEGAs*** (orange) and our full NLO and Sommerfeld corrected cross section (blue). All other parameters are fixed to those given for Scenario I in Tab. 8.1. The red dot corresponds to the Scenario I. The green contours correspond to the relative contribution of the process $\tilde{\tau}_1\tilde{\tau}_1^* \to t\bar{t}$ to the total annihilation cross section.

renormalisation scheme are remarkably reduced! The same holds in certain cases for variations of the μ_R scale. Finally a warning: The comparison of theoretical and experimental uncertainties may confuse. An experimental uncertainty implies an expectation value lying between the boundary values. In our estimation of the theoretical one, one must not deduce that the truth lies between those two schemes. Moreover, there are a couple of more schemes (e.g. take simply everything in dimensional reduction) and their usage highly depends on the process. Especially in the MSSM, they are not easy to define consistently. For the case that this can be done successfully, this approach still cannot cover constant terms. Their values have to be determined only using exact calculations of higher orders whose size we are trying to give. We conclude: As one cannot define a true/an expectation value for the calculations, the reduction of the gaps between different schemes is the only way to predict reliable results.

8.1.4. On Gravitinos

In order to consequently bring the quantisation of fundamental interactions to an end, a theory of quantum gravity still has to be developed. Although a manifold of ideas was discussed in the last decades, a quantisation often turned out to be perturbatively non-renormalisable. Nonetheless, it is natural to assume gravitons to mediate gravity like the other gauge bosons do in the remaining interactions. These particles, thought as quantised gravitational waves, have to carry a spin of 2 as gravity acts only attractively and the gauge field is the energy-stress tensor of rank 2. SUSY transformations then produce spin-3/2 gravitinos obeying the Rarita-Schwinger equation of motion. We previously mentioned the gauge-mediated SUSY-breaking (GMSB) which is mediated to the visible sector of supersymmetric particles at a certain scale. The GMSB scale $\langle F \rangle$ is then related to the gravitino mass $m_{\tilde{G}}$ and the reduced Planck mass M_P by $m_{\tilde{G}} = \langle F \rangle / (\sqrt{3} M_P)$. Gravitinos are the LSPs (and therefore dark matter candidates) in scenarios of a SUSY breaking via a gauge-singlet chiral superfield S and quark- and lepton-like messenger fields that we discussed before. We give some references that treat gravitino dark matter under the given conditions: [68,69]. Now, we skip over details and come to our omnipresent object of desire. The relic density $\Omega_{\tilde{G}} h^2$ of frozen-out gravitinos comes into being in a twofold manner:

$$\Omega_{\tilde{G}} h^2 \;=\; \Omega_{\tilde{G}}^{th} h^2 + \Omega_{\tilde{G}}^{non-th} h^2 \tag{8.5}$$

The non-thermal gravitino production is based on the decay of the NSLP which shall be later the scalar tau (only, if R-parity is conserved). Every NLSP usually decays into a gravitino and the SM partner of the NLSP, so the relic density is related to the known value for staus in a very simple way [70]:

$$\Omega_{\tilde{G}}^{non-th} h^2 = \frac{m_{\tilde{G}}}{m_{NLSP}} \Omega_{NLSP}^{th} h^2 \tag{8.6}$$

The nature of the second constituent, the thermal production, is a bit harder to motivate [70,71] and has the following form:

$$\Omega_{\tilde{G}}^{th} h^2 = 0.27 \left(\frac{T_R}{10^{10}\,\mathrm{GeV}} \right) \left(\frac{100\,\mathrm{GeV}}{m_{\tilde{G}}} \right) \left(\frac{m_{\tilde{g}}}{1\,\mathrm{TeV}} \right)^2 \tag{8.7}$$

The formula involves the gluino mass $m_{\tilde{g}}$ of the particular scenario and the reheating temperature T_R. This quantity comes from the end of the inflationary expansion. This moment of expansion of the very early Universe happened in a supercooled way (temperature drops by 10^5 in the most models). In order to get back to the pre-inflationary temperature, a thermalisation or reheating must occur. One defines T_R as temperature value to reach this realm again, although the actual value is unknown. It is, however, possible to estimate T_R beyond 10^9 GeV to explain the baryon asymmetry by leptogenesis. The method to derive the upper equation is, on top, only reliable if T_R lies above 10^7 GeV. Details on the reheating temperature can be found in [73]. In Fig. 8.7 a numerical investigation of the parameters from above is shown that may illustrate the dependences a bit more.

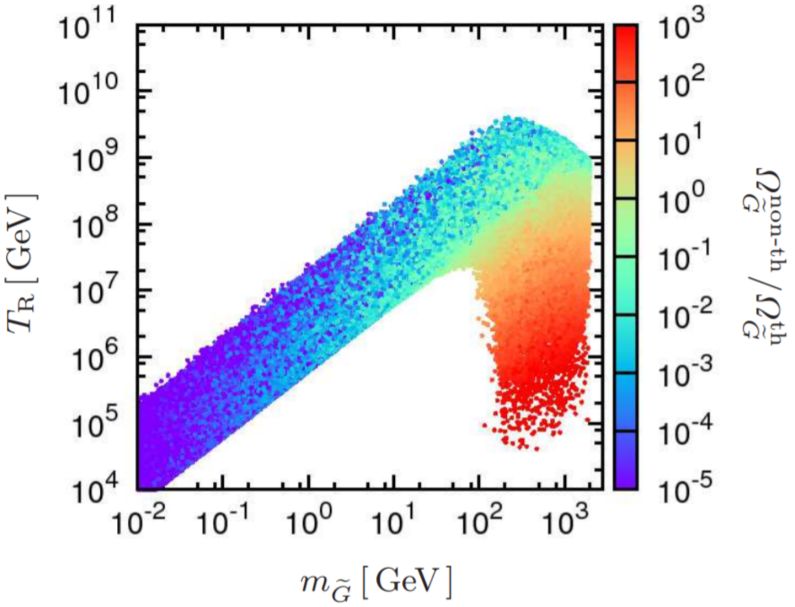

Figure 8.7.: A detailed study of the importance of non-thermal and thermal gravitino production depending on their masses and the reheating temperature [69].

At the end, we should lose some words about the stau lifetime that can be written in the following form:

$$t_{\tilde{\tau}_1} \simeq \left(6100\,s\right)\left(\frac{1\;TeV}{m_{\tilde{\tau}_1}}\right)^5\left(\frac{m_{\tilde{G}}}{100\;GeV}\right)^2 \lesssim 6000\,s \tag{8.8}$$

The abundance of light elements after primordial nucleosynthesis has to be preserved, so a maximum lifetime for SUSY particles must be incorporated [74,75]. With this condition, the gravitino mass is often constrained to be an order of magnitude smaller than the stau mass. The ATLAS analysis was performed for neutralino relic densities. This fact together with the liftetime constraint made it nearly impossible to find a promising scenario in the set of the ATLAS points, given that we are interested in the non-thermal production of gravitinos. Indeed, an allowed scenario would have been found, but a too large contribution of thermally produced gravitinos would make our corrections worthless, as no corrected cross section appears. We therefore decided to construct an illustrative scenario in order to show what can principally be done with the stau annihilation cross section. With relatively light stau masses around 2 TeV, while other particles have masses around 5 TeV, we were able to generate a parameter set fulfilling the lifetime constraint as well as our hope of big non-thermal contributions (we called it Scenario II). Thus, the gravitino mass lies around 400 GeV. A Planck-compatible result can then be achieved with a reheating temperature of $T_{\text{R}} \approx \mathcal{O}(10^7)$ GeV .

Similarly to the neutralino relic analysis, we illustrate in Fig. 8.8 the shift induced by NLO and Sommerfeld corrections - now in the $m_{\tilde{G}}$–T_R plane. Again, the shift is far

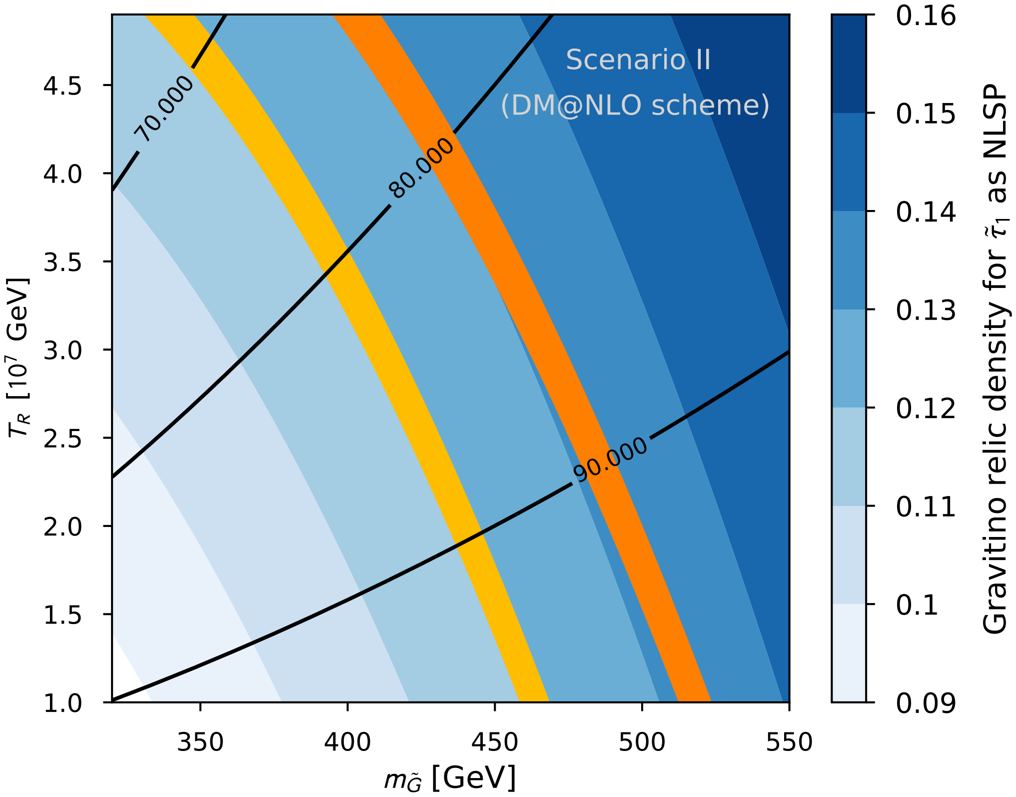

Figure 8.8.: Parameter regions in the $m_{\tilde{G}}$–T_R plane which are compatible with the Planck limits for the case of gravitino dark matter, where the stau relic density has been computed using *micrOMEGAs* (yellow) and our full NLO and Sommerfeld corrected cross section in the *DM@NLO* scheme (orange). All other parameters are fixed to those given for Scenario II in Tab. 8.1. The blue contours correspond to the gravitino relic density based on the *micrOMEGAs* calculation. The black lines indicate the relative non-thermal contribution in percent to the total gravitino relic density, again based on the *micrOMEGAs* calculation.

	value
$M_{\tilde{q}_L}$	3796.6
$M_{\tilde{t}_L}$	2535.0
$M_{\tilde{u}_R}$	3995.0
$M_{\tilde{t}_R}$	1258.6
$M_{\tilde{d}_R}$	3133.2
$M_{\tilde{b}_R}$	3303.7
$M_{\tilde{\ell}_L}$	3134.1
$M_{\tilde{\tau}_L}$	1503.9
$M_{\tilde{\ell}_R}$	2102.5
$M_{\tilde{\tau}_R}$	1780.4
Q	1784.6

	I
M_1	1278.4
M_2	-2093.5
M_3	1267.15
A_t	2755.3
A_b	-2320.9
A_τ	-1440.3
$\tan\beta$	15.5
μ	-3952.55
m_{A^0}	3624.8

Table 8.3.: Scenario, analogously to those in Tab. 8.1, in the (19+3)-pMSSM parameter space containing a remarkable impact of stop annihilation into gluon pairs for the neutralino relic density. All dimensionful quantities are given in GeV.

beyond the experimental uncertainty and the additional terms should be taken into account: They are responsible for a shift of about 50 GeV for the gravitino mass, or (equivalently) for a fixed gravitino mass of 450 GeV, T_R has to be doubled in order to still satisfy the experimental data.

Finally note, that this kind of gravitino cosmology underlies several strong assumptions. We do not only demand the SUSY conjecture to be true, but also the quantisation of gravity by tensor bosons (gravitons) and the theory of inflation as well. Seen from a viewpoint of philosophy of science, this construction of dark matter candidates and their investigation is based on a very unstable ground.

8.2. Stop Annihilation Into Gluons

Currently, the NLO results in order to investigate their impact on the Planck-compatible ribbon are not available yet. Nonetheless, we have the possibility to present an interesting scenario (Table 8.3) in analogy to the previous one to analyse the contributions of the different channels of stop annihilation into gluon pairs. The mass degeneracy between the neutralino and $m_{q_t^R}$ has the consequence that almost every important process for the LSP relic density contains stops in the initial state. More precisely, we have our process of interest (38,6 %), stop annihilation into top quarks (30,5 %) and coannihilation into a gluon and a top (9 %). Luckily, the second process has been already implemented, therefore our *DM@NLO* corrections are very dominant in this scenario. Our scenario features again bino-like neutralinos. In Fig. 8.9 we performed a scan in the neighbourhood of the ATLAS point (red dot) in the plane analogous to the stau annihilation process. In this case we deal with considerably higher masses and also the relative contribution to the

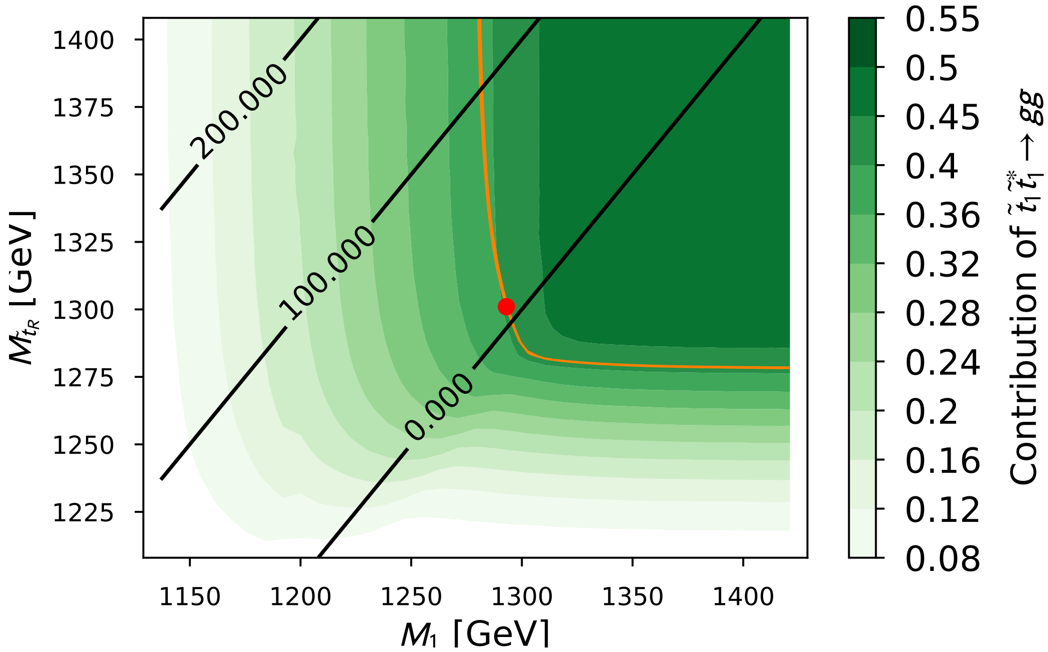

Figure 8.9.: Planck-compatible relic density ribbon of *micrOMEGAs*. The red point denotes the point of the ATLAS scenario from Tab. 8.3. The ribbon is plotted in the $(M_{\tilde{t}_R}, M_1)$ plane. A contour provides information about the mass difference (for neutralino LSP, only positive values are relevant). We give relative contributions of $\tilde{t}_1\tilde{t}_1^* \to gg$ to the neutralino relic density using the green colour bar.

relic density is bigger. In general, one could find scenarios with fairly high percentages up to 70 %. The chosen soft parameter is the right-handed stop mass - a strong mixing leads to the lighter stop. In Fig. 8.10 we did something new and decomposed the Born cross section into its channels. The four-vertex - the simplest diagram - turns out to be by far the most relevant one. It decreases for high momenta whereas t- and u-channel increase. At higher energies they may collide, but the maximum of the thermal distribution is already around 260 GeV. One should not be confused by the s-channel as the process has to be seen inclusively. The single channel does not occur in Nature. The *micrOMEGAs* result are rather congruent with our *DM@NLO* code, the renormalisation scheme does not visibly affect the results.

The diagrams may drastically change in another scenario; moreover, the analysis is only for illustrative purposes to show how the process and its single channels behave and that promising scenarios do exist. As there appear far more corrections than in stau annihilation with electroweak initial states, we expect bigger corrections and a slower convergence of the perturbative series. With a maximum of the thermal distribution at low centre-of-mass energies, a QCD Sommerfeld enhancement should be visible as

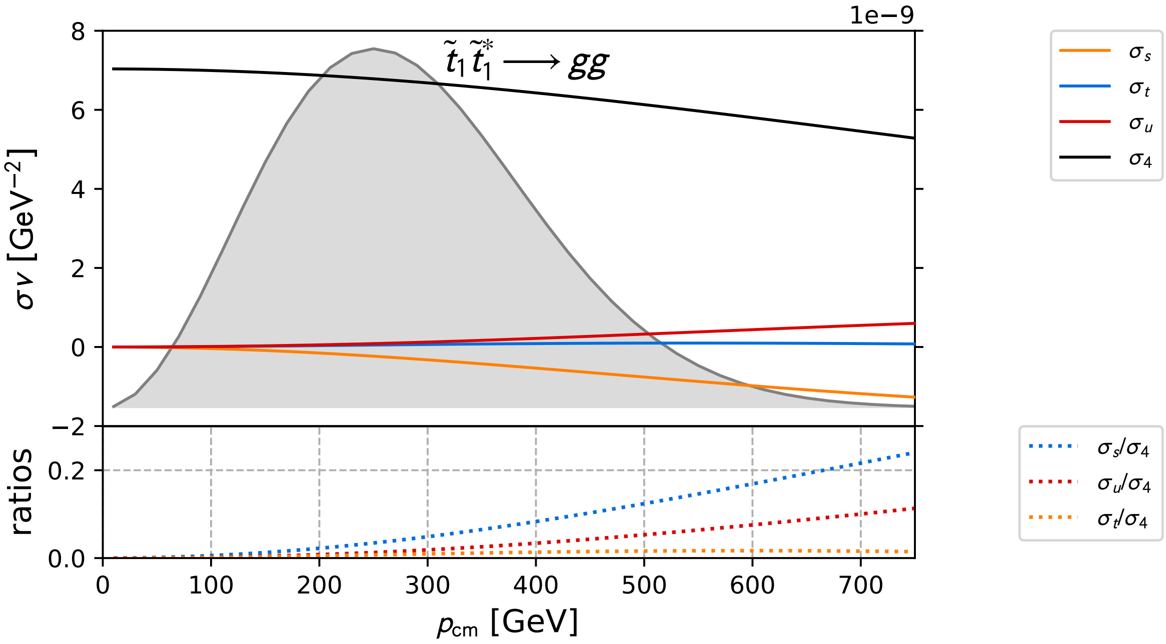

Figure 8.10.: Annihilation cross section, dependent on the centre-of-mass energy p_{cm}. We give absolute and relative (below) contributions of the different channels s, t, u and the four-vertex, denoted by σ_4, for the stop annihilation into a gluon pair. The grey area indicates a thermal distribution in arbitrary units.

well. Generally, the stronger coupling leads to the assumption of a stronger impact on the final cross section than an exchange of infinitely many photons. Nevertheless, one should keep attractive and repulsive colour potentials in mind - depending on the colour decomposition effects they could cancel each other.

9. Conclusion and Outlook

Before this thesis comes to an end, we briefly recapitulate what was achieved within the last year and, maybe even more important, what has to be done in the future to finish the stop annihilation. Over and above that, it might be interesting to discuss how the *DM@NLO* project may go on.

We started with an overview of the current dark matter research - about promising and falsified models, some experimental constraints and especially SUSY giving birth to the lightest neutralino which we appointed to the main dark matter constituent. Subsequently, we explained the basic ideas of *DM@NLO*. The stop annihilation into gluon pairs involves some non-trivial QCD like the appearance of Faddeev-Popov ghosts and (not necessary, but convenient) a colour decomposition into irreducible representations. With a short group theoretical introduction, we explained the procedure in greater detail - as a cooking recipe for coming processes. Where do all these peculiar supersymmetric particles come from? Using the group theory part, we roughly derived the algebraic origin of squarks & Co. and pondered why SUSY might be promising. At this point, all necessary foundations were set out - let us now repeat the achievements in the stop annihilation process:

- implementation of born cross section, in accordance with *mircOMEGAs* and the results of S. Schmiemann
- colour decomposition of the single channels
- numerical analysis of tree level + parameter scan
- remaining Passarino-Veltman integrals (for 3-gluon topology) were implemented
- UV-convergent propagator corrections were fully implemented
- vertex corrections calculated and implemented (successful renormalisation, one case of doubt explained in Appendix D)
- automatic box calculation with interferences by *FeynCalc* code
- manually calculated amplitudes of all real emissions (for cross-check by the successor)

Furthermore, some integration methods and preliminary results regarding the dipole subtraction method for massive initial scalars have been developed (Chapter 6).

The thesis continued with the second process (stau annihilation into heavy quarks), where some NLO corrections have already been performed in a previous work. We completed the virtual and real corrections for the vector boson exchange and compared an analytical treatment of the gluon emission with the numerically performed dipole subtraction and came to the same result. Electroweak corrections in the form of a QED Sommerfeld enhancement were added. Interestingly, they almost cancelled the SUSY-QCD calculations at NLO. Therefore, by an accident, we discovered the considerable dependence of the results on the renormalisation scheme. The Born cross section strongly differs when changing the scheme, whereas the corrections were more or less left untouched. In the course of that, we also varied the renormalisation scale and investigated the sensitivity of the results by modified Coulomb scales.

In total, we could estimate the reliability of our NLO and Sommerfeld corrections with the theoretical uncertainties appearing in such variations. We found an interesting scenario in the SUSY parameter space in which the stau-antistau annihilation into heavy quarks was relatively important. The vicinity of this point was intensively studied - the Planck-compatible ribbon was visibly shifted by our corrections. We applied our calculations to gravitino dark matter physics and showed, how gravitino mass and the reheating temperature in the postinflationary Universe are shifted using our precise cross section. This happened with an artificially constructed scenario just for illustrative purposes as the ATLAS points got into conflict with the stau lifetime constraint from primordial nucleosynthesis. The results were published in [69].

In the near future, the *DM@NLO* project will finally come to an end. The successor of the author will possibly finish the stop annihilation into gluons being the last process of interest for SUSY dark matter coannihilation processes (eventually, light gluinos may represent further coannihilation partners). After the successful development of the dipoles for initial scalars, an automatisation of the real interferences seems desirable. In these diagrams an interesting challenge appears: The interface to the stop annihilation into heavy quarks - as the same $2 \to 3$ diagram appears in both processes. A Sommerfeld enhancement should be very easily implementable as all necessary tools are already existent. Nonetheless, the phenomenon of attractive and repulsive colour potentials may enrich the investigation. In current research in the area of dark matter (co-)annihilations, a handful of new ideas have been rediscovered from exotic QCD and quarkonium formations, as the formation of bound states made of the initial particles. The multiple Higgs exchange leading to Sommerfeld-like ladder diagrams is a further method to achieve greater precision (especially in the low-energy regime) with small effort. In suitable scenarios one may think about the application of these methods to *DM@NLO*.

Ultimately, the *DM@NLO* code might be published as a whole. Furthermore, turning the diagrams around could easily lead to predictions for direct detection with accuracies at next-to-leading order. The library of implemented Passarino-Veltman integrals and dipoles are very helpful for further processes (not necessarily related to SUSY) as well. Thus, the *DM@NLO* project may turn out as very useful in various contexts.

A. Some Algebra

A.1. Miscellaneous Relations

In order to use the technique of dimensional regularisation, one has to deal with Dirac matrices in D dimensions. The known identities from the Minkowski space can change! The following relations simplified the calculations:

$$\gamma^\mu \gamma_\mu = D \tag{A.1}$$

$$\gamma^\alpha \gamma^\mu \gamma_\alpha = (2-D)\gamma^\mu \tag{A.2}$$

$$\gamma^\alpha \gamma^\mu \gamma^\nu \gamma_\alpha = 4g^{\mu\nu} - (4-D)\gamma^\mu \gamma^\nu \tag{A.3}$$

$$\gamma^\alpha \gamma^\mu \gamma^\nu \gamma^\rho \gamma_\alpha = -2\gamma^\rho \gamma^\nu \gamma^\mu + (4-D)\gamma^\mu \gamma^\nu \gamma^\rho \tag{A.4}$$

In D dimensions the Dirac traces are the same like in the common Minkowski space:

$$\mathrm{Tr}(\gamma^\mu \gamma^\nu) = 4g^{\mu\nu} \to \mathrm{Tr}(\not{a}\not{b}) = 4ab \tag{A.5}$$

$$\mathrm{Tr}(\gamma^\mu \gamma^\nu \gamma^\lambda \gamma^\rho) = 4(g^{\mu\nu} g^{\lambda\rho} - g^{\mu\lambda} g^{\nu\rho} + g^{\mu\rho} g^{\nu\lambda}) \tag{A.6}$$

$$\begin{aligned}\mathrm{Tr}(\gamma^\mu \gamma^\nu \gamma^\lambda \gamma^\rho \gamma^\sigma \gamma^\tau) = 4(&2g^{\mu\nu} g^{\lambda\rho} g^{\sigma\tau} - g^{\mu\nu} g^{\lambda\sigma} g^{\rho\tau} - g^{\mu\lambda} g^{\nu\tau} g^{\rho\sigma} \\ &+ g^{\mu\lambda} g^{\nu\sigma} g^{\rho\tau} + g^{\mu\rho} g^{\nu\tau} g^{\lambda\sigma} - g^{\mu\rho} g^{\nu\sigma} g^{\lambda\tau} + g^{\mu\tau} g^{\nu\lambda} g^{\rho\sigma} \\ &- g^{\mu\sigma} g^{\nu\lambda} g^{\rho\tau} - g^{\lambda\rho} g^{\mu\tau} g^{\nu\sigma} + g^{\mu\sigma} g^{\rho\lambda} g^{\tau\nu} \\ &+ g^{\mu\rho} g^{\nu\lambda} g^{\sigma\tau} - g^{\mu\lambda} g^{\nu\rho} g^{\sigma\tau})\end{aligned} \tag{A.7}$$

$$\mathrm{Tr}(\gamma_1^\mu \cdot \ldots \cdot \gamma_n^\sigma) = \mathrm{Tr}(\gamma^5 \gamma_1^\mu \cdot \ldots \cdot \gamma_n^\sigma) = 0 \qquad (n \quad \text{odd}) \tag{A.8}$$

A.2. Projection Operators

The concept of chirality was born in the context of the observation of parity-violating processes by Madame Wu. The coupling of weakly interacting gauge bosons is highly dependent on the chirality of the particles. The projection operators filter the left- and right-handed part out of the entire Dirac spinor:

$$P_R = \frac{1+\gamma^5}{2} \qquad P_L = \frac{1-\gamma^5}{2} \qquad \text{with} \quad \gamma^5 = i\gamma^0\gamma^1\gamma^2\gamma^3 \tag{A.9}$$

$$P_R P_L = 0 \tag{A.10}$$

$$P_R P_R = P_R \qquad P_L P_L = P_L \quad \text{(idempotent)} \tag{A.11}$$

$$\mathrm{Tr}(P_L) = \mathrm{Tr}(P_R) = 2 \tag{A.12}$$

They become important in case of quark-squark-gaugino mixing, when left- and right-handed part carry a different vertex factor. In other cases, the two projection operators can simply be added to a unity matrix.

A.3. Colour Algebra

The algebraic background of the following equations needed for computing the colour factors was already explained in Section 3.1. Therefore, we just give all of the used properties of colour algebra (in the general form arising from the SU(N) group) [76,77,78].

$$\mathrm{Tr}(T^a) = 0 \tag{A.13}$$

$$\mathrm{Tr}(T^a T^b) = \frac{1}{2}\delta_{ab} \tag{A.14}$$

$$\{T^a, T^b\} = \frac{1}{N}\delta_{ab} + d^{abc}T^c \tag{A.15}$$

$$T^a_{ij}T^a_{kl} = \frac{1}{2}\left(\delta_{il}\delta_{jk} - \frac{1}{N}\delta_{ij}\delta_{kl}\right) \tag{A.16}$$

In principal, these relations are sufficient for the calculation of colour factors, nonetheless a couple of properties that can be derived from the previous ones save much time during the calculations:

$$f^{abc} = -2i\mathrm{Tr}(T^a[T^b, T^c]) \tag{A.17}$$

$$d^{abc} = 2\mathrm{Tr}(T^a\{T^b, T^c\}) \tag{A.18}$$

$$T^a T^b = \frac{1}{2}\left(\frac{1}{N}\delta_{ab} + (d^{abc} + if^{abc})T^c\right) \tag{A.19}$$

$$f^{acd}f^{bcd} = N\delta_{ab} \tag{A.20}$$

$$d^{abc}T^c = \{T^a, T^b\} - \frac{1}{N}\delta_{ab} \tag{A.21}$$

$$\mathrm{Tr}(T^a T^b T^c) = \frac{1}{4}(d^{abc} + if^{abc}) \tag{A.22}$$

$$T^a T^b T^a = -\frac{1}{2N}T^b \tag{A.23}$$

$$\mathrm{Tr}(T^a T^b T^a T^c) = -\frac{1}{4N}\delta_{bc} \tag{A.24}$$

$$f^{acd}d^{bcd} = 0 \tag{A.25}$$

$$f^{ade}f^{bef}f^{cfd} = \frac{N}{2}f^{abc} \tag{A.26}$$

$$d^{abc}d^{abd} = \left(\frac{N^2-4}{N}\right)\delta_{cd} \tag{A.27}$$

$$d^{abc}T^aT^b = \frac{N^2-4}{2N}T^c \tag{A.28}$$

$$f^{abc}T^aT^b = \frac{iN}{2}T^c \tag{A.29}$$

$$d^{abc}T^aT^bT^c = \frac{N^2-4}{2N}C_F \tag{A.30}$$

$$f^{pak}f^{kbl}f^{lcp} = -\frac{3}{2}f^{abc} \tag{A.31}$$

$$d^{pak}f^{kbl}f^{lcp} = \frac{3}{2}d^{abc} \tag{A.32}$$

$$d^{pak}d^{kbl}f^{lcp} = \frac{5}{6}f^{abc} \tag{A.33}$$

$$d^{pak}d^{kbl}d^{lcp} = -\frac{1}{2}d^{abc} \tag{A.34}$$

$$f^{abe}d^{cde} + f^{ace}d^{bde} + f^{ade}d^{bce} = 0 \tag{A.35}$$

$$f^{abe}d^{cde} + f^{cbe}d^{ade} + f^{dbe}d^{ace} = 0 \tag{A.36}$$

$$f^{abe}f^{cde} = \frac{2}{N}\left(\delta_{ac}\delta_{bd} - \delta_{ad}\delta_{bc}\right) + d^{ace}d^{bde} - d^{bce}d^{ade} \tag{A.37}$$

$$d^{abk}d^{kcl} + d^{bck}d^{kal} + d^{cak}d^{kbl} = \frac{1}{N}\left(\delta_{ab}\delta_{cl} + \delta_{ac}\delta_{bl} + \delta_{al}\delta_{bc}\right) \tag{A.38}$$

The following abbreviations are common (arithmetically expressed for the $SU(3)$ group):

$$C_F = \frac{(N^2-1)}{2N} = \frac{4}{3} \qquad T_F = \frac{1}{2} \tag{A.39}$$

The last normalisation factor is often called Dynkin index.

Within the loop calculations for the four-vertex, fairly complicated colour structures appear. We refer to [27], where the *Mathematica* package *color.m* is introduced. One can also export the source code from this reference.

B. Propagators and Couplings

All momenta k_1, k_2 and k_3 go from left to the right.

(a) 2-squark-gluon:

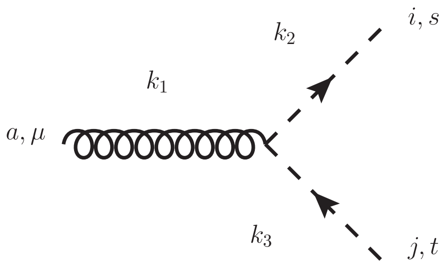

$$-ig_s T^a_{st}(k_2 - k_3)_\mu \delta_{ij}$$

Changing the direction of the arrows leads to an additional minus sign.

(b) 2-quark-gluon:

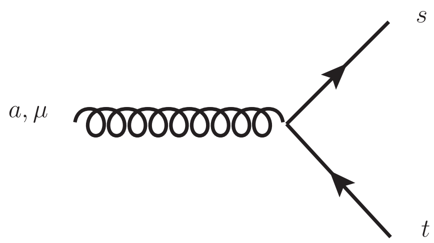

$$-ig_s T^a_{st}\gamma_\mu$$

(c) 2-ghost-gluon:

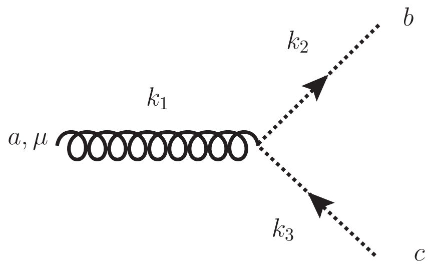

$$-g_s f_{abc} k_{2\mu}$$

It should be noted that only the particle, not the anti-particle, contributes to the vertex factor.

(d) 3-gluon:

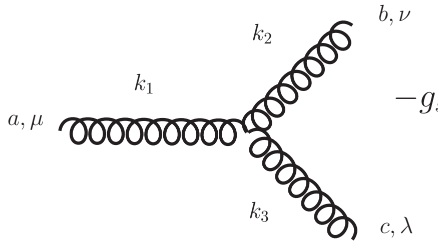

$$-g_s f_{abc}[(k_1 + k_2)_\lambda g_{\mu\nu} + (k_3 - k_2)_\mu g_{\nu\lambda} - (k_3 + k_1)_\nu g_{\mu\lambda}]$$

The minus sign originally means i^2 as one imaginary unit is contained in the colour factor.

(e) 4-gluon:

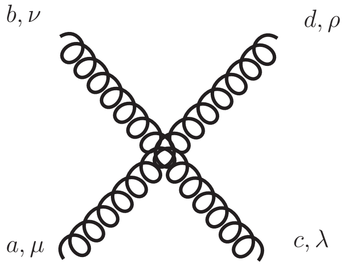

$$\begin{aligned} -ig_s^2[&f_{eab}f_{ecd}(g_{\mu\lambda}g_{\nu\rho} - g_{\mu\rho}g_{\nu\lambda}) \\ &+f_{eac}f_{edb}(g_{\mu\rho}g_{\nu\lambda} - g_{\mu\nu}g_{\rho\lambda}) \\ &+f_{ead}f_{ebc}(g_{\mu\nu}g_{\lambda\rho} - g_{\mu\lambda}g_{\nu\rho})] \end{aligned}$$

(f) 2-gluino-gluon:

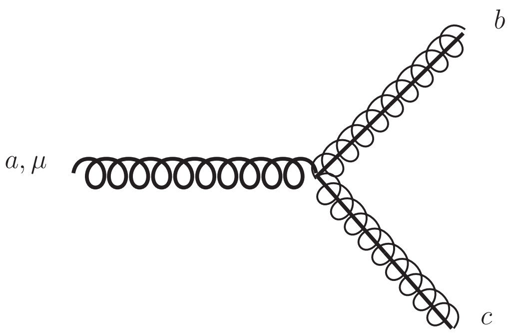

$$-g_s f_{abc}\gamma_\mu$$

(g) 2-squark-2-gluon:

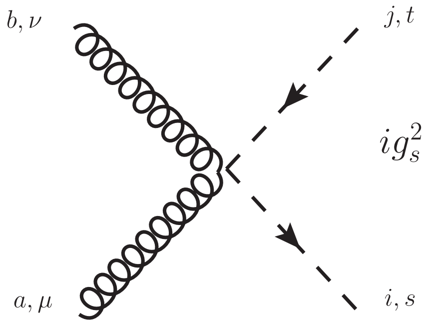

$$ig_s^2(\tfrac{1}{3}\delta_{ab}\delta_{st} + d_{abc}T^c_{st})g_{\mu\nu}\delta_{ij}$$

To express the next vertex factors we have to define the mixing of the squark types.

$$\begin{pmatrix}\tilde{q}_1\\ \tilde{q}_2\end{pmatrix} = \mathbf{R}^{\tilde{q}}\begin{pmatrix}\tilde{q}_L\\ \tilde{q}_R\end{pmatrix} = (R_{iL}, R_{iR})\begin{pmatrix}\tilde{q}_L\\ \tilde{q}_R\end{pmatrix} = \begin{pmatrix}\cos\theta_{\tilde{q}} & \sin\theta_{\tilde{q}}\\ -\sin\theta_{\tilde{q}} & \cos\theta_{\tilde{q}}\end{pmatrix}\begin{pmatrix}\tilde{q}_L\\ \tilde{q}_R\end{pmatrix} \tag{B.1}$$

Furthermore, we introduce for the vertex of four interacting squarks (we define with $\alpha = 1$ the stop sector and with 2 the sbottom sector):

$$A^\alpha_{ij} = R^\alpha_{i1}R^\alpha_{j1} - R^\alpha_{i2}R^\alpha_{j2} = \begin{pmatrix}\cos 2\theta_{\tilde{q}_\alpha} & -\sin 2\theta_{\tilde{q}_\alpha}\\ -\sin 2\theta_{\tilde{q}_\alpha} & -\cos 2\theta_{\tilde{q}_\alpha}\end{pmatrix} \tag{B.2}$$

The fermion flow makes it necessary to distinguish between two different Feynman rules:

(h) quark-squark-gluino:

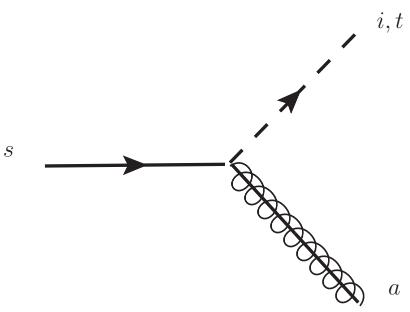

$$\sqrt{2}ig_sT^a_{st}(R_{iL}P_L - R_{iR}P_R)$$

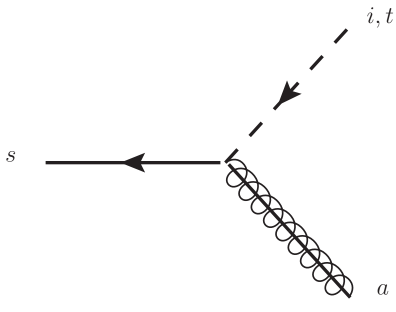

$$\sqrt{2}ig_sT^a_{st}(R_{iL}P_R - R_{iR}P_L)$$

(i) 4-squark:

Four interacting squarks lead to a lengthy expression: We sum over a, but not over the index α.

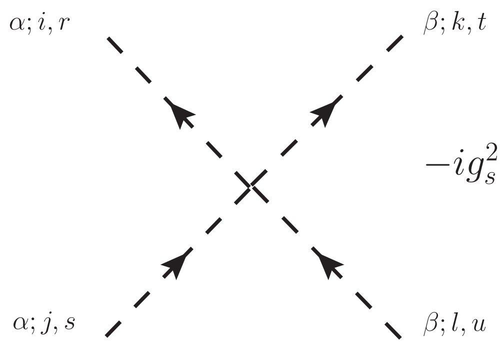

$$-ig_s^2[T^a_{rs}T^a_{tu}A^\alpha_{ij}A^\beta_{kl} + \delta_{\alpha\beta}T^a_{ru}T^a_{ts}A^\alpha_{il}A^\beta_{kj}]$$

In this chapter we used the Feynman rules in [79]. There exist uncountable other definitions, the direction of momenta, charge and fermion flows have to be handled with care.

C. Tree Level Calculations

C.1. Kinematics

A convenient way to express the cross section is the usage of the Mandelstam variables, defined via

$$s = (p_1 + p_2)^2 = (k_1 + k_2)^2 \tag{C.1}$$

$$t = (p_1 - k_1)^2 = (p_2 - k_2)^2 \tag{C.2}$$

$$u = (p_1 - k_2)^2 = (p_2 - k_1)^2 \tag{C.3}$$

fulfilling the relation

$$s + t + u = \sum_{i=1}^{4} m_i^2 = p_1^2 + p_2^2 + k_1^2 + k_2^2 \tag{C.4}$$

C.2. Born Cross Sections and Their Interferences

Although some amplitudes were mentioned in the main part of this thesis, the expression in Mandelstam variables was totally excluded, furthermore the amplitudes of the interferences. Of course, there is no interference of ghosts with other channels. Some other expectable interferences are forbidden by the colour decomposition. Finally, one should keep in mind that every squared amplitude needs a prefactor $\frac{1}{2 \cdot 9}$ since we are treating identical particles in the final state and we have to average the possible colours. The colours themselves will not be given here as it was done in detail in the chapter on decomposition.

$$\mathcal{M}_s = \frac{-ig_s^2}{s}(p_2 - p_1)^\alpha g_{\alpha\rho}[g^{\rho\nu}(k_1 + 2k_2)^\mu + g^{\mu\nu}(k_1 - k_2)^\rho - g^{\mu\rho}(2k_1 + k_2)^\nu]\epsilon_\mu^*(k_1)\epsilon_\nu^*(k_2) \tag{C.5}$$

$$|\bar{\mathcal{M}}_s|^2 = -\frac{g_s^4}{s^2}(3s^2 + 8sm_{\tilde{t}_1}^2 - 2m_{\tilde{t}_1}^2(6s + 14m_{\tilde{t}_1}^2 - 20t) - 20(ts + t^2)) \tag{C.6}$$

$$\mathcal{M}_t = (2p_1 - k_1)^\mu \frac{ig_s^2}{t - m_{\tilde{t}_1}^2}(2p_2 - k_2)^\nu \epsilon_\mu^*(k_1)\epsilon_\nu^*(k_2) \tag{C.7}$$

$$|\bar{\mathcal{M}}_t|^2 = \frac{g_s^4}{(t - m_{\tilde{t}_1}^2)^2}(2m_{\tilde{t}_1}^2 + 2t)^2 \tag{C.8}$$

$$\mathcal{M}_u = (2p_1 - k_2)^\mu \frac{ig_s^2}{t - m_{\tilde{t}_1}^2}(2p_2 - k_1)^\nu \epsilon_\mu^*(k_2)\epsilon_\nu^*(k_1) \tag{C.9}$$

$$|\bar{\mathcal{M}}_u|^2 = \frac{g_s^4}{(u - m_{\tilde{t}_1}^2)^2}(-2s + 6m_{\tilde{t}_1}^2 - 2t)^2 \tag{C.10}$$

$$\mathcal{M}_4 = ig_s^2 g^{\mu\nu}\epsilon_\mu^*(k_1)\epsilon_\nu^*(k_2) \tag{C.11}$$

$$|\bar{\mathcal{M}}_4|^2 = 4g_s^4 \tag{C.12}$$

$$\mathcal{M}_{gh} = -i\frac{g_s^2}{s}(p_2 - p_1)^\alpha g_{\alpha\rho}(k_1)_\rho - i\frac{g_s^2}{s}(p_2 - p_1)^\alpha g_{\alpha\rho}(k_2)_\rho \tag{C.13}$$

$$|\bar{\mathcal{M}}_{gh}|^2 = \frac{g_s^4}{s^2} \cdot 2(s - 2m_{\tilde{t}_1}^2 + 2t)^2 \tag{C.14}$$

We continue with interferences:

$$|\mathcal{M}_s\mathcal{M}_t| = \frac{1}{2}\frac{g_s^4}{s \cdot (t - m_{\tilde{t}_1}^2)}[s^2 + 8m_{\tilde{t}_1}^4 + 4ts - m_{\tilde{t}_1}^2(8s + 8t + 4m_{\tilde{t}_1}^2)] \tag{C.15}$$

$$|\mathcal{M}_s\mathcal{M}_u| = \frac{1}{2}\frac{g_s^4}{s \cdot (u - m_{\tilde{t}_1}^2)}[10s^2 + 16m_{\tilde{t}_1}^4 + 16ts - 8t^2 - m_{\tilde{t}_1}^2(32s + 16t)] \tag{C.16}$$

$$|\mathcal{M}_t\mathcal{M}_u| = -\frac{2g_s^4}{(t - m_{\tilde{t}_1}^2)(u - m_{\tilde{t}_1}^2)}(4m_{\tilde{t}_1}^2 - s)^2 \tag{C.17}$$

$$|\mathcal{M}_t\mathcal{M}_4| = -\frac{g_s^4}{(t - m_{\tilde{t}_1}^2)}(4t + 4m_{\tilde{t}_1}^2 - s) \tag{C.18}$$

$$|\mathcal{M}_u\mathcal{M}_4| = -\frac{g_s^4}{(u - m_{\tilde{t}_1}^2)}(12m_{\tilde{t}_1}^2 - 4t - 5s) \tag{C.19}$$

These results were implemented into the code in a twofold manner: in earlier work of S. Schmiemann and by the author of the thesis. Both are in accordance with *mircOMEGAs*. Furthermore, S. Schmiemann was able to reproduce the same cross section in the light-cone gauge instead of using ghosts.

D. NLO Calculations

D.1. Dimensional Regularisation

In Chapter 5 we mentioned the calculation of loop diagrams, but did not pay attention to the explicit performance. Here, we give the most important tools for the integration over the momenta within loops. In order to get rid of the ill-defined corrections (explained in the section about renormalisation), one has to make these contributions calculable. This can successfully be worked out using dimensional regularisation/reduction schemes (there are further methods like the one of Pauli-Villars, cut-off scheme, ...). The loop integrals get analytically continued to an arbitrary, complex number of dimensions D separating the ill-defined parts to a singular and a non-singular contribution:

$$\int d^4q \rightarrow \mu^{(4-D)/2} \int d^Dq \tag{D.1}$$

μ keeps the mass dimension of the equation equal. After integration, we take the limit $D \rightarrow 4$ and singular poles in the form of $2/(D-4)$ occur. One can imagine that every possible loop leads to the same kind of integrals. Passarino and Veltman [80] discovered this fact and developed a general type of loop integrals, the so-called Passarino-Veltman integrals. First, we write them generically:

$$T^N_{\mu_1,...,\mu_M}(p_1,...,p_{N-1},m_0,...,m_{N-1}) \tag{D.2}$$

$$= \frac{(2\pi\mu)^{(4-D)/2}}{i\pi^2} \cdot \int d^Dq \frac{q_{\mu_1}...q_{\mu_M}}{[q^2-m^2+i\epsilon][(q+p_1)^2-m_1^2+i\epsilon]...[(q+p_{N-1})^2-m_{N-1}^2+i\epsilon]}$$

This integral describes a generic loop of the form in the figure below [81]. It has to be noted that the sign of the momenta p_i depends on their chosen direction in the Feynman diagram. As a convention, one uses the nomenclature $T^1 \rightarrow A$, $T^2 \rightarrow B$ and so on. The basic idea behind the evaluation of loop diagrams is the possibility of expressing every $T^N_{\mu_1,...,\mu_M}(p_1,...,p_{N-1},m_0,...,m_{N-1})$ as a linear combination of the scalar integrals (no q in the numerator) A to D. The scalar integrals used in the calculations have the obvious form:

$$A_0 = \frac{(2\pi\mu)^{4-D}}{i\pi^2} \cdot \int d^Dq \frac{1}{[q^2-m^2+i\epsilon]} \tag{D.3}$$

$$B_0 = \frac{(2\pi\mu)^{4-D}}{i\pi^2} \cdot \int d^Dq \frac{1}{[q^2-m^2+i\epsilon][(q+p_1)^2-m_1^2+i\epsilon]} \tag{D.4}$$

$$C_0 = \frac{(2\pi\mu)^{4-D}}{i\pi^2} \cdot \int d^Dq \frac{1}{[q^2-m^2+i\epsilon][(q+p_1)^2-m_1^2+i\epsilon][(q+p_2)^2-m_2^2+i\epsilon]} \tag{D.5}$$

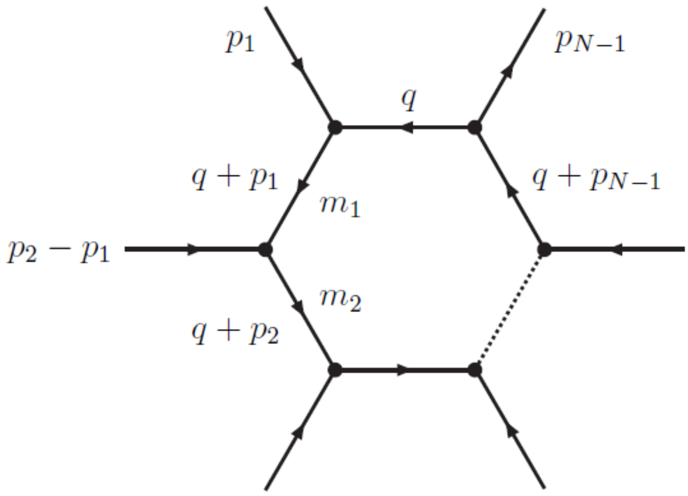

The arguments of these functions of course depend on the momentum convention as we illustrated for the 3- and 4-point function. So how is it possible to express the tensor

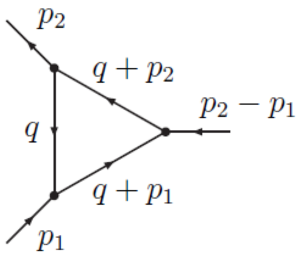

$$\equiv C_0(p_1^2, (p_1-p_2)^2, p_2^2, m_0^2, m_1^2, m_2^2)$$

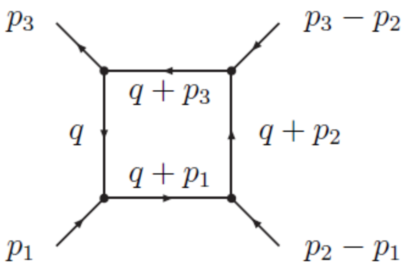

$$\equiv D_0(p_1^2, p_{21}^2, p_{32}^2, p_3^2, p_2^2, p_{13}^2, m_0^2, m_1^2, m_2^2, m_3^2)$$

integrals via these scalar ones? The answer is tensor reduction: In analogy to contracting tensors one can work out the reduced form of the $T^N_{\mu_1,\dots,\mu_M}(p_1,\dots,p_{N-1},m_0,\dots,m_{N-1})$:

$$B^\mu = p_1^\mu B_1 \tag{D.6}$$

$$B^{\mu\nu} = g^{\mu\nu} B_{00} + p_1^\mu p_1^\nu B_{11} \tag{D.7}$$

$$C^\mu = p_1^\mu C_1 + p_2^\mu C_2 \tag{D.8}$$

$$C^{\mu\nu} = g^{\mu\nu} C_{00} + \sum_{i,j=1}^{2} p_i^\mu p_j^\nu C_{ij} \tag{D.9}$$

$$C^{\mu\nu\alpha} = \sum_{i=1}^{2}(g^{\mu\nu}p_i^\alpha + g^{\nu\alpha}p_i^\mu + g^{\alpha\mu}p_i^\nu)C_{00i} + \sum_{i,j,k=1}^{2} p_i^\mu p_j^\nu p_k^\alpha C_{ijk} \tag{D.10}$$

$$D^\mu = \sum_{i=1}^{3} p_i^\mu D_i \tag{D.11}$$

$$D^{\mu\nu} = g^{\mu\nu}D_{00} + \sum_{i,j=1}^{3} p_i^\mu p_j^\nu D_{ij} \tag{D.12}$$

$$D^{\mu\nu\alpha} = \sum_{i=1}^{3}(g^{\mu\nu}p_i^\alpha + g^{\nu\alpha}p_i^\mu + g^{\alpha\mu}p_i^\nu)D_{00i} + \sum_{i,j,k=1}^{3} p_i^\mu p_j^\nu p_k^\alpha D_{ijk} \tag{D.13}$$

Those scalar integrals also decay in the four mentioned basic integrals, for instance:

$$B_1 = \frac{1}{2p_1^2}(A_0(m_0) - A_0(m_1) - (p_1^2 - m_1^2 + m_0^2)B_0) \tag{D.14}$$

They can be calculated in a rather involved way. In the results, the following variable $\epsilon := \frac{4-D}{2}$ will appear (dependent on conventions); furthermore, we remember the Gamma function:

$$\Gamma(x) = \int_0^{+\infty} e^{-t}t^{x-1}\mathrm{d}t \tag{D.15}$$

The number $\partial_x\Gamma(x)|_{x=1} = \gamma_E$ is called Euler-Mascheroni constant and has the value 0,5772. Finally, the A_0 is given by:

$$A_0 = m^2(\epsilon^{-1} - \gamma_E + \ln 4\pi - \ln\left(\frac{m^2}{\mu^2}\right) + 1 + \mathcal{O}(\epsilon)) := m^2(\Delta - \ln\left(\frac{m^2}{\mu^2}\right) + 1 + \mathcal{O}(\epsilon)) \tag{D.16}$$

With the Feynman parametrisation

$$\frac{1}{ab} = \int_0^1 \mathrm{d}x \frac{1}{(a(1-x)+bx)^2} \tag{D.17}$$

$$\frac{1}{abc} = \int_0^1 \mathrm{d}x \int_0^{1-x} \mathrm{d}y \frac{1}{(a(1-x-y)+bx+cy)^3} \tag{D.18}$$

one calculates

$$B_0 = \Delta - \int_0^1 \mathrm{d}x \ln\left(\frac{x^2p_1^2 - x(p_1^2 - m_1^2 + m_0^2) + m_0^2 - i\epsilon}{\mu^2}\right) \tag{D.19}$$

C_0 is too long to be mentioned it in this appendix. Divergences appear only in some tensor integrals as we see in the two tables.

Integral	UV div.	$(D-4)\times$ Integral
$A_0(m^2)$	$m^2\Delta$	$(D-4)\times A_0 = -2m^2$
$A_2(m^2)$	$\frac{m^4}{4}\Delta$	$(D-4)\times A_2 = -2\frac{m^4}{4}$
$B_0(p^2,m_0^2,m_1^2)$	Δ	$(D-4)\times B_0 = -2$
$B_1(p^2,m_0^2,m_1^2)$	$-\frac{1}{2}\Delta$	$(D-4)\times B_1 = 1$
$B_{00}(p^2,m_0^2,m_1^2)$	$-\left(\frac{p^2}{12}-\frac{1}{4}(m_0^2+m_1^2)\right)\Delta$	$(D-4)\times B_{00} = \left(\frac{p^2}{6}-\frac{1}{2}(m_0^2+m_1^2)\right)$
B_{11}	$\frac{1}{3}\Delta$	$(D-4)\times B_{11} = -\frac{2}{3}$
$\dot{B}_{00}$	$-\frac{1}{12}\Delta$	$(D-4)\times \dot{B}_{00} = \frac{1}{6}$
C_{00}	$\frac{1}{4}\Delta$	$(D-4)\times C_{00} = -\frac{1}{2}$
C_{00i}	$-\frac{1}{12}\Delta$	$(D-4)\times C_{00i} = \frac{1}{6}$
D_{0000}	$\frac{1}{24}\Delta$	$(D-4)\times D_{0000} = -\frac{1}{12}$

Integral	IR div. (small mass)	IR & collinear pole
$\dot{B}_0(m^2,\lambda^2,m^2) = \dot{B}_0(m^2,m^2,\lambda^2)$	$-\frac{1}{2m^2}\ln\lambda^2$	$\frac{1}{2m^2}\frac{1}{\varepsilon'}$
$\dot{B}_1(m^2,m^2,\lambda^2)$	$\frac{1}{2m^2}\ln\lambda^2$	$-\frac{1}{2m^2}\frac{1}{\varepsilon'}$
$\dot{B}_1(m^2,\lambda^2,m^2)$	0	0
$\dot{B}_{11}(m^2,m^2,\lambda^2)$	$-\frac{1}{2m^2}\ln\lambda^2$	$\frac{1}{2m^2}\frac{1}{\varepsilon'}$
$C_0(m_1^2,s,m_2^2,\lambda^2,m_1^2,m_2^2)$	$-\frac{\ln\beta_0}{\kappa}\ln\lambda^2$	$\frac{\ln\beta_0}{\kappa}\frac{1}{\varepsilon'}$
$C_0(m^2,s,0,0,m^2,0)$	-	$\frac{1}{s-m^2}\frac{\Gamma(1-\varepsilon')}{2\varepsilon'^2}\left(\frac{4\pi\mu^2m^2}{(m^2-s)^2}\right)^{-\varepsilon'}$
$C_0(0,s,0,0,0,0)$	-	$\frac{1}{s}\frac{\Gamma(1-\varepsilon')}{\varepsilon'^2}\left(\frac{4\pi\mu^2}{-s}\right)^{-\varepsilon'}$

Figure D.1.: UV and IR divergences of Passarino-Veltman integrals [81]

D.2. Tensor Reduction of Three-Point Functions

The most of the tensor integrals are already implemented in the *DM@NLO* code, so one had less work regarding tensor reduction. The three-gluon topology however requires the knowledge of the decomposition of $C^{\mu\nu\rho}$, given by

$$C^{\mu\nu\rho} = \sum_{i=1}^{2}(g^{\mu\nu}p_i^\rho + g^{\nu\rho}p_i^\mu + g^{\rho\mu}p_i^\nu)C_{00i} + \sum_{i,j,k=1}^{2} p_i^\mu p_j^\nu p_k^\rho C_{ijk} \tag{D.20}$$

which means that the components C_{001}, C_{002}, C_{111}, C_{112}, C_{122} and C_{222} have to be identified with linear combinations of already known tensors. There exists a procedure to reduce every tensor integral to the scalar basis T_0^N, but it is only necessary to end up with any implemented integrals, generically worked out in [60]. Let us apply this set of rules, starting with a contraction of the integral momentum q^μ with an external one:

$$q.p_k = \frac{1}{2}[\mathcal{D}_k - \mathcal{D}_0 - f_k], \qquad f_k = p_k^2 - m_k^2 + m_0^2 \tag{D.21}$$

The $\mathcal{D}_k$ are the factors in the denominator of the respective tensor integral. For this multiplication we define

$$R^{N,k}_{\mu_1\dots\mu_{P-1}} := T^N_{\mu_1\dots\mu_P} p_k^{\mu_P} = \frac{1}{2}\left[T^{N-1}_{\mu_1\dots\mu_{P-1}}(k) - T^{N-1}_{\mu_1\dots\mu_{P-1}}(0) - f_k \cdot T^N_{\mu_1\dots\mu_{P-1}}\right] \tag{D.22}$$

where the argument k appears, if the propagator $\mathcal{D}_k$ was cancelled. For the number of momenta $P > 1$ we can also contract $g^{\mu\nu}q_\mu q_\nu \to \mathcal{D}_0 + m_0^2$, so we define again:

$$R^{N,00}_{\mu_1\dots\mu_{P-2}} = T^N_{\mu_1\dots\mu_P} g^{\mu_{P-1}\mu_P} = T^{N-1}_{\mu_1\dots\mu_{P-2}}(0) + m_0^2 T^N_{\mu_1\dots\mu_{P-2}} \tag{D.23}$$

These reductions yield a set of $N-1$ linear equations for each tensor integral, expressed via a representation matrix X_{N-1}. We assume the matrix to be non-singular, otherwise the algorithm would break down. For $M < N$ Lorentz vectors we can give the result:

$$T^N_{00i_1\dots i_{P-2}} = \frac{1}{D+P-2-M}\left[R^{N,00}_{i_1\dots i_{P-2}} - \sum_{k=1}^{M} R^{N,k}_{ki_1\dots i_{P-2}}\right] \tag{D.24}$$

$$T^N_{ki_1\dots i_{P-1}} = (X_M^{-1})_{k\tilde{k}}\left[R^{N,\tilde{k}}_{i_1\dots i_{P-1}} - \sum_{r=1}^{P-1} \delta^{\tilde{k}}_{i_r} T^N_{00i_1\dots i_{r-1}i_{r+1}\dots i_{P-1}}\right] \tag{D.25}$$

The representation matrix X_2 and its inverse read:

$$X_2 = \begin{pmatrix} p_1^2 & p_1.p_2 \\ p_1.p_2 & p_2^2 \end{pmatrix} \qquad (X_2)^{-1} = \frac{1}{\det X_2}\begin{pmatrix} p_2^2 & -p_1.p_2 \\ -p_1.p_2 & p_1^2 \end{pmatrix} \tag{D.26}$$

where the determinant can be expressed via the Källen function:

$$\det X_2 = p_1^2 p_2^2 - (p_1.p_2)^2 = -\frac{1}{4}\lambda[(p_2 - p_1)^2, p_1^2, p_2^2] \tag{D.27}$$

Applying these formulae leads to:

$$C_{001} = \frac{1}{2}\frac{1}{D-1}\left(f_2 C_{12} + 2m_0^2 C_1 + f_1 C_{11} - B_0^1 - 2B_1^1\right) \tag{D.28}$$

$$C_{002} = \frac{1}{2}\frac{1}{D-1}\left(B_1^1 + f_1 C_{12} + 2m_0^2 C_2 + f_2 C_{22}\right) \tag{D.29}$$

The expansion of $\frac{1}{D-1}$ using the geometric series yields the ultraviolet divergence:

$$\frac{1}{3-2\epsilon} = \frac{1}{3}\sum_{i=0}^{\infty}\frac{(2\epsilon)^i}{3^i} \approx \frac{3+2\epsilon}{9} \tag{D.30}$$

The convergent integrals read:

$$C_{111} = -\frac{2}{\lambda}[p_1^2(-B_0^1 - 2B_1^1 - B_{11}^1 - f_1 C_{11} + 4C_{001}) + p_1.p_2(-B_0^1 - 2B_1^1 - B_{11}^1 - f_2 C_{11})] \tag{D.31}$$

$$C_{112} = -\frac{2}{\lambda}[p_1.p_2(-B_0^1 - 2B_1^1 - B_{11}^1 - f_1 C_{11} + 4C_{001}) + p_2^2(-B_0^1 - 2B_1^1 - B_{11}^1 - f_2 C_{11})] \tag{D.32}$$

$$C_{122} = -\frac{2}{\lambda}[p_1^2(-B_{11}^1 - C_{22}f_1 + B_{11}^2) + p_1.p_2(-B_{11}^1 - f_2 C_{22} - 4C_{002})] \tag{D.33}$$

$$C_{222} = -\frac{2}{\lambda}[p_1.p_2(-B_{11}^1 - C_{22}f_1 + B_{11}^2) + p_2^2(-B_{11}^1 - f_2 C_{22} - 4C_{002})] \tag{D.34}$$

D.3. Self-Energies

First, we define the denominators of the tensor integrals:

$$\mathcal{D}_1 = q^2 - m_1^2 \qquad \mathcal{D}_2 = (q+p)^2 - m_2^2 \tag{D.35}$$

Π denotes a self-energy, the lower index stands for the virtually corrected particle, the upper one for the particles in the loops.

D.3.1. Gluon self-energy

In this case, the amplitude can be separated into two components, a transversal (T) and a longitudinal (L) one:

$$\Pi_g = \epsilon_\mu(p)\frac{-ig_s^2}{16\pi^2}\left[\left(g^{\mu\nu} - \frac{p^\mu p^\nu}{p^2}\right)\Pi^T(p^2) + \frac{p^\mu p^\nu}{p^2}\Pi^L(p^2)\right]\epsilon_\nu^*(p) \tag{D.36}$$

We are interested in Π_T and will give only this contribution.

Quark loop/gluino loop:

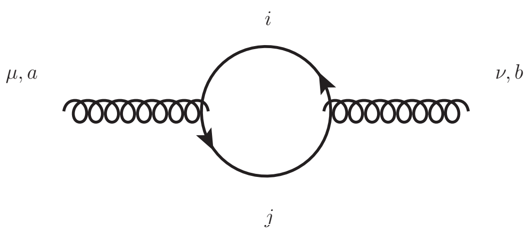

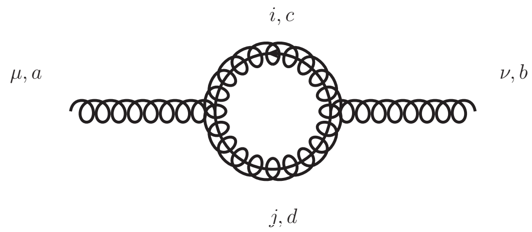

We give the general amplitude for this topology and insert specific couplings for quarks and gluinos afterwards.

$$\begin{aligned}\Pi_g^{ff} &= \mu^{\frac{4-D}{2}} \frac{-i}{16\pi^2} g_s^2 \int_q \frac{1}{\mathcal{D}_1\mathcal{D}_2} (-1) i^4 \\ &\times \mathrm{Tr}[\gamma^\mu (g_1^L P_L + g_1^R P_R)(\not{q} + m_1)\gamma^\nu (g_2^L P_L + g_2^R P_R)(\not{p} + \not{q} + m_2)]\epsilon_\nu^*(p)\end{aligned} \tag{D.37}$$

$$\begin{aligned}\Pi_g^{ff,T} &= \epsilon_\mu(p) \frac{-i g_s^2}{16\pi^2} g^{\mu\nu} [2m_1 m_2 (g_1^L g_2^R + g_1^R g_2^L) B_0 - 2(g_1^L g_2^L + g_1^R g_2^R) \\ &\times (p^2 B_1 + m_1^2 B_0 + A_0(m_2^2) - 2B_{00}]\epsilon_\nu^*(p)\end{aligned} \tag{D.38}$$

In general, we can equate $L = R$. The couplings for the gluinos read $g_1 = -g_s \gamma^\mu f^{acd}$ and $g_2 = -g_s \gamma^\nu f^{cbd}$, so the colour factor becomes $-N\delta_{ab}$. This loop gets an additional symmetry factor of 1/2 as gluinos are Majorana fermions. The couplings for the quarks read $g_1 = -i g_s T^a_{ji} \gamma^\mu$ and $g_2 = -i g_s T^b_{ij} \gamma^\nu$, so the colour factor becomes T_F.

Gluon loop:

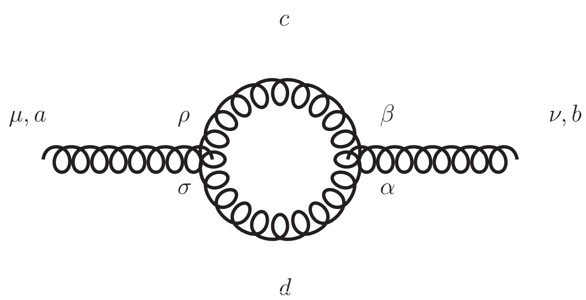

$$\Pi_g^{gg} = \epsilon_\mu(p) \mu^{\frac{4-D}{2}} \frac{1}{2} \frac{-i}{16\pi^2} g_s^2 \int_q \frac{1}{\mathcal{D}_1\mathcal{D}_2} i^2 f^{acd} f^{bdc} \Gamma^{\mu\rho\sigma} \Gamma^{\nu\alpha\beta} g_{\rho\beta} g_{\sigma\alpha} \epsilon_\nu^*(p) \tag{D.39}$$

$$\Gamma^{\mu\rho\sigma} = g^{\mu\rho}(p-q)^\sigma + g^{\rho\sigma}(2q+p)^\mu - g^{\sigma\mu}(2p+q)^\rho \tag{D.40}$$

$$\Gamma^{\alpha\beta\nu} = g^{\alpha\beta}(p+2q)^\nu + g^{\beta\nu}(p-q)^\mu - g^{\alpha\nu}(2p+q)^\beta \tag{D.41}$$

$$\Pi_g^{gg,T} = \epsilon_\mu(p) \frac{-i}{16\pi^2} g_s^2 (-N\delta_{ab}) \frac{1}{2} (10B_{00} + 2p^2 B_1 + 5p^2 B_0 + 2A_0) \epsilon_\nu^*(p) \tag{D.42}$$

Squark loop:

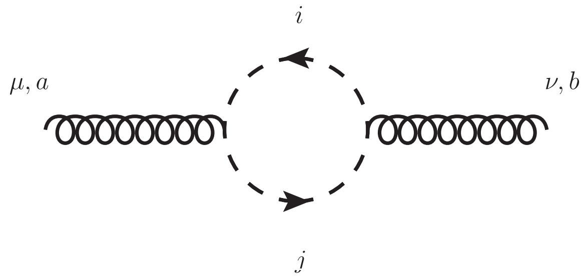

$$\Pi_g^{\tilde{q}\tilde{q}} = \epsilon_\mu(p)\mu^{\frac{4-D}{2}} \frac{-i}{16\pi^2} g_s^2 \int_q \frac{1}{\mathcal{D}_1\mathcal{D}_2} i^4 T^a_{ji} T^b_{ij} (p+2q)^\mu (p+2q)^\nu \epsilon^*_\nu(p) \tag{D.43}$$

$$\Pi_g^{\tilde{q}\tilde{q},T} = \epsilon_\mu(p) \frac{-ig_s^2}{16\pi^2} T_F \delta_{ab} \cdot 4B_{00} \epsilon^*_\nu(p) \tag{D.44}$$

Ghost loop:

Since they behave quite peculiar - as scalars, they obey Fermi-Dirac statistics - we need a (-1) factor to accommodate the closed ghost loop. The colour structure is equivalent to the gluon loop.

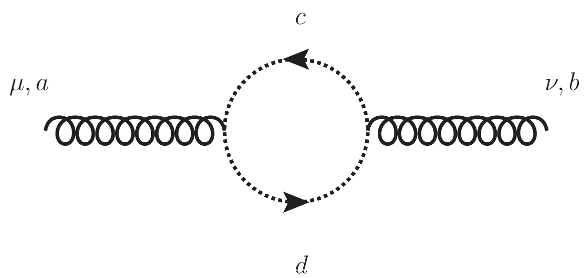

$$\Pi_g^{gh} = \epsilon_\mu(p)\mu^{\frac{4-D}{2}} \frac{-i}{16\pi^2} g_s^2 \int_q \frac{1}{\mathcal{D}_1\mathcal{D}_2} i^2 (-1) f^{acd} f^{bdc} (p+q)^\mu q^\nu \epsilon^*_\nu(p) \tag{D.45}$$

$$\Pi_g^{gh,T} = \epsilon_\mu(p) \frac{ig_s^2}{16\pi^2} (-N\delta_{ab}) B_{00} \epsilon^*_\nu(p) \tag{D.46}$$

Squark 1-point loop:

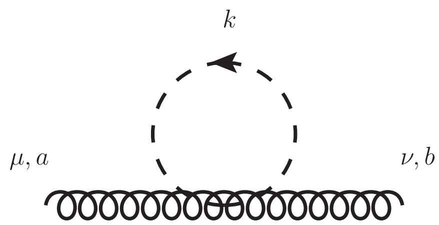

This tadpole is quite simple, so we only give

$$\Pi_g^{\tilde{q},T} = \epsilon_\mu(p)\frac{-i}{16\pi^2}g_s^2\{T^a,T^b\}A_0(m_{\tilde{q}}^2)\epsilon_\nu^*(p) \tag{D.47}$$

Gluon 1-point loop:

This one is even easier than the previous: We remember the Jacobi identity of our structure constants and see that the amplitude vanishes.

D.3.2. Squark self-energy

Quark-gluino loop:

The non-trivial mixing within this vertex can be found in App. B about couplings.

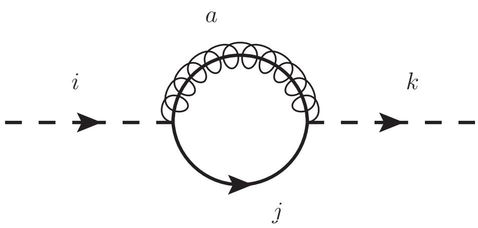

$$\begin{aligned}\Pi_{\tilde{q}}^{q\tilde{g}} = \mu^{\frac{4-D}{2}}\frac{i}{8\pi^2}g_s^2\int_q\frac{1}{\mathcal{D}_1\mathcal{D}_2}i^4T_{ji}^aT_{kj}^a(-1)\mathrm{Tr}[(R_{1L}P_L\\ -R_{1R}P_R)(\not{p}+\not{q}+m_q)(R_{1L}P_R-R_{1R}P_L)(\not{q}+m_{\tilde{g}})\end{aligned} \tag{D.48}$$

$$\Pi_{\tilde{q}}^{q\tilde{g}} = \mu^{\frac{4-D}{2}}\frac{iC_F}{8\pi^2}g_s^2\delta_{ik}[-2m_qm_{\tilde{g}}R_{1L}R_{1R}B_0+(R_{1L}^2+R_{1R}^2)(m_{\tilde{g}}B_0+p^2B_1+A_0(m_q^2))] \tag{D.49}$$

Squark-gluon loop:

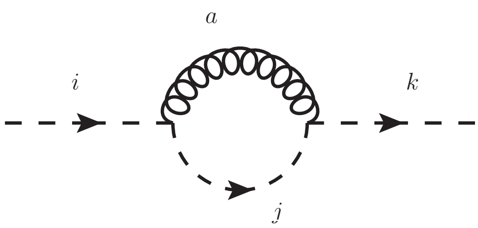

$$\Pi_{\tilde{q}}^{g\tilde{q}} = \mu^{\frac{4-D}{2}}\frac{i}{16\pi^2}g_s^2\int_q\frac{1}{\mathcal{D}_1\mathcal{D}_2}(-i)^4T_{ji}^aT_{kj}^a(2p+q)^\nu g^{\mu\nu}(2p+q)^\mu \tag{D.50}$$

$$\Pi_{\tilde{q}}^{g\tilde{q}} = \mu^{\frac{4-D}{2}} \frac{iC_F}{16\pi^2} g_s^2 \delta_{ik}(4p^2(B_0 + B_1) + A_0(m^2)) \tag{D.51}$$

Squark 1-point loop:

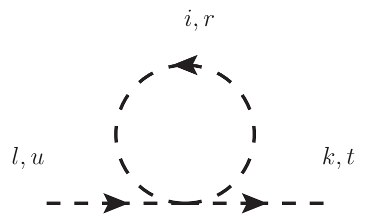

Again, the tadpole diagrams are more than simple:

$$\Pi_{\tilde{q}}^{\tilde{q}} = \mu^{\frac{4-D}{2}} \frac{i}{16\pi^2} g_s^2 (T_{rr}^a T_{tu}^a A_{ii} A_{kl} + T_{ru}^a T_{rt}^a A_{il} A_{ik}) \int_q \frac{1}{\mathcal{D}_1} \tag{D.52}$$

$$\Pi_{\tilde{q}}^{\tilde{q}} = \mu^{\frac{4-D}{2}} \frac{i}{16\pi^2} g_s^2 T_F A_{ik}^2 A_0(m_{\tilde{q}}^2) \tag{D.53}$$

Gluon one-point loop:

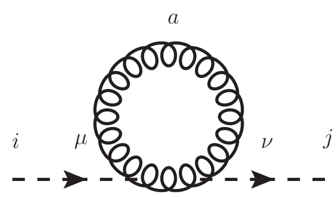

$$\Pi_{\tilde{q}}^{g} = \mu^{\frac{4-D}{2}} \frac{i}{16\pi^2} g_s^2 \int_q \frac{1}{\mathcal{D}_1} \{T^a, T^a\} g^{\mu\nu} g_{\mu\nu} \tag{D.54}$$

$$\Pi_{\tilde{q}}^{g} = \mu^{\frac{4-D}{2}} \frac{i}{16\pi^2} g_s^2 D A_0(m_g^2) = 0 \tag{D.55}$$

As the gluon is massless and $A_0(0) = 0$, we have no contribution.

D.4. Renormalisation

The principles of renormalisation were briefly explained in the main part - but the explicit expressions of the counterterms are still remaining. We first show how to renormalise the squark and gluon sector to construct the counterterms and give afterwards the needed terms to absorb the UV divergence for the vertices and self-energies of our process.

D.4.1. Squark Sector

The bare and shifted Lagrangian was already shown in 5.2.1. We continue with decomposing the matrix element $\mathcal{M}$ of the one-scalar irreducible two-point function $\mathcal{M} = i[\delta_{ij}(k^2 - m_{\tilde{q}_i}^2)\hat{\Pi}_{ij}(k^2)]$ into the Born contribution and the parts from the one-loop corrected self-energy (note that i, j are the indices for the squark mass eigenstate basis):

$$\hat{\Pi}_{ij}(k^2) = \Pi_{ij}(k^2) - \delta_{ij}\delta m_{\tilde{q}_i}^2 + \frac{1}{2}(k^2 - m_{\tilde{q}_{i,j}}^2)(\delta Z_{ij} + \delta Z_{ji}^*) \tag{D.56}$$

The expression contains the renormalised self-energy $\Pi_{ij}(k^2)$ and its corresponding counterparts (mass and wave function). The next step is, as described in Section 5.2, the application of the on-shell renormalisation conditions (5.21) providing the following expressions

$$\delta m_{\tilde{q}_i}^2 = \mathrm{Re}\Pi_{ii}(m_{\tilde{q}_i}^2) \tag{D.57}$$

$$\delta Z_{ij} = \frac{2}{m_{\tilde{q}_i}^2 - m_{\tilde{q}_j}^2}\mathrm{Re}\Pi_{ij}(m_{\tilde{q}_j}^2), i \neq j \tag{D.58}$$

$$\delta Z_{ii} = -\mathrm{Re}\frac{\partial}{\partial k^2}\Pi_{ii}(k^2)|_{k^2=m_{\tilde{q}_i}^2} \tag{D.59}$$

Gluon loop contribution:

$$\delta Z_{\tilde{q}}^{g} = C_F\frac{g_s^2}{16\pi^2}(2B_0(k^2, 0, m_{\tilde{q}}) + 2(k^2 + m_{\tilde{q}}^2)\dot{B}_0(k^2, 0, m_{\tilde{q}})) \tag{D.60}$$

Gluino loop contribution:

$$\delta Z_{\tilde{q}}^{\tilde{g}} = C_F\frac{g_s^2}{16\pi^2}[((R_{1L}^2+R_{1R}^2)(m_{\tilde{g}}^2+m_q^2+k^2)-4R_{1L}R_{1R}m_{\tilde{g}}m_q)\dot{B}_0(k^2, m_{\tilde{g}}, m_q)-B_0(k^2, m_{\tilde{g}}, m_q)] \tag{D.61}$$

The mass term, however, is easily derived by substituting the internal momentum by the squark mass in the self-energies.

D.4.2. Gluon Wave Function

The renormalisation starts once again with the bare Lagrangian, in this case given by the free-field Proca density for vector particles:

$$\mathcal{L} = -\frac{1}{4}(\partial_\mu(A_0^a)_\nu - \partial_\nu(A_0^a)_\mu)(\partial^\mu(A_0^a)^\nu - \partial^\nu(A_0^a)^\mu) \tag{D.62}$$

The matrix element for the irreducible two-point function can be expressed as follows, where the gluon self-energy $\hat{\Pi}_{\mu\nu}$ was splitted in transversal and longitudinal parts:

$$\mathcal{M} = -i\epsilon^\mu(k)\left[\left(g_{\mu\nu} - \frac{k_\mu k_\nu}{k^2}\right)\hat{\Pi}_T(k^2) + \frac{k_\mu k_\nu}{k^2}\hat{\Pi}_L(k^2)\right]\epsilon^{*\nu}(k) \tag{D.63}$$

The Ward identity together with the renormalisation conditions

$$\mathrm{Re}[\hat{\Pi}_{\mu\nu}(k^2)]|_{k^2=0}\epsilon^{*\nu}(k) = 0 \tag{D.64}$$

$$\lim_{k^2\to 0}\frac{1}{k^2}\mathrm{Re}[\hat{\Pi}_{\mu\nu}(k^2)]\epsilon^{*\nu}(k) = -\epsilon^{\mu}(k) \tag{D.65}$$

tells us that the longitudinal one is negligible. The corrected self-energy therefore has the following form, after the conditions were applied:

$$\hat{\Pi}_T(k^2) = \Pi_T(k^2) + k^2\delta Z^g \qquad \delta Z_g = -\mathrm{Re}\frac{\partial}{\partial k^2}\Pi_T(k^2)|_{k^2=0} \tag{D.66}$$

Starting from the self-energies, we again derive the δZ_g term:

Squark loop contribution:

$$\delta Z_g^{\tilde{q}} = T_F\frac{g_s^2}{144\pi^2}(3B_0(k^2,m_{\tilde{q}}^2,m_{\tilde{q}}^2) - 12m_{\tilde{q}}^2\dot{B}_0(k^2,m_{\tilde{q}}^2,m_{\tilde{q}}^2)) \tag{D.67}$$

Quark loop contribution:

$$\delta Z_g^{q} = T_F\frac{g_s^2}{36\pi^2}(6m_q^2\dot{B}_0(k^2,m_q^2,m_q^2) + 3B_0(k^2,m_q^2,m_q^2)) \tag{D.68}$$

Gluino loop contribution:

$$\delta Z_g^{\tilde{g}} = N\frac{g_s^2}{72\pi^2}(6m_q^2\dot{B}_0(k^2,m_{\tilde{g}}^2,m_{\tilde{g}}^2) + 3B_0(k^2,m_{\tilde{g}}^2,m_{\tilde{g}}^2)) \tag{D.69}$$

Gluon loop contribution:

$$\delta Z_g^{g} = -N\frac{57g_s^2}{576\pi^2}B_0(k^2,0,0) \tag{D.70}$$

Ghost loop contribution:

$$\delta Z_g^{gh} = -N\frac{3g_s^2}{576\pi^2}B_0(k^2,0,0) \tag{D.71}$$

The one-point loops do not contribute to the counterterm. For an obvious reason, a mass counterterm does not exist.

It remains the renormalisation of the strong coupling. For this procedure we need the vertex corrections from below, so we continue later.

D.5. Vertex Corrections

As we had to struggle with more than 40 vertex corrections, we can only give the result (which again means the whole amplitude and the expression with Passarino-Veltman integrals).
One should notice, that every vertex already carries factor $\mu^{\frac{4-D}{2}}$. It is more convenient to introduce the shorthand-notation:

$$\mu^{4-D}\mu^{\frac{4-D}{2}}\int\frac{d^Dq}{(2\pi)^D} = \mu^{\frac{4-D}{2}}\frac{i}{16\pi^2}\int_q \tag{D.72}$$

Again, the vertex amplitude reads $\mathcal{A}^{\cdots}_{\cdots}$ - the upper index contains the particles within the loops, the lower one stands for the corrected vertex from the tree level diagrams (3-gluon, gluon-2-ghost, 2-squark-2-gluon, 2-squark-gluon). In front of the expression, a possible non-trivial symmetry factor may be written, as introduced in 5.2.2. Let us start with the most complicated structure of the vector-vector-vector-topology:

3-GLUON CORRECTIONS

The colour factors can be factorised with the Born cross section colour factor f^{abc} in the most cases. We always express the colour structure in the first equation via all needed elements of the colour algebra and in the second one the factorisation or at least a representation with the colour basis.
We briefly comment on the potentially enormous simplification: After having performed the tensor reduction, one obtains 14 different kinematical structures (1 to 8: $k_i^\mu k_j^\nu k_k^\rho$ for $i, j, k = 1, 2$ and 9 to 14: $k_i^\mu g^{\nu\rho}$, $k_i^\nu g^{\mu\rho}$, $k_i^\rho g^{\nu\mu}$, more on the code). A linear combination of the last six yields the tree level amplitude - therefore, they have to contain the divergences, whereas all others stay convergent, at least summed up. Using the properties of the indistinguishable final gluons, one can simplify all these structures to less (some commentaries are left in the code). Moreover, the renormalisation can be split into pure Standard Model parts and SUSY parts since the three-gluon topology has some diagrams where SUSY particles do not appear at all. This requires adapted coupling and wave function renormalisation to check the finiteness separately. Only the quark loop is responsible for treating the divergences in the counterterm, the different gluon and ghost loops should cancel themselves.

Complicated integrands may drastically differ, but have numerically equivalent expressions in terms of Passarino-Veltman integrals, depending on the chosen substitution techniques!

3-gluon loop:

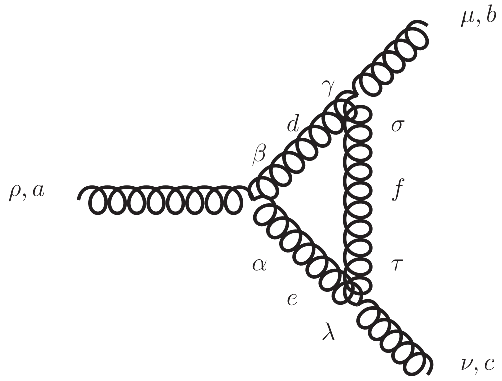

$$\mathcal{A}_g^{ggg} = \mu^{\frac{4-D}{2}} \frac{i}{16\pi^2} g_s^3 i^3 f^{ade} f^{dbf} f^{fce} \int_q \frac{-i^6}{\mathcal{D}_0\mathcal{D}_1\mathcal{D}_2} \Gamma^{\alpha\beta\rho} g^{\alpha\lambda} \Gamma^{\lambda\tau\nu} g^{\tau\sigma} \Gamma^{\gamma\mu\sigma} g^{\gamma\beta} \tag{D.73}$$

with

$$\Gamma^{\alpha\beta\rho} = g^{\rho\beta}(2k_1 + k_2 - q)^\alpha + g^{\beta\alpha}(k_2 - k_1 + 2q)^\rho - g^{\rho\alpha}(q + k_1 + 2k_2)^\beta \tag{D.74}$$

$$\Gamma^{\lambda\tau\nu} = g^{\lambda\tau}(k_2 + 2q)^\nu + g^{\tau\nu}(k_2 - q)^\lambda - g^{\nu\lambda}(2k_2 + q)^\tau \tag{D.75}$$

$$\Gamma^{\gamma\mu\sigma} = g^{\gamma\sigma}(2q - k_1)^\mu - g^{\sigma\mu}(q + k_1)^\gamma + g^{\mu\gamma}(2k_1 - q)^\sigma \tag{D.76}$$

$$\begin{aligned}
\mathcal{A}_g^{ggg} = \frac{g_s^3}{16\pi^2}\{-\frac{iN}{2} f^{abc} \times [&3k_2^\rho k_1^\mu k_1^\nu + q^\rho k_1^\mu k_1^\nu + 16k_2^\rho k_2^\mu k_1^\nu - 3k_1^\rho q^\mu k_1^\nu \\
&-13k_2^\rho q^\mu k_1^\nu + 3k_1^\rho k_1^\mu k_2^\nu - 3k_2^\rho k_1^\mu k_2^\nu - 4q^\rho k_1^\mu k_2^\nu \\
&-3k_1^\rho k_2^\mu k_2^\nu + 3q^\rho k_2^\mu k_2^\nu - 2k_1^\rho q^\mu k_2^\nu - 6k_2^\rho q^\mu k_2^\nu \\
&+9q^\rho q^\mu k_2^\nu - 6k_1^\rho k_1^\mu q^\nu - 2k_2^\rho k_1^\mu q^\nu - 9q^\rho k_1^\mu q^\nu \\
&-13k_1^\rho k_2^\mu q^\nu + 3k_2^\rho k_2^\mu q^\nu - 9k_1^\rho q^\mu q^\nu + 9k_2^\rho q^\mu q^\nu \\
&18q^\rho q^\mu q^\nu + g^{\rho\mu}(-4k_1.k_2 k_1^\nu - 8k_1.q k_1^\nu + 4q^2 k_1^\nu + 10q^\nu k_1.k_2 \\
&-4k_2^\nu k_1.q + 3k_2^\nu k_2.q + 2q^\nu k_2.q + 3q^2 k_2^\nu + 2q^2 q^\nu) \\
&+g^{\mu\nu}(k_1^\rho k_1.k_2 - 3k_2^\rho k_1.k_2 - 14q^\rho k_1.k_2 + 3k_1^\rho k_1.q + k_2^\rho k_1.q - 2q^\rho k_1.q \\
&+k_1^\rho k_2.q + 3k_2^\rho k_2.q + 2q^\rho k_2.q - 3(k_1^\rho - k_2^\rho)q^2 + 2q^2 q^\rho) \\
&+g^{\nu\rho}(4k_2^\mu k_1.k_2 + 10q^\mu k_1.k_2 + 3k_1^\mu k_1.q - 2q^\mu k_1.q - 4k_1^\mu k_2.q - 8k_2^\mu k_2.q \\
&-3q^2 k_1^\mu - 4q^2 k_2^\mu + 2q^\mu q^2)]\}
\end{aligned} \tag{D.77}$$

3-fermion loop:

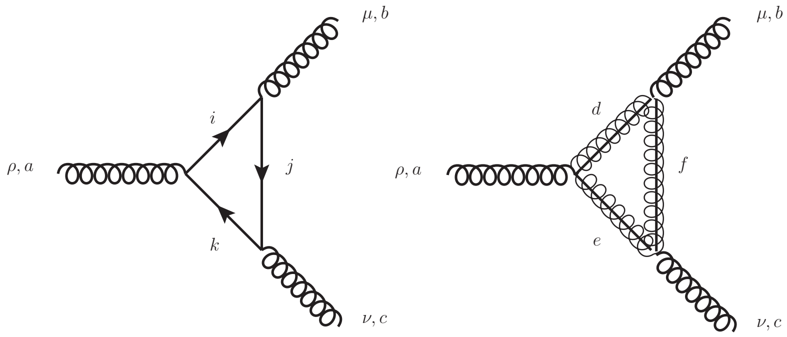

The gluino loop and the quark loop have the same topology, so only the coupling constants are different, the tensor reduction is untouched by this change. It is important to take both directions of the fermion flow into consideration! For the gluinos as Majorana particles there is no need to distinguish between two diagrams. Furthermore, the diagrams differs from each other within the colour structure.

$$\begin{aligned} \mathcal{A}_g^{fff} &= \mu^{\frac{4-D}{2}} \frac{iF_{col}}{16\pi^2} g_s^3 i^6 \int_q (-1) \frac{1}{\mathcal{D}_0\mathcal{D}_1\mathcal{D}_2} \\ \times \quad & \mathrm{Tr}[\gamma^\mu(\not{q} - \not{k}_1 + m_{f_1})\gamma^\rho(\not{q} + \not{k}_2 + m_{f_2})\gamma^\nu(\not{q} + m_{f_3})] \end{aligned} \tag{D.78}$$

$$\begin{aligned} \mathcal{A}_g^{fff} = \frac{4i \cdot C_F}{16\pi^2} g_s^3 [& g^{\nu\rho}(-m_{f_2}m_{f_3}k_1^\mu - m_{f_1}m_{f_3}k_2^\mu + q^\mu k_1.k_2 - k_2^\mu k_1.q + (m_{f_1}m_{f_2} + m_{f_2}m_{f_3} \\ & -m_{f_1}m_{f_3})q^\mu + k_1^\mu k_2.q - 2q^\mu k_2.q + (k_1^\mu + k_2^\mu - q^\mu)q^2] + g^{\mu\rho}[m_{f_2}m_{f_3}k_1^\nu \\ & +m_{f_1}m_{f_3}k_2^\nu + (m_{f_2}m_{f_1} - m_{f_2}m_{f_3} + m_{f_1}m_{f_3})q^\nu k_1.k_2 + (k_2^\nu + 2q^\nu)k_1.q \\ & -k_1^\nu k_2.q - q^2(k_1^\nu + k_2^\nu - q^\nu)] + g^{\mu\nu}[-m_{f_2}m_{f_3}k_1^\rho + (-m_{f_2}m_{f_1} + m_{f_2}m_{f_3} + m_{f_1}m_{f_3})q^\rho \\ & -k_1.k_2q^\rho + (k_1^\rho + k_2^\rho)k_1.q + q^2(k_1^\rho - k_2^\rho - q^\rho] - q^\mu k_2^\nu k_1^\rho - k_2^\mu q^\nu k_1^\rho \\ & -2q^\mu q^\nu k_1^\rho - q^\mu k_1^\nu k_2^\rho - k_1^\mu q^\nu k_2^\rho + 2q^\mu q^\nu k_2^\rho + k_2^\mu k_1^\nu q^\rho \\ & -k_1^\mu k_2^\nu q^\rho + 2q^\mu k_2^\nu q^\rho - 2k_1^\mu q^\nu q^\rho + 4q^\mu q^\nu q^\rho] \end{aligned} \tag{D.79}$$

Regarding the gluinos/quarks, the colour factor is given by:

$$F_{col}^{\tilde{g}} = i^3 f^{ade} f^{dbf} f^{fce} = -i\frac{N}{2} f^{abc} \tag{D.80}$$

$$F_{col}^{q} = T_{ik}^a T_{kj}^c T_{ji}^b = -\frac{d^{abc} - if^{abc}}{4} \tag{D.81}$$

3-squark:

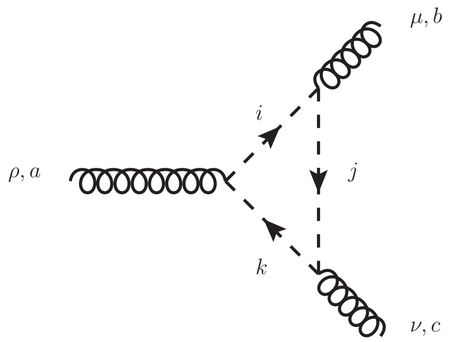

$$\mathcal{A}_g^{\tilde{q}\tilde{q}\tilde{q}} = \mu^{\frac{4-D}{2}} \frac{i}{16\pi^2} g_s^3 T_{ik}^a T_{kj}^c T_{ji}^b \int_q \frac{i^6}{\mathcal{D}_0\mathcal{D}_1\mathcal{D}_2} (2q - k_1 + k_2)^\rho (2q - k_1)^\mu (2q + k_2)^\nu \quad \text{(D.82)}$$

$$\mathcal{A}_g^{\tilde{q}\tilde{q}\tilde{q}} = \frac{-g_s^3}{16\pi^2} \frac{d^{abc} - if^{abc}}{4} [8C^{\mu\nu\rho} + 4C^{\mu\rho} k_2^\nu - 4C^{\mu\nu}(k_1 - k_2)^\rho$$
$$-4C^{\rho\nu} k_1^\mu - 2C^\rho k_1^\mu k_2^\nu - 2C^\mu (k_1 - k_2)^\rho k_2^\nu + 2C^\nu (k_1 - k_2)^\rho k_1^\mu + (k_1 - k_2)^\rho k_1^\mu k_2^\nu] \quad \text{(D.83)}$$

2-gluon loop A:

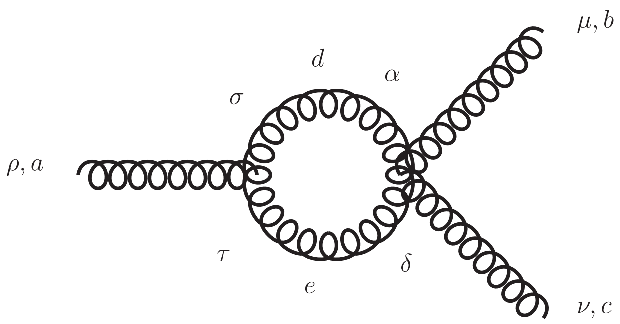

Loops with two virtual gluons can occur in three different ways. But only two are in fact different, if one rotates the diagram in a three-dimensional space. One finds a symmetry factor standing in front of the amplitudes.

$$\mathcal{A}_g^{gg} = \mu^{\frac{4-D}{2}} \frac{1}{2} \frac{i}{16\pi^2} g_s^3 (-i^4) \int_q \frac{1}{\mathcal{D}_0\mathcal{D}_1} \Gamma^{\rho\sigma\tau} g^{\sigma\alpha} g^{\tau\delta}$$
$$\times \left[(g^{\alpha\nu} g^{\delta\mu} - g^{\alpha\delta} g^{\mu\nu}) f_1 + (g^{\alpha\mu} g^{\delta\nu} - g^{\alpha\delta} g^{\mu\nu}) f_2 + (g^{\alpha\mu} g^{\delta\nu} - g^{\alpha\nu} g^{\mu\delta}) f_3 \right] \quad \text{(D.84)}$$

$$\Gamma^{\rho\sigma\tau} = g^{\rho\sigma}(k_1 + k_2 + q)_\tau - g^{\sigma\tau}(2q - k_1 - k_2)_\rho - g^{\rho\tau}(2k_1 + 2k_2 - q)_\sigma \quad \text{(D.85)}$$

$$\mathcal{A}_g^{gg} = \frac{1}{2}\frac{g_s^3}{16\pi^2}\Big[f_1[(4B^\rho g^{\mu\nu} + B^\mu g^{\rho\nu} + B^\nu g^{\mu\rho}) + B_0((k_1+k_2)^\mu g^{\rho\nu}$$
$$-2(k_1+k_2)^\nu g^{\mu\rho})] + [f_2[(4B^\rho g^{\mu\nu} + B^\mu g^{\rho\nu} + B^\nu g^{\mu\rho}) + B_0((k_1+k_2)^\nu g^{\rho\mu} \tag{D.86}$$
$$-2(k_1+k_2)^\mu g^{\nu\rho})] + 3f_3[(k_1+k_2)^\nu g^{\mu\rho} - (k_1+k_2)^\mu g^{\nu\rho}]\Big]$$

$$f_1 = \frac{iN}{2}f^{abc} \qquad f_2 = -\frac{iN}{2}f^{abc} \qquad f_3 = iNf^{abc} \tag{D.87}$$

2-gluon loop B,C:

Due to indistinguishable final states, the two diagrams are equivalent - easily shown diagrammatically by rotation at the axis of the four-gluon vertex.

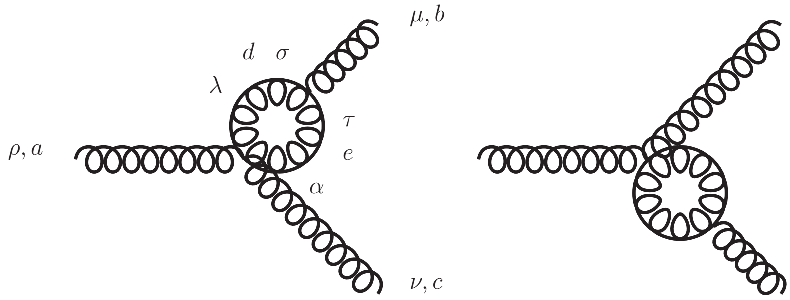

$$\mathcal{A}_g^{gg} = \mu^{\frac{4-D}{2}}\frac{1}{2}\frac{i}{16\pi^2}g_s^3\int_q \frac{(-i^4)}{\mathcal{D}_0\mathcal{D}_1}\Gamma^{\sigma\mu\tau}g^{\sigma\lambda}g^{\tau\alpha}$$
$$\times\Big[(g^{\nu\alpha}g^{\rho\lambda} - g^{\nu\lambda}g^{\rho\alpha})f_1 + (g^{\nu\lambda}g^{\rho\alpha} - g^{\rho\nu}g^{\alpha\lambda})f_2 + (g^{\rho\nu}g^{\alpha\lambda} - g^{\nu\alpha}g^{\rho\lambda})f_3\Big] \tag{D.88}$$

$$\Gamma^{\sigma\mu\tau} = g^{\sigma\mu}(q+k_1)^\tau + g^{\mu\tau}(q-2k_1)^\sigma - g^{\sigma\tau}(2q-k_1)^\mu \tag{D.89}$$

$$\mathcal{A}_g^{gg} = \frac{1}{2}\frac{g_s^3}{16\pi^2}\Big[3f_1(k_1^\nu g^{\mu\rho} - k_1^\rho g^{\mu\nu})B_0 + f_2[(k_1^\rho g^{\mu\nu}$$
$$-2k_1^\nu g^{\mu\rho} - 2k_1^\mu g^{\nu\rho})B_0 + 4B^\mu g^{\nu\rho} + B^\nu g^{\mu\rho}$$
$$+B^\rho g^{\nu\mu}] + f_3[(-k_2^\rho g^{\mu\nu} + 2k_2^\nu g^{\mu\rho} + 2k_2^\mu g^{\nu\rho}) \tag{D.90}$$
$$\times \quad B_0 - 4B^\mu g^{\nu\rho} - B^\nu g^{\mu\rho} - B^\rho g^{\nu\mu}]\Big]$$

$$f_1 = iNf^{abc} \qquad f_2 = \frac{iN}{2}f^{abc} \qquad f_3 = \frac{iN}{2}f^{abc} \tag{D.91}$$

2-squark loop A:

The diagrammatic structure of the 2-gluon loop can be transferred to the following squark loops:

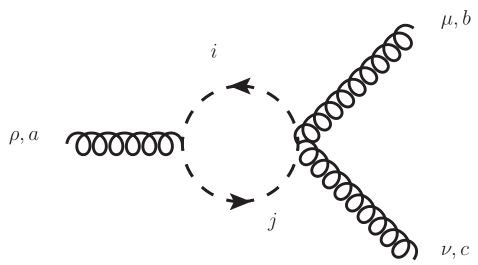

$$\mathcal{A}_g^{\tilde{q}\tilde{q},A} = \mu^{\frac{4-D}{2}} \frac{i}{16\pi^2} g_s^3 T^a_{ji} \{T^b, T^c\}_{ij} \int_q \frac{i^4}{\mathcal{D}_0 \mathcal{D}_1} (2q - k_1 - k_2)^\rho g^{\mu\nu} \tag{D.92}$$

$$\mathcal{A}_g^{\tilde{q}\tilde{q},A} = -\frac{1}{16\pi^2} g_s^3 \frac{d^{abc}}{2} (2B^\rho - (k_1 + k_2)^\rho B_0) g^{\mu\nu} \tag{D.93}$$

2-squark loop B,C:

Once again, we consider only the left diagram.

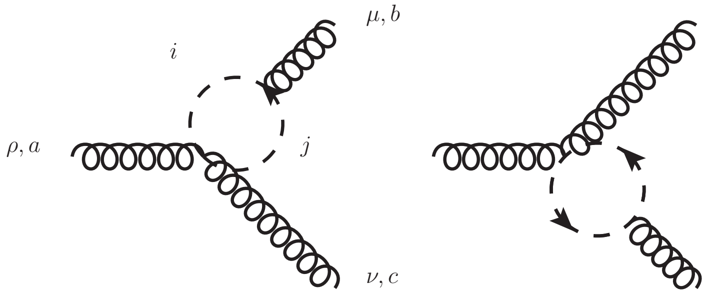

$$\mathcal{A}_g^{\tilde{q}\tilde{q},B} = \mu^{\frac{4-D}{2}} \frac{i}{16\pi^2} g_s^3 T^b_{ij} \{T^a, T^c\}_{ji} \int_q \frac{-i^4}{\mathcal{D}_0 \mathcal{D}_1} (2q - k_1)^\mu g^{\rho\nu} \tag{D.94}$$

$$\mathcal{A}_g^{\tilde{q}\tilde{q},B} = \frac{1}{16\pi^2} g_s^3 \frac{d^{abc}}{2} (2B^\mu - k_1^\mu B_0) g^{\rho\nu} \tag{D.95}$$

3-ghost loop:

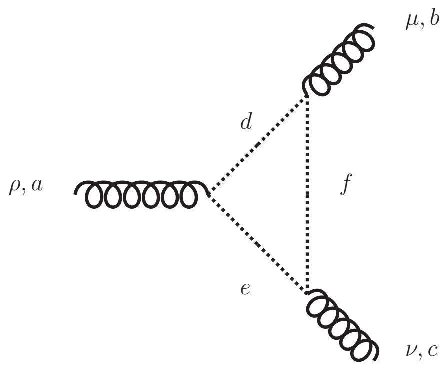

The ghost loop has to be separated into two directions of ghost flows in analogy to the closed flows in the loops from above. They are nevertheless numerically equivalent. We give results for a clockwise flow:

$$\mathcal{A}_g^{3gh} = \mu^{\frac{4-D}{2}} \frac{i}{16\pi^2} g_s^3 i^3 f^{ade} f^{dbf} f^{fce} \int_q (-1) \frac{i^6}{\mathcal{D}_0\mathcal{D}_1\mathcal{D}_2} (k_1 - q)^\rho q^\mu (q + k_2)^\nu \tag{D.96}$$

$$\mathcal{A}_g^{3gh} = \frac{-i}{16\pi^2} g_s^3 \frac{N}{2} f^{abc} (-C^{\mu\nu\rho} - C^{\rho\mu} k_2^\nu + C^{\mu\nu} k_1^\rho + C^\mu k_1^\rho k_2^\nu) \tag{D.97}$$

The UV-divergent parts are eliminated by the counterterm

$$ig_s \left(\frac{\delta g_s}{g_s} + \frac{3\delta Z_g}{2} \right) \tag{D.98}$$

GLUON-2-GHOST CORRECTIONS

Ghost exchange:

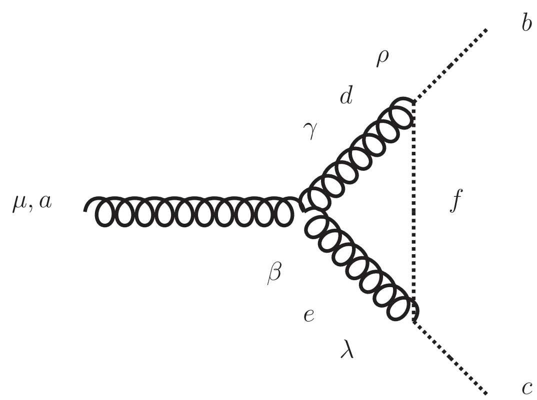

The virtual gluon could decay into to different diagrams dependent on the position of ghost and anti-ghost. We therefore have for each corrections always two diagrams (flow directions - A: bottom-up, B: top-down).

$$\mathcal{A}_{gh}^{gh-gg,A} = \mu^{\frac{4-D}{2}} \frac{i}{16\pi^2} g_s^3 i^3 f^{ade} f^{dbf} f^{fce} \int_q \frac{i^6}{\mathcal{D}_0\mathcal{D}_1\mathcal{D}_2} \Gamma^{\mu\gamma\beta} g^{\gamma\rho} g^{\beta\lambda} q^\lambda k_1^\rho \tag{D.99}$$

$$\Gamma^{\mu\gamma\beta} = g^{\mu\gamma}(2k_1 + k_2 - q)^\beta + g^{\beta\gamma}(2q + k_2 - k_1)^\mu - (k_1 + 2k_2 + q)^\gamma g^{\mu\beta} \tag{D.100}$$

$$\mathcal{A}_{gh}^{gh-gg,A} = -\frac{i}{16\pi^2}\frac{N}{2} f^{abc} g_s^3 [-2C^\mu k_1.k_2 + C^{\mu\nu} k_1^\nu - B_0 k_1^\mu + C^\nu(4k_1^\mu k_2^\nu - k_1^\mu k_1^\nu)] \tag{D.101}$$

$$\mathcal{A}_{gh}^{gh-gg,B} = \mu^{\frac{4-D}{2}} \frac{i}{16\pi^2} g_s^3 i^3 f^{ade} f^{dbf} f^{fce} \int_q \frac{i^6}{\mathcal{D}_0\mathcal{D}_1\mathcal{D}_2} \Gamma^{\alpha\gamma\beta} g^{\gamma\rho} g^{\beta\lambda} q^\rho k_2^\lambda \tag{D.102}$$

$$\mathcal{A}_{gh}^{gh-gg,B} = -\frac{i}{16\pi^2}\frac{N}{2} f^{abc} g_s^3 [2C^\mu k_1.k_2 + C^{\mu\nu} k_2^\nu - B_0 k_2^\mu + C^\nu(-2k_2^\mu k_2^\nu - k_2^\mu k_2^\nu)] \tag{D.103}$$

Gluon exchange:

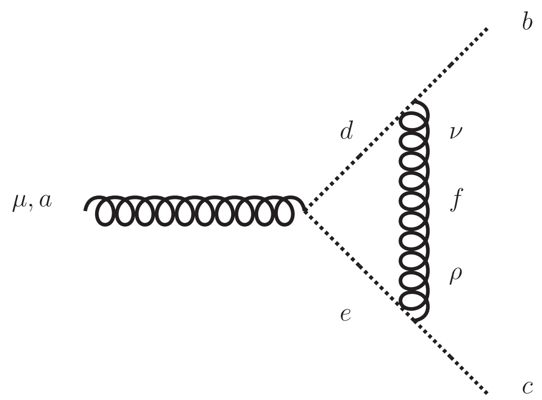

$$\mathcal{A}_{gh}^{2gh-g,A} = \mu^{\frac{4-D}{2}} \frac{i}{16\pi^2} i^3 f^{ade} f^{dbf} f^{fce} g_s^3 \int_q \frac{-i^6}{\mathcal{D}_0\mathcal{D}_1\mathcal{D}_2} k_1.(q + k_2)(k_1 - q)^\mu \tag{D.104}$$

$$\mathcal{A}_{gh}^{2gh-g,A} = -\frac{i}{16\pi^2}\frac{N}{2} f^{abc} g_s^3 k_1.k_2 (k_1^\mu(C_0 + C_1) - k_2^\mu C_2 + k_1^\mu C_2 - k_1^\mu C_{12} - k_2^\mu C_{22}) \tag{D.105}$$

$$\mathcal{A}_{gh}^{2gh-g,B} = \mu^{\frac{4-D}{2}} \frac{i}{16\pi^2} i^3 f^{ade} f^{dbf} f^{fce} g_s^3 \int_q \frac{-i^6}{\mathcal{D}_0\mathcal{D}_1\mathcal{D}_2}(q+k_2)^\mu k_2.(q-k_1) \tag{D.106}$$

$$\mathcal{A}_{gh}^{2gh-g,B} = -\frac{i}{16\pi^2}\frac{N}{2} f^{abc} g_s^3 [k_1.k_2(-k_2^\mu(C_0+C_1+C_2+C_{12}) + k_1^\mu(C_1+C_{11})) + k_2^\mu C_{00}] \tag{D.107}$$

It remains the renormalisation procedure.

FOUR-VERTEX CORRECTIONS

This vertex mostly has no complicated kinematical structures. However, the colour algebra as well as combinatorics are quite intricate in this context! Colour factors and Passarino-Veltman integrals have been checked twice, partly based on previous calculations by S. Schmiemann. Large parts of ultraviolet divergences cancel themselves without taking the counterterm into account. One finds the striking pattern that loops containing two scalars/bosons subtract divergences of three scalars/bosons in a loop. It remains to investigate combinatorial factors again since they currently seem to be the only reason how to absorb the last poles.

Regarding the four-vertex, the gluon has four possibilities to build a loop:

<u>Gluon exchange A (left):</u>

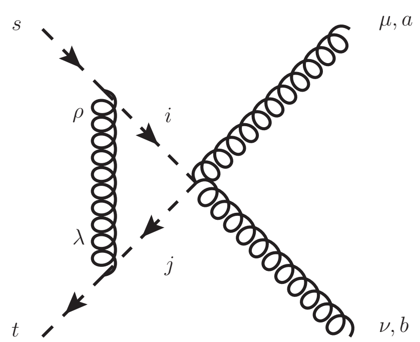

$$\mathcal{A}_4^{gA} = \mu^{\frac{4-D}{2}} \frac{i}{16\pi^2} g_s^4 \int_q \frac{1}{\mathcal{D}_0\mathcal{D}_1\mathcal{D}_2}(i^6)\{T^a,T^b\}T^c_{is}T^c_{tj} g^{\mu\nu}(2p_1-q)_\rho g^{\rho\lambda}(2p_2+q)_\lambda \tag{D.108}$$

$$\begin{aligned}\mathcal{A}_4^{gA} &= \frac{g_s^4}{16\pi^2}\left(\frac{C_F}{N}\delta_{ab}\delta_{ts} - \frac{1}{2N}d^{abc}T^c_{ts}\right) \\ \times &\quad (4p_1.p_2C_0 + 2(p_1.p_2C_2 - m_1^2C_1 + p_1.p_2C_2 - m_2^2C_2) - B_0)g^{\mu\nu}\end{aligned} \tag{D.109}$$

Gluon exchange B (right):

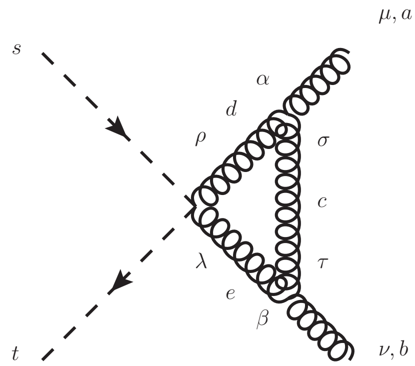

$$\mathcal{A}_4^{gB} = \mu^{\frac{4-D}{2}} \frac{i}{16\pi^2} g_s^4 \left(\frac{1}{N}\delta_{st}\delta_{de} + d^{def} T_{ts}^f\right) f^{dac} f^{cbe} \int_q \frac{-i^4}{\mathcal{D}_0\mathcal{D}_1\mathcal{D}_2} g^{\rho\alpha} g^{\sigma\tau} g^{\lambda\beta}$$
$$\times \quad (g^{\alpha\mu}(2k_1 - q)_\sigma + g^{\alpha\sigma}(2q - k_1)_\mu - g^{\mu\sigma}(q + k_1)_\alpha)$$
$$\times \quad (g^{\beta\tau}(2q + k_2)_\nu - g^{\nu\tau}(q - k_2)_\beta - g^{\beta\nu}(q + 2k_2)_\tau) \tag{D.110}$$

$$\mathcal{A}_4^{gB} = -\left(\frac{3}{2} d^{abd} T_{ts}^d + \delta_{ab}\delta_{ts}\right) \frac{g_s^4}{16\pi^2} [(4k_1^\nu k_2^\mu - 2k_2^\nu k_1^\mu - 5g^{\mu\nu} k_1.k_2) C_0 + 10C^{\mu\nu}$$
$$-k_1.k_2 g^{\mu\nu}(C_1 + C_2) + 2B_0 g^{\mu\nu} - 4k_1^\mu C^\nu + 4k_2^\nu C^\mu - k_1^\nu C^\mu + k_2^\mu C^\nu] \tag{D.111}$$

Gluon exchange C (above):

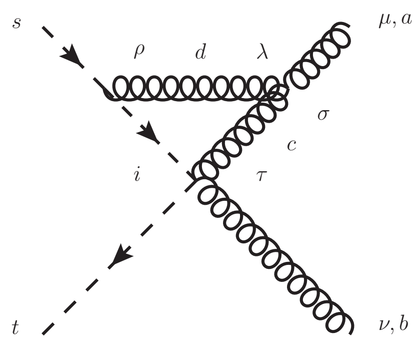

$$\mathcal{A}_4^{gC} = \mu^{\frac{4-D}{2}} \frac{i}{16\pi^2} g_s^4 \int_q \frac{1}{\mathcal{D}_0\mathcal{D}_1\mathcal{D}_2} (-i^6) f^{acd} \{T^c, T^b\} T_{is}^d$$
$$\times \quad (2p_1 - q)_\rho g^{\rho\lambda} g^{\sigma\nu} [(q + k_1)_\sigma g^{\mu\lambda} - (2k_1 - q)_\lambda g^{\mu\sigma} + (k_1 - 2q)_\mu g^{\lambda\sigma}] \tag{D.112}$$

$$\mathcal{A}_4^{gC} = \frac{3}{4}\left(-d^{abd} - if^{abd}\right)T_{ts}^d \cdot \frac{g_s^4}{16\pi^2}[-g^{\mu\nu}(4p_1.k_1C_0 + B_0 \\ +2p_1.k_1(C_1 + C_2) + 2m_1^2C_1) + 2(p_1^\mu k_1^\nu + k_1^\mu p_1^\nu)C_0 - C^\mu k_1^\nu \\ +2p_1^\mu C^\nu - k_1^\mu C^\nu - 4p_1^\nu C^\mu + C^{\mu\nu}] \tag{D.113}$$

Gluon exchange D (below):

Take a three-dimensional look on the gluon exchange C: By rotating, we obtain the same for the gluon exchange above - the cross section contribution is, naturally, equal.

We do not give the u-channel-like contributions since they are easily calculated by changing the outgoing momenta and the colours a and b so that the colour structure needs a changed sign in the if^{abc} basis vector.
Once again, we have to treat four possible ways of exchanging a squark (we exclude the u-channel-like diagrams once more).

Squark exchange A(left)

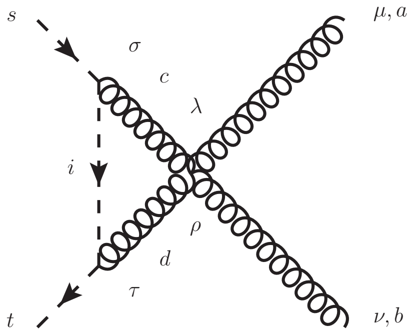

$$\mathcal{A}_4^{\tilde{q}A} = \mu^{\frac{4-D}{2}}\frac{i}{16\pi^2}g_s^4\int_q \frac{-i^6}{\mathcal{D}_0\mathcal{D}_1\mathcal{D}_2}T_{is}^cT_{ti}^d(p_1+q)_\lambda(q-p_2)_\rho \\ \times \quad [f^{edc}f^{eba}(g_{\mu\lambda}g_{\nu\rho} - g_{\mu\rho}g_{\nu\lambda}) + f^{edb}f^{eac}(g_{\mu\rho}g_{\nu\lambda} - g_{\mu\nu}g_{\rho\lambda}) + f^{eda}f^{ecb}(g_{\mu\nu}g_{\rho\lambda} - g_{\mu\lambda}g_{\nu\rho})] \tag{D.114}$$

$$\mathcal{A}_4^{\tilde{q}A} = \frac{g_s^4}{16\pi^2}\{(F_2 - F_3)[(-C_{00} + B_0 + m_0^2C_0 + p_1.p_2(C_2 + C_1 - C_0) \\ -m_1^2C_1 - m_2^2C_2)g^{\mu\nu} + p_1^\mu p_1^\nu(C_1 - C_{11}) \\ +p_2^\mu p_2^\nu(C_2 - C_{22})] + p_1^\mu p_2^\nu[F_1(C_0 - C_1 - C_2) \\ +F_2C_{12} + F_3(C_2 + C_1 - C_{12})] + p_2^\mu p_1^\nu[F_1(C_2 + C_1 - C_0) \\ +F_2(C_0 - C_2 - C_1 + C_{12}) - F_3C_{12}]\} \tag{D.115}$$

$$F_1 = -\frac{iN}{2} f^{abc} \tag{D.116}$$

$$F_2 = -\frac{1}{2}\delta_{ab}\delta_{ts} + \frac{N}{4}\Big(if^{abc} - d^{abc}\Big)T^c_{ts} \tag{D.117}$$

$$F_3 = \frac{1}{2}\delta_{ab}\delta_{ts} + \frac{N}{4}\Big(if^{abc} + d^{abc}\Big)T^c_{ts} \tag{D.118}$$

Squark exchange B (right):

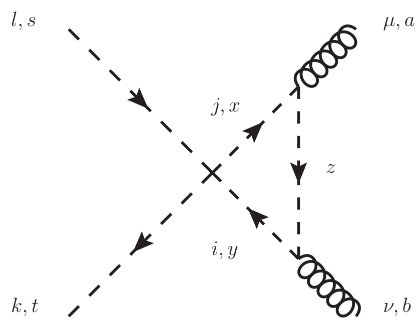

$$\begin{aligned}\mathcal{A}_4^{\tilde{q}B} = \mu^{\frac{4-D}{2}} \frac{i}{16\pi^2} g_s^4 [T^c_{yx}T^c_{ts}A_{ij}A_{11} + T^c_{ys}T^c_{tx}A_{i1}A_{1j}]T^a_{xz}T^b_{zy} \\ \times \int_q \frac{1}{\mathcal{D}_0\mathcal{D}_1\mathcal{D}_2}(i^6)(2q+k_1)_\mu(2q-k_2)_\nu\end{aligned} \tag{D.119}$$

$$\begin{aligned}\mathcal{A}_4^{\tilde{q}B} = \frac{g_s^4}{16\pi^2}[T^c_{yx}T^c_{ts}A_{ij}A_{11} + T^c_{ys}T^c_{tx}A_{i1}A_{1j}]T^a_{xz}T^b_{zy}[4C_{00}g^{\mu\nu} + k_1^\mu k_1^\nu(2C_1 + 4C_{11}) \\ + k_2^\mu k_2^\nu(4C_{22} + 2C_2) - k_1^\mu k_2^\nu(4C_{12} + 2C_2) - k_2^\mu k_1^\nu(C_0 + 2C_1 + 4C_{12})]\end{aligned} \tag{D.120}$$

$$F_1 = \frac{1}{4}d^{abc}T^c_{ts} + \frac{i}{4}f^{abc}T^c_{ts} \tag{D.121}$$

$$F_2 = \frac{N^2-1}{4N^2}\delta_{ab}\delta_{ts} - \frac{1}{4N}d^{abc}T^c_{ts} - \frac{i}{4N}f^{abc}T^c_{ts} \tag{D.122}$$

with

$$[T^c_{yx}T^c_{ts}A_{ij}A_{11} + T^c_{ys}T^c_{tx}A_{i1}A_{1j}]T^a_{xz}T^b_{zy} = F_1A_{ij}A_{11} + F_2A_{i1}A_{1j} \tag{D.123}$$

Squark exchange C (above):

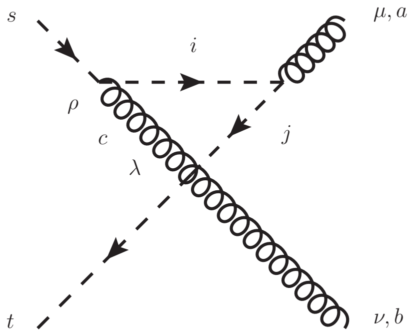

$$\mathcal{A}_4^{\tilde{q}C} = \mu^{\frac{4-D}{2}} \frac{i}{16\pi^2} g_s^4 \int_q \frac{1}{\mathcal{D}_0\mathcal{D}_1\mathcal{D}_2} (-i^6)\{T^b, T^c\} T^a_{ji} T^c_{is} g^{\rho\lambda} g^{\lambda\nu} (q+p_1)_\rho (2q-k_1)_\mu \quad \text{(D.124)}$$

$$\begin{aligned}\mathcal{A}_4^{\tilde{q}C} &= -\left[\frac{N^2-2}{4N^2}\delta_{ab}\delta_{ts} + \frac{1}{2N}\left(-d^{abc} + i f^{abc}\right) T^c_{ts}\right] \frac{g_s^4}{16\pi^2} \\ &\times \quad (2C^{\mu\nu} + 2p_1^\nu C^\mu - k_1^\mu C^\nu - p_1^\nu k_1^\mu)\end{aligned} \quad \text{(D.125)}$$

Squark exchange D (below):

This amplitude does not have to be treated for the same reason as in case of gluon exchange.

Gluon loop:

Combinatorics yields a symmetry factor of 1/2.

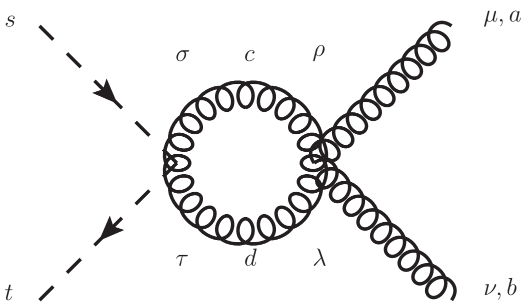

$$\begin{aligned}\mathcal{A}_4^{gg} = \mu^{\frac{4-D}{2}} \frac{1}{2} \frac{i}{16\pi^2} g_s^4 \{T^d, T^c\}_{tj} \int_q \frac{1}{\mathcal{D}_0\mathcal{D}_1} (-i^4) g^{\sigma\tau} g^{\sigma\rho} g^{\tau\lambda} \\ \times [f^{eab} f^{ecd}(g_{\mu\rho}g_{\nu\lambda} - g_{\nu\rho}g_{\mu\lambda}) + f^{eac} f^{edb}(g_{\nu\rho}g_{\mu\lambda} \\ -g_{\mu\nu}g_{\rho\lambda}) + f^{ead} f^{ebc}(g_{\mu\nu}g_{\rho\lambda} - g_{\mu\rho}g_{\nu\lambda})]\end{aligned} \quad \text{(D.126)}$$

$$\mathcal{A}_4^{gg} = \frac{g_s^4}{16\pi^2}\frac{1}{2}(-B_0)\Bigg[(1-D)\cdot(\delta_{ab}\delta_{ts} + \frac{N}{2}d^{abd}T^d_{ts}) + (D-1)\cdot(-\delta_{ab}\delta_{ts} - \frac{N}{2}d^{abd}T^d_{ts})\Bigg] \tag{D.127}$$

The tensor reductions for the coming loops are trivial, so we only give the amplitude.

Squark loop:

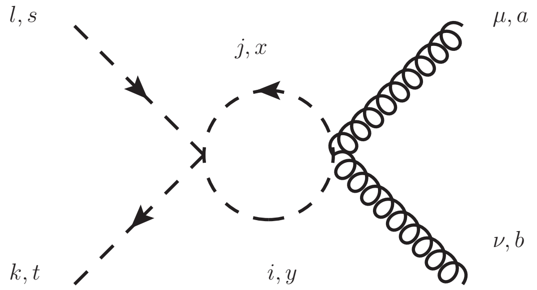

$$\mathcal{A}_4^{\tilde{q}\tilde{q}} = \mu^{\frac{4-D}{2}}\frac{i}{16\pi^2}g_s^4[T^c_{yx}T^c_{ts}A_{ij}A_{11} + T^c_{ys}T^c_{tx}A_{i1}A_{1j}]\{T^a,T^b\}\int_q \frac{i^4}{\mathcal{D}_0\mathcal{D}_1}g^{\mu\nu} \tag{D.128}$$

$$F_1 = \frac{1}{2}d^{abc}T^c_{ts} \tag{D.129}$$

$$F_2 = \frac{N^2-1}{2N^2}\delta_{ab}\delta_{ts} - \frac{1}{2N}d^{abc}T^c_{ts} \tag{D.130}$$

with

$$[T^c_{yx}T^c_{ts}A_{ij}A_{11} + T^c_{ys}T^c_{tx}A_{i1}A_{1j}]\{T^a,T^b\} = F_1A_{ij}A_{11} + F_2A_{i1}A_{1j} \tag{D.131}$$

Squark-gluon loop:

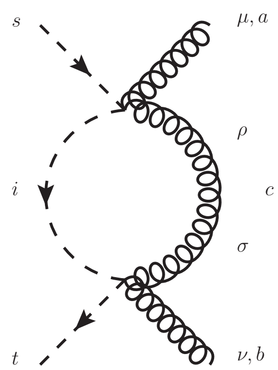

$$\mathcal{A}_4^{g\tilde{q}} = \mu^{\frac{4-D}{2}} \frac{i}{16\pi^2} g_s^4 \int_q \frac{1}{\mathcal{D}_0 \mathcal{D}_1} (-i^4) g^{\mu\rho} g^{\rho\sigma} g^{\sigma\nu} \{T^a, T^c\}\{T^b, T^c\} \tag{D.132}$$

$$\{T^a, T^c\}\{T^b, T^c\} = \frac{N^2-2}{2N^2}\delta_{ab}\delta_{ts} + \frac{N^2-4}{4N}\left[d^{abc} + i f^{abc}\right] T^c_{ts} \tag{D.133}$$

We end with the counterterm:

$$i g_s^2 \left(2\frac{\delta g_s}{g_s}\delta_{ij} + \delta Z_g \delta_{ij} + \delta Z_{ij} + \delta Z^*_{ji} \right) \tag{D.134}$$

In this vertex the term g_s^2 has to be renormalised. Hence, as we stop before NNLO, we take in fact the mixing term of the binomial which is still at NLO, carrying a factor 2.

2-SQUARK-GLUON CORRECTIONS

The general structure of this topology was calculated with the help of [12] where the generic diagram was evaluated (in the convention below; note, that also Mandelstam variables change). By rotating and renaming the momenta, we enjoy the advantage of having the opportunity to describe five vertex corrections with one (two for t-, u-channel and one for the left hand side of the s-channel).

From the convention of momenta, it follows that

$$\mathcal{D}_0 = q^2 - M_0^2 \qquad \mathcal{D}_1 = (q-p_1)^2 - M_1^2 \qquad \mathcal{D}_2 = (q-p_2)^2 - M_2^2 \tag{D.135}$$

Gluon-2-squark loop:

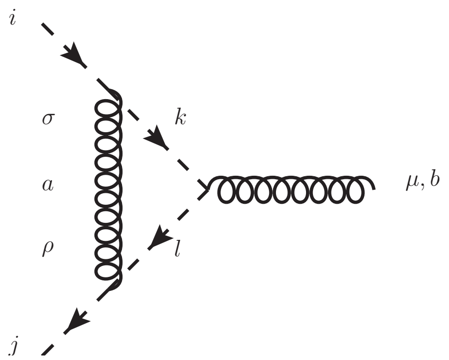

$$\mathcal{A}_s^{g\tilde{q}\tilde{q}} = \mu^{\frac{4-D}{2}} \frac{i}{16\pi^2} g_s^3 T^B_{lk} T^a_{jl} T^a_{ki} (-i^6) \int_q \frac{1}{\mathcal{D}_0\mathcal{D}_1\mathcal{D}_2} (2q-p_1-p_2)^\mu (q-2p_1)^\sigma g_{\sigma\rho} (q-2p_2)^\rho \tag{D.136}$$

$$
\begin{aligned}
\mathcal{A}_s^{g\tilde{q}\tilde{q}} =& \frac{g_s^3}{16\pi^2}\left(\frac{1}{2N}T^a_{ji}\right)\Big\{2(p_1-p_2)^\mu B_1 + 2p_1^\mu B_0 - 2p_1^\mu M_0^2 C_1 - 2p_2^\mu M_0^2 C_2 \\
& - 4[(p_1+p_2)^\mu C_{00} + p_1^\mu(p_1^2+p_1.p_2)C_{11} + p_2^\mu(p_2^2+p_1.p_2)C_{22} \\
& + p_1^\mu(p_2^2+p_1.p_2)C_{12} + p_2^\mu(p_1^2+p_1.p_2)C_{12}] - 8p_1.p_2(p_1^\mu C_1 + p_2^\mu C_2) \\
& - (p_1+p_2)^\mu[B_0 + M_0^2C_0 + 2p_1^2C_1 + 2p_2^2C_2 + 2p_1.p_2(C_1+C_2+2C_0)]\Big\}
\end{aligned} \tag{D.137}
$$

Squark-2-gluon loop:

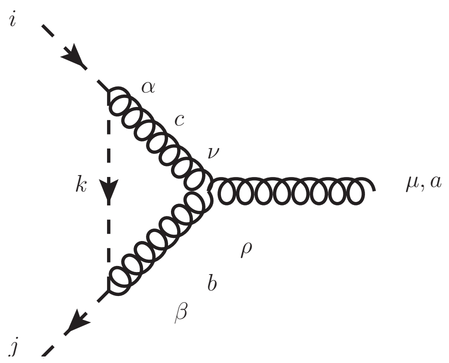

$$
\mathcal{A}_s^{gg\tilde{q}} = \mu^{\frac{4-D}{2}}\frac{i}{16\pi^2}g_s^3 f^{abc}T^c_{ki}T^b_{jk}i^6\int_q \frac{1}{\mathcal{D}_0\mathcal{D}_1\mathcal{D}_2}\Gamma^{\mu\nu\rho}g_{\nu\alpha}(q+p_1)^\alpha g_{\rho\beta}(q+p_2)^\beta \tag{D.138}
$$

$$
\Gamma^{\mu\nu\rho} = g^{\mu\nu}(p_2-2p_1+q)^\rho + g^{\nu\rho}(p_1+p_2-2q)^\mu + g^{\rho\mu}(q-2p_2+p_1)^\nu \tag{D.139}
$$

$$
\begin{aligned}
\mathcal{A}_s^{gg\tilde{q}} =& -\frac{g_s^3}{16\pi^2}\left(\frac{N}{2}T^a_{ji}\right)\Big\{p_1^\mu[2B_0 + 2M_0^2C_0 - 2C_{00} + (p_2^2 - p1.p_2)C_0 \\
& - (p_2^2 - 3p_1.p_2)C_1 - (3p_2^2 - p_1.p_2)C_2 - 2(p_1^2+p_1.p_2)C_{11} - 2(p_2^2+p_1.p_2)C_{12}] \\
& + p_2^\mu[2B_0 + 2M_0^2C_0 - 2C_{00} + (p_1^2 - p1.p_2)C_0 - (3p_1^2 - p_1.p_3)C_1) \\
& - (p_1^2 - 3p_1p_2)C_2 - 2(p_1^2+p_1.p_2)C_{12} - 2(p_2^2+p_1.p_2)C_{22}]\Big\}
\end{aligned} \tag{D.140}
$$

Quark-2-gluino loop:

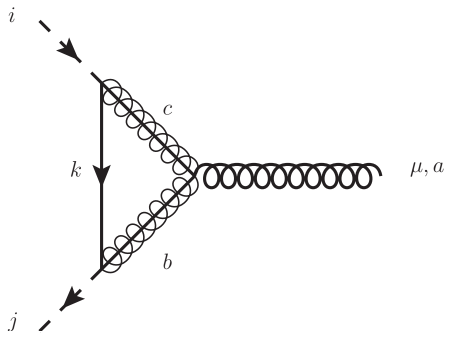

$$
\begin{aligned}
\mathcal{A}_s^{q\tilde{g}\tilde{g}} =& \mu^{\frac{4-D}{2}} \frac{i}{16\pi^2}(-i^6) g_s^3 f^{abc} T^c_{ki} T^b_{jk} \int_q (-1) \frac{1}{\mathcal{D}_0 \mathcal{D}_1 \mathcal{D}_2} \\
& \mathrm{Tr}[(g_2^L P_L + g_2^R P_R)(\not{q} + M_0)(g_1^L P_L + g_1^R P_R) \\
\times \quad & (\not{q} - \not{p}_1 + M_1)\gamma^\mu (g_0^L P_L + g_0^R P_R)(\not{q} - \not{p}_2 + M_2)]
\end{aligned} \tag{D.141}
$$

$$
g_0^L = 1 \qquad g_0^R = 1 \tag{D.142}
$$

$$
g_1^L = \sqrt{2} R_{1R} \qquad g_1^R = -\sqrt{2} R_{1L} \tag{D.143}
$$

$$
g_2^L = -\sqrt{2} R_{1L} \qquad g_2^R = \sqrt{2} R_{1R} \tag{D.144}
$$

$$
\begin{aligned}
\mathcal{A}_s^{q\tilde{g}\tilde{g}} =& \Big\{ 2M_0 M_1 (g_2^L g_1^L g_0^R + g_2^R g_1^R g_0^L)(p_1^\mu C_1 + p_2^\mu (C_2 + C_0) \\
&+ 2M_0 M_2 (g_2^L g_1^L g_0^L + g_2^R g_1^R g_0^R)(p_1^\mu (C_1 + C_0) + p_2^\mu C_2) \\
&+ 2M_1 M_2 (g_2^L g_1^R g_0^L + g_2^R g_1^L g_0^R)(p_1^\mu C_1 + p_2^\mu C_2) \\
&- 2(g_2^L g_1^R g_0^R + g_2^R g_1^L g_0^L)((p_1 - p_2)^\mu B_1 + p_1^\mu B_0 - M_0^2 (p_1^\mu C_1 + p_2^\mu C_2) \\
&+ p_1.p_2 (p_1^\mu C_1 + p_2^\mu C_2) - (B_0 + M_0^2 C_0)(p_1 + p_2)^\mu - p_1^\mu (p_1.p_2 C_1 + p_2^2 C_2) \\
&- p_2^\mu (p_1^2 C_1 + p_1.p_2 C_2)) \Big\} \times \frac{g_s^3}{16\pi^2} \frac{N}{2} T^a_{ji} (-1)
\end{aligned} \tag{D.145}
$$

Gluino-2-quark loop:

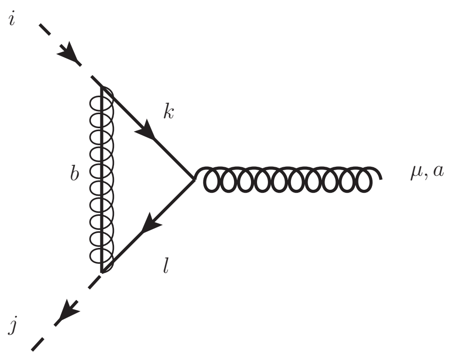

Apparently, we expect the same topology due to a generic fermion loop. But the couplings are different as well as the colour factors:

$$g_0^L = -1 \qquad g_0^R = -1 \tag{D.146}$$

$$g_1^L = \sqrt{2}R_{1R} \qquad g_1^R = -\sqrt{2}R_{1L} \tag{D.147}$$

$$g_2^L = -\sqrt{2}R_{1L} \qquad g_2^R = \sqrt{2}R_{1R} \tag{D.148}$$

The kinematical structure is identical, so that we only express the different colour factor by $C_F = i\frac{1}{2N}T^a_{ji}$.

Gluon loop:

For this diagram, a look at the colour structure is again less time-consuming:

$$C_F = f^{abc}\left(\frac{1}{N}\delta_{ab} + d_{abc}T^c\right) = 0 \tag{D.149}$$

C_F is so to speak an orthogonality relation of the eigendirections in colour space. Hence, we do not have to take this contribution into account.

Squark loop:

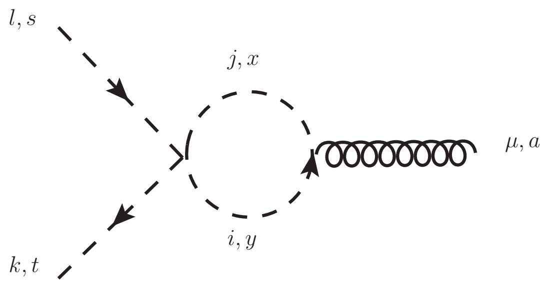

$$\mathcal{A}_s^{\tilde{q}} = \mu^{\frac{4-D}{2}} \frac{i}{16\pi^2} g_s^3 i^4 T^a_{xy} [T^c_{yx} T^c_{ts} A_{ij} A_{11} + T^c_{ys} T^c_{tx} A_{i1} A_{1j}] \int_q \frac{1}{\mathcal{D}_0 \mathcal{D}_1} (2q - p_1 - p_2)^\mu \tag{D.150}$$

$$\mathcal{A}_s^{\tilde{q}} = \frac{g_s^3}{16\pi^2}\left(\frac{1}{2}T^a_{tu}A_{ij}A_{11} - \frac{1}{2N}T^a_{tu}A_{i1}A_{1j}\right)(-(p_1+p_2)^\mu B_0 + 2B^\mu) \tag{D.151}$$

Squark-gluon loop:

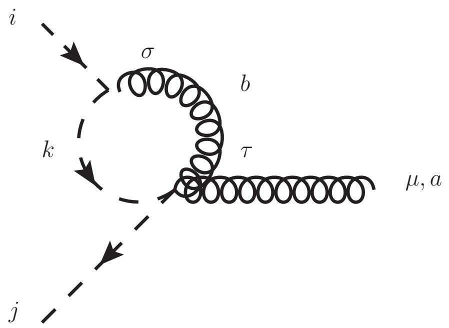

$$\mathcal{A}_s^{g\tilde{q}A} = \mu^{\frac{4-D}{2}} \frac{i}{16\pi^2} g_s^3 T_{ki}^b \{T^a, T^b\}_{jk} \int_q \frac{1}{\mathcal{D}_0 \mathcal{D}_1} g^{\sigma\tau} g^{\tau\mu} (q+p_1)^\sigma \tag{D.152}$$

$$\mathcal{A}_s^{g\tilde{q}A} = \frac{g_s^3}{16\pi^2} \left(\frac{N}{2} - \frac{1}{N} \right) T_{ji}^a (B^\mu + p_1^\mu B_0) \tag{D.153}$$

After having calculated the amplitudes one can decompose these vertices into two amplitudes, keeping in mind that one of them vanishes due to the Ward identity (if the vector particle is on-shell, so not in the case of the s-channel).

$$\mathcal{A}_s = \mu^{\frac{4-D}{2}} \frac{i}{16\pi^2} \Big[\mathcal{A}_s^+ (p_1+p_2)^\mu + \mathcal{A}_s^- (p_1-p_2)^\mu \Big] \tag{D.154}$$

This is of course much more time-saving than evaluating every possible kinematical structure of the 3-gluon topology. The vertex counterterm reads:

$$-ig_s \left(\frac{\delta g_s}{g_s} \delta_{ij} + \frac{\delta Z_g}{2} \delta_{ij} + \delta Z_{ij} + \delta Z_{ji}^* \right) \tag{D.155}$$

D.5.1. The Renormalisation of the Strong Coupling Constant

In every vertex needed for our NLO calculation, the strong coupling constant g_s, also expressed by $\alpha_s = \frac{g_s^2}{4\pi}$ appears - so it is unsurprising to renormalise g_s, too. First, we look upon the general behaviour of α_s - the evolution of the strong coupling in perturbative QCD is controlled by a perturbative series (β-function) yielding us the scale dependence (physical scale Q):

$$\beta(\alpha_s) = Q^2 \frac{\partial \alpha_s}{\partial Q^2} = -\left(\frac{\alpha_s}{4\pi} \right)^2 \sum_n \left(\frac{\alpha_s}{4\pi} \right)^n \beta_n \tag{D.156}$$

In those QCD calculations, one can determine the values of β_i by calculating the corresponding loop integrals of order $i+1$ and obtains (for the number of flavours n_f active at the scale Q and working within the minimal subtraction scheme) [82]:

$$\beta_0 = 11 - \frac{2}{3} n_f \qquad \beta_1 = 102 - \frac{38}{3} n_f \qquad \beta_2 = \frac{2857}{2} - \frac{5033}{18} n_f + \frac{325}{54} n_f^2 \tag{D.157}$$

This series may diverge already at finite energies (Landau pole) and the perturbative approach breaks down. Lattice-QCD, however, provides a means to perform predictive calculations beyond the perturbative realm. In our case, some additional SUSY-specific terms appear. An easy way to derive $\delta g_s/g_s$, needed in every vertex counterterm (see above), is simply to compare the UV-divergent parts of a particular vertex correction with the corresponding counterterms from wave function renormalisation (e.g. the 2-squark-gluon vertex). As the δZ_{ij} and the δZ_g terms subtract the Δ-terms of the tensor integrals in this vertex only partially, exactly the remaining Δ-terms have to be within the $\delta g_s/g_s$ result in order to make the whole vertex correction UV finite. Working in dimensional reduction, we obtain (separately for SM and SUSY where we encounter again the β_0)

$$\left(\frac{\delta g_s}{g_s}\right)^{SM,\overline{DR}} = \frac{\alpha_s}{8\pi}\Delta\left(\frac{2}{3}n_f - \frac{11}{3}C_A\right) \qquad \left(\frac{\delta g_s}{g_s}\right)^{SUSY,\overline{DR}} = \frac{\alpha_s}{8\pi}\Delta\left(\frac{1}{3}n_f + \frac{2}{3}C_A\right) \tag{D.158}$$

and, in total, the last counterterm we need for the renormalisation [39]:

$$\left(\frac{\delta g_s}{g_s}\right)^{\overline{DR}} = \frac{\alpha_s}{8\pi}\Delta(n_f - 3C_A) \tag{D.159}$$

D.6. Box Diagrams

The full amplitudes of the calculated box diagrams are even longer, so we only give the amplitude, again. First of all, we will again define the denominators:

$$\mathcal{D}_1 = q^2 - M_1^2 \qquad \mathcal{D}_2 = (q + p_1)^2 - M_2^2 \tag{D.160}$$

$$\mathcal{D}_3 = (q + p_1 + p_2)^2 - M_3^2 \qquad \mathcal{D}_4 = (q + k_1)^2 - M_4^2$$

These expressions belong to the following convention (internal momenta go counter-clockwise):

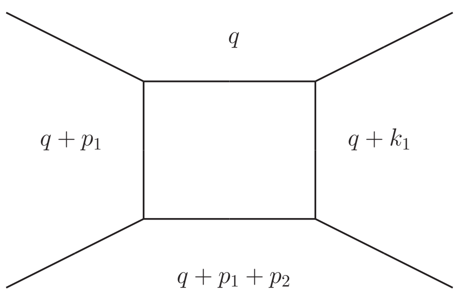

For a time-saving evaluation, we wrote a FeynCalc file performing the tensor reduction in (bosonic) box diagrams automatically, including all helpful substitutions and simplifications. The output is a Fortran code containing the nomenclature of our code. For illustrative purposes, we give an example of a non-trivial substitution - a q^4 in the numerator- shrinking the complexity of the Passarino-Veltman integrals enormously. We begin with adding a zero:

$$M_1^2 \cdot \int d^D q \frac{q^2}{\mathcal{D}_1\mathcal{D}_2\mathcal{D}_3\mathcal{D}_4} + \int d^D q \frac{q^2(q^2 - M_1^2)}{\mathcal{D}_1\mathcal{D}_2\mathcal{D}_3\mathcal{D}_4} \tag{D.161}$$

We repeat that step for the first term, in the second term we introduce $\tilde{q} = q + p_1$:

$$M_1^4 D_0 + M_1^2 C_0 + \int d^D \tilde{q} \frac{\tilde{q}^2 - 2\tilde{q}.p_1 + m_{\tilde{t}_1}}{[\tilde{q}^2 - M_2^2][(\tilde{q}+p_2)^2 - M_3^2][(\tilde{q}+k_1-p_1)^2 - M_4^2]} \tag{D.162}$$

Be aware of the different arguments in the Passarino-Veltman integrals after substitution. The poles are still the same. We add a zero for the third time and interpret $\tilde{q}.p_1$ as $\tilde{q}_\mu p_1^\mu$:

$$M_1^4 D_0 + C_0(M_1^2 + M_2^2 + m_{\tilde{t}_1}) + 2p_1.p_2 C_1 + 2C_2(k_1.p_1 - m_{\tilde{t}_1}) + B_0 \tag{D.163}$$

The alternative would have been the contraction of $D^{\mu\mu\nu\nu}$ which is clearly no alternative.

We start with the integer-spin diagrams, continue with fermionic boxes and finish with ghost final states for gauge invariance. The number of boxes in Chapter 4 is reduced by taking only diagrams into account that have considerably different structures and cannot be obtained via substitutions.

Box 1:

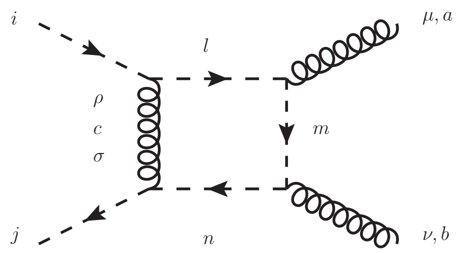

$$B_1 = \frac{ig_s^4}{16\pi^2}\frac{(2\pi\mu)^{4-D}}{i\pi^2} T^c_{li}T^a_{ml}T^b_{nm}T^c_{jn} \int \frac{d^D q}{\mathcal{D}_1\mathcal{D}_2\mathcal{D}_3\mathcal{D}_4} i^8 (p_1 - q)_\rho \quad \times \\ (2q + k_1)_\mu (2q + p_1 + p_2 + k_1)_\nu g^{\sigma\rho}(q + p_1 + 2p_2)_\sigma \epsilon^*_\mu(p)\epsilon^*_\nu(p) \tag{D.164}$$

Box 2:

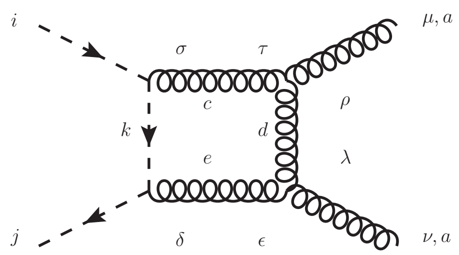

$$B_2 = \frac{ig_s^4}{16\pi^2}\frac{(2\pi\mu)^{4-D}}{i\pi^2}f^{adc}f^{dbe}T^e_{jk}T^c_{ki}\int\frac{d^Dq}{\mathcal{D}_1\mathcal{D}_2\mathcal{D}_3\mathcal{D}_4} \times$$
$$i^6(q+2p_1)^\sigma(p_2-q-p_1)^\delta g^{\delta\epsilon}\Gamma^{\nu\epsilon\lambda}g^{\rho\lambda}\Gamma^{\rho\tau\mu}g^{\sigma\tau}\epsilon^*_\mu(p)\epsilon^*_\nu(p) \quad \text{(D.165)}$$

$$\Gamma^{\nu\epsilon\lambda} = (2q+p_1+p_2+k_1)^\nu g^{\epsilon\lambda} + (k_2-q-k_1)^\epsilon g^{\nu\lambda} - (k_2+q+p_1+p_2)^\lambda g^{\nu\epsilon}$$
$$\Gamma^{\rho\tau\mu} = (k_1-q)^\rho g^{\tau\mu} - (q+2k_1)^\tau g^{\mu\rho} + (2q+k_1)^\mu g^{\rho\tau}$$

Box 3:

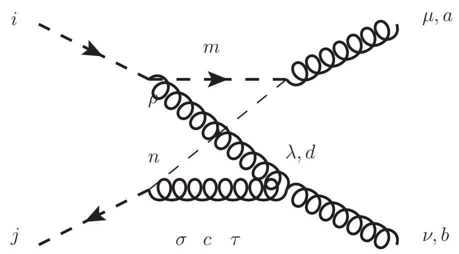

$$B_3 = -\frac{g_s^4}{16\pi^2}\frac{i(2\pi\mu)^{4-D}}{i\pi^2}T^d_{mi}T^a_{nm}T^c_{jn}f^{dbc}i^7\int\frac{d^Dq}{\mathcal{D}_1\mathcal{D}_2\mathcal{D}_3\mathcal{D}_4} \times$$
$$(q-p_1)^\rho(2q+p_1)^\mu(q+p_2+k_1)^\sigma g^{\sigma\tau}g^{\lambda\rho}\Gamma^{\lambda\nu\tau}\epsilon^*_\mu(p)\epsilon^*_\nu(p) \quad \text{(D.166)}$$

$$\Gamma^{\lambda\nu\tau} = g^{\lambda\nu}(q+p_1+k_2)^\tau + g^{\tau\nu}(q+p_1-2k_2)^\lambda - g^{\tau\lambda}(2q+2p_1-k_2)^\nu$$

Box 4:

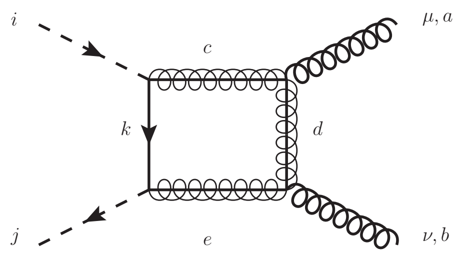

$$B_4 = \frac{g_s^4}{16\pi^2}\frac{i(2\pi\mu)^{4-D}}{i\pi^2}T^c_{ki}T^e_{jk}f^{cad}f^{dbe}\int\frac{d^Dq}{\mathcal{D}_1\mathcal{D}_2\mathcal{D}_3\mathcal{D}_4}i^6(-1) \times$$
$$\mathrm{Tr}[(g^1_LP_L+g^1_RP_R)(\not{q}+m_{\tilde{g}})\gamma^\mu(\not{q}+\not{k}_1+m_{\tilde{g}})\gamma^\nu$$
$$(\not{q}+\not{p}_1+\not{p}_2+m_{\tilde{g}})(g^3_LP_L+g^3_RP_R)(\not{q}+\not{p}_1+m_q)]\epsilon^*_\mu(p)\epsilon^*_\nu(p) \quad \text{(D.167)}$$

$$g^1_L = \sqrt{2}R_{1R} \qquad g^1_R = -\sqrt{2}R_{1L} \qquad g^3_L = -\sqrt{2}R_{1L} \qquad g^3_R = \sqrt{2}R_{1R}$$

Box 5:

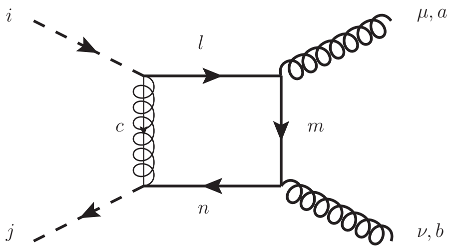

$$B_5 = \frac{g_s^4}{16\pi^2}\frac{i(2\pi\mu)^{4-D}}{i\pi^2}T^c_{li}T^a_{ml}T^b_{nm}T^c_{jn}\int\frac{d^Dq}{\mathcal{D}_1\mathcal{D}_2\mathcal{D}_3\mathcal{D}_4}i^8(-1) \quad \times$$
$$\mathrm{Tr}[(g_L^1P_L+g_R^1P_R)(\not{q}+\not{p}_1+m_{\tilde{g}})(g_L^3P_L+g_R^3P_R)$$
$$(\not{q}+\not{p}_1+\not{p}_2+m_q)\gamma^\nu(\not{q}+\not{k}_1+m_q)\gamma^\mu(\not{q}+m_q)]\epsilon^*_\mu(p)\epsilon^*_\nu(p) \tag{D.168}$$

$$g_L^1=\sqrt{2}R_{1R} \qquad g_R^1=-\sqrt{2}R_{1L} \qquad g_L^3=-\sqrt{2}R_{1L} \qquad g_R^3=\sqrt{2}R_{1R}$$

Box 6:

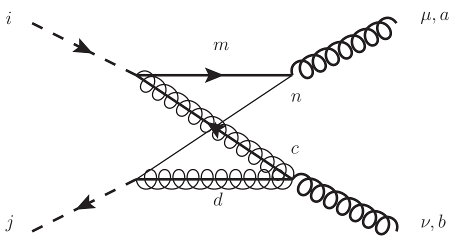

$$B_6 = \frac{g_s^4}{16\pi^2}\frac{i(2\pi\mu)^{4-D}}{i\pi^2}T^c_{mi}T^a_{nm}T^d_{jn}f^{cbd}(-1)\int\frac{d^Dq}{\mathcal{D}_1\mathcal{D}_2\mathcal{D}_3\mathcal{D}_4} \quad \times$$
$$\mathrm{Tr}[\gamma^\nu(\not{q}+\not{p}_1-\not{k}_2+m_{\tilde{g}})(g_L^3P_L+g_R^3P_R)(\not{q}+\not{k}_1+m_q)$$
$$\gamma^\mu(\not{q}+m_q)(g_L^1P_L+g_R^1P_R)(\not{q}+\not{p}_1+m_{\tilde{g}})]\epsilon^*_\mu(p)\epsilon^*_\nu(p) \tag{D.169}$$

$$g_L^1=\sqrt{2}R_{1R} \qquad g_R^1=-\sqrt{2}R_{1L} \qquad g_L^3=-\sqrt{2}R_{1L} \qquad g_R^3=\sqrt{2}R_{1R}$$

Finally, we give the two boxes with ghosts in the final state:

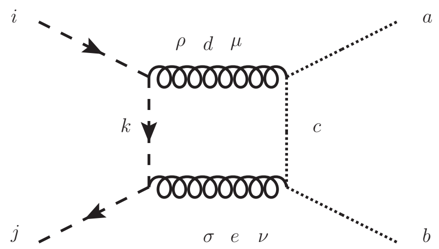

Box 7:

$$B_7 = \frac{g_s^4}{16\pi^2}\frac{i(2\pi\mu)^{4-D}}{i\pi^2}(-i^6) f^{acd} f^{cbe} T^e_{jk} T^d_{ki} \int \frac{d^D q}{\mathcal{D}_1\mathcal{D}_2\mathcal{D}_3\mathcal{D}_4} \times \\ (2p_1+q).k_1 \cdot (p_2-q-p_1).(k_1+q) \tag{D.170}$$

Box 8:

$$B_8 = \frac{g_s^4}{16\pi^2}\frac{i(2\pi\mu)^{4-D}}{i\pi^2}(-i^6) f^{acd} f^{cbe} T^e_{jk} T^d_{ki} \int \frac{d^D q}{\mathcal{D}_1\mathcal{D}_2\mathcal{D}_3\mathcal{D}_4} \times \\ (2p_1+q).(k_1+q) \cdot (p_2-q-p_1).k_2 \tag{D.171}$$

D.7. Real Emissions: Analytical Phase Space Integrals

We used a generic 12-dimensional integral for the phase space integration of the stau annihilation; its explicit expressions were worked out in [30].

$$I^{j_1,\ldots,j_m}_{i_1,..,i_n}(m_0,m_1,m_2) = \frac{1}{\pi^2}\int \frac{d^3p_1}{2E_1}\frac{d^3p_2}{2E_2}\frac{d^3q}{2E_q}\delta(p_0-p_1-p_2-q)\frac{(\pm 2qp_{j_1})\ldots(\pm 2qp_{j_m})}{(\pm 2qp_{i_1})\ldots(\pm 2qp_{i_n})} \tag{D.172}$$

The integrated squared amplitude of the real emission

$$\frac{1}{F}\int |\bar{\mathcal{M}}|^2 dPS^{(3)} \tag{D.173}$$

can be written now via linear combinations of these integrals. First we have to introduce some special abbreviations like the Källen root function (compare to $\lambda(\ldots)$ in Section 6)

$$\kappa = \kappa(m_0^2, m_1^2, m_2^2) = \sqrt{m_0^4 + m_1^4 + m_2^4 - 2(m_0^2m_1^2 + m_0^2m_2^2 + m_1^2m_2^2)} \tag{D.174}$$

occurring in the β_i that have the following form:

$$\beta_0 = \frac{m_0^2 - m_1^2 - m_2^2 + \kappa}{2m_1m_2} \quad \beta_1 = \frac{m_0^2 - m_1^2 + m_2^2 - \kappa}{2m_0m_2} \quad \beta_2 = \frac{m_0^2 + m_1^2 - m_2^2 - \kappa}{2m_2m_1} \tag{D.175}$$

They fulfil the property

$$\beta_0\beta_1\beta_2 = 1\,. \tag{D.176}$$

Moreover, the Spence function appears:

$$\mathrm{Sp}(z) = \mathrm{Li}_2(z) = -\int_0^z \frac{\ln(1-u)}{u} du = \sum_{k=1}^{\infty} \frac{z^k}{k^2}\,. \tag{D.177}$$

The integrals decay into IR-finite and IR-divergent ones. The singular expressions can be easily identified due to their artificial mass λ. The indices are exchangable by exchanging m_1 and m_2. The singularities are subtracted with the following terms:

$$I_{00} = \frac{1}{4m_0^4}\left[\kappa \ln\left(\frac{\kappa^2}{\lambda m_0 m_1 m_2}\right) - \kappa - (m_1^2 - m_2^2)\ln\left(\frac{\beta_1}{\beta_2}\right) - m_0^2 \ln \beta_0\right] \tag{D.178}$$

$$I_{11} = \frac{1}{4m_1^2 m_2^2}\left[\kappa \ln\left(\frac{\kappa^2}{\lambda m_0 m_1 m_2}\right) - \kappa - (m_0^2 - m_2^2)\ln\left(\frac{\beta_0}{\beta_2}\right) - m_0^2 \ln \beta_1\right] \tag{D.179}$$

$$\begin{aligned} I_{01} = \frac{1}{4m_0^2}\Bigg[&2\ln\left(\frac{\lambda m_0 m_1 m_2}{\kappa^2}\right)\ln(\beta_2) + 2\ln^2(\beta_2) - \ln^2(\beta_0) - \ln^2(\beta_1) \\ &+2Sp(1-\beta_2^2) - Sp(1-\beta_1^2) - Sp(1-\beta_1^2)\Bigg] \end{aligned} \tag{D.180}$$

$$\begin{aligned} I_{12} = \frac{1}{4m_0^2}\Bigg[&2\ln\left(\frac{\lambda m_0 m_1 m_2}{\kappa^2}\right)\ln(\beta_0) + 2\ln^2(\beta_0) - \ln^2(\beta_1) - \ln^2(\beta_2) \\ &+2Sp(1-\beta_0^2) - Sp(1-\beta_1^2) - Sp(1-\beta_2^2)\Bigg] \end{aligned} \tag{D.181}$$

The last one cancels the divergences of the $C_0(m_1^2, s, m_2^2, \lambda^2, m_1^2, m_2^2)$, whereas the first two remove the poles of the counterterms. There are various IR-finite integrals:

$$I = \frac{1}{4m_0^2}\left[\frac{\kappa}{2}(m_0^2 + m_1^2 + m_2^2) + 2m_0^2 m_1^2 \ln(\beta_2) + 2m_0^2 m_2^2 \ln(\beta_1) + 2m_1^2 m_1^2 \ln(\beta_0)\right] \tag{D.182}$$

$$I_0 = \frac{1}{4m_0^2}\left[-2m_1^2 \ln(\beta_2) - 2m_2^2 \ln(\beta_1) - \kappa\right] \tag{D.183}$$

$$I_1 = \frac{1}{4m_0^2}\left[-2m_0^2 \ln(\beta_2) - 2m_2^2 \ln(\beta_0) - \kappa\right] \tag{D.184}$$

$$I_0^1 = \frac{1}{4m_0^2}\left[m_1^4 \ln(\beta_2) - m_2^2(2m_0^2 - 2m_1^2 + m_2^2)\ln(\beta_1) - \frac{\kappa}{4}(m_0^2 - 3m_1^2 + 5m_2^2)\right] \tag{D.185}$$

$$I_1^0 = \frac{1}{4m_0^2}\left[m_1^4 \ln(\beta_2) - m_2^2(2m_1^2 - 2m_0^2 + m_2^2)\ln(\beta_1) - \frac{\kappa}{4}(m_1^2 - 3m_0^2 + 5m_2^2)\right] \tag{D.186}$$

$$I_2^1 = \frac{1}{4m_0^2}\left[m_1^4\ln(\beta_0) - m_0^2(2m_2^2 - 2m_1^2 + m_0^2)\ln(\beta_1) - \frac{\kappa}{4}(m_2^2 - 3m_1^2 + 5m_0^2)\right] \quad \text{(D.187)}$$

$$I_{00}^{12} = -\frac{1}{4m_0^2}\left[m_1^4\ln(\beta_2) + m_2^4\ln(\beta_1) + \frac{\kappa^3}{6m_0^2} + \frac{\kappa}{4}(3m_1^2 + 3m_2^2 - m_0^2)\right] \quad \text{(D.188)}$$

$$I_{11}^{02} = -\frac{1}{4m_0^2}\left[m_1^4\ln(\beta_2) + m_2^4\ln(\beta_0) + \frac{\kappa^3}{6m_1^2} + \frac{\kappa}{4}(3m_0^2 + 3m_2^2 - m_1^2)\right] \quad \text{(D.189)}$$

$$I_{11}^{00} = \frac{1}{4m_0^2}\left[2m_2^2(m_1^2 + m_2^2 - m_0^2)\ln(\beta_0) + \frac{\kappa^3}{6m_1^2} + 2\kappa m_2^2\right] \quad \text{(D.190)}$$

$$I_{00}^{11} = \frac{1}{4m_0^2}\left[2m_2^2(m_0^2 + m_2^2 - m_1^2)\ln(\beta_1) + \frac{\kappa^3}{6m_0^2} + 2\kappa m_2^2\right] \quad \text{(D.191)}$$

$$I_{11}^{22} = \frac{1}{4m_0^2}\left[2m_0^2(m_0^2 + m_1^2 - m_2^2)\ln(\beta_2) + \frac{\kappa^3}{6m_1^2} + 2\kappa m_0^2\right] \quad \text{(D.192)}$$

E. Technical Details: Sommerfeld Enhancement

This collection of formulae starts with recapitulating the zero-distance Green's function to the Hamiltonian describing the dynamics of the quasi-stauonium, given as an expansion up to NLO:

$$G(0; \sqrt{s} + i\Gamma_{\tilde{\tau}_1}) = \frac{\alpha(\mu_C) m_{\tilde{\tau}_1}^2}{4\pi} \times \left[g_{LO} + \frac{\alpha(\mu_G)}{4\pi} g_{NLO} + \mathcal{O}(\alpha^2) \right] \tag{E.1}$$

We define the quantities

$$\kappa = \frac{i\alpha(\mu_C)}{2v} \tag{E.2}$$

$$v = \sqrt{\frac{\sqrt{s} + i\Gamma_{\tilde{\tau}_1} - 2m_{\tilde{\tau}_1}}{m_{\tilde{\tau}_1}}} \tag{E.3}$$

$$L = \ln\left(\frac{i\mu_C}{2m_{\tilde{\tau}_1} v} \right) \tag{E.4}$$

and the function

$$\psi^{(n)}(1-\kappa) = \frac{d^n}{dz^n} \left(\gamma_E + \frac{d}{dz}\Gamma(z)|_{z=1-\kappa} \right) \tag{E.5}$$

with the Gamma function

$$\Gamma(x) = \int_0^{+\infty} e^{-t} t^{x-1} \mathrm{d}t \tag{E.6}$$

and the Euler-Mascheroni constant $d/dz\Gamma(z)_{z=1} = \gamma_E = 0,5772$ to express $g_{(N)LO}$ given by

$$g_{LO} = -\frac{1}{2\kappa} + L - \psi^{(0)} \tag{E.7}$$

$$\begin{aligned} g_{NLO} = &\beta_0[L^2 - 2L(\psi^{(0)} - \kappa\psi^{(1)}) + \kappa\psi^{(2)} + (\psi^{(0)})^2 \\ &- 3\psi^{(1)} - 2\kappa\psi^{(0)}\psi^{(1)} + 4{}_4F_2(1,1,1,1;2,2,1-\kappa;1)] \\ &+ a_1(L - \psi^{(0)} + \kappa\psi^{(1)}) \end{aligned}$$

with

$$a_1 = -\frac{20}{9}\sum_f Q_f^2 \qquad \beta_0 = -\frac{4}{3}\sum_f Q_f^2 \tag{E.8}$$

The sum contains all fermions f up to the scale of the typical momentum exchange.

One special function still needs our attention, the generalised hypergeometric function. Before treating them, we discuss how to get rid of the double counting of the LO contribution as it was calculated in the tree level diagrams: We expand the expression from above in powers of the fine-structure constant and see that the term $-\frac{1}{2\kappa}$ yields the only LO contribution. This term of course has to be subtracted, namely:

$$\Im\{G_{LO}(0; \sqrt{s} + i\Gamma_{\tilde{\tau}_1})\} = m_{\tilde{\tau}_1}^2 \Im\left\{\frac{iv}{4\pi}\right\} \tag{E.9}$$

Now we turn back to the hypergeometric function ${}_pF_q$. Using again the Eulerian Gamma function, we can express it via

$${}_pF_q(a_1, ..., a_p; b_1, ..., b_q; z) = \sum_{k=0}^{\infty} \prod_{i=1}^{p} \frac{\Gamma(k + a_i)}{\Gamma(a_i)} \prod_{j=1}^{q} \frac{\Gamma(b_j)}{\Gamma(k + b_j)} \frac{z^k}{k!} \tag{E.10}$$

To use parameters a, b yielding poles is naturally restricted. This special function contains, in its general form, several trigonometric functions, the (modified) Bessel functions and more. The trivial case ${}_0F_0(;;z)$ is the complex exponential function. Unsatisfactorily, the convergence of this series underlies diverse constraints. If $p < q + 1$ **(a)**, the ratio criterion claims the quotient of the coefficients to be bounded, going towards zero. This implies convergence for finite z. For the important case $p = q + 1$ **(b)**, the ratio criterion gives an unclear answer. The divergence for $|z| > 1$ is obvious, our $|z = 1|$ is instead difficult to treat. Absolute convergence is guaranteed for the case

$$\mathrm{Re}\left(\sum_{j=1}^{q} b_j - \sum_{i=1}^{p} a_i\right) > 0 \tag{E.11}$$

and if not, we can at least give a convergence condition for real z arguments, $z \to 1$:

$$(1 - z)\frac{d}{dz} \log({}_pF_q(a_1, ..., a_p; b_1, ..., b_q; z^p)) = \sum_{i=1}^{p} a_i - \sum_{j=1}^{q} b_j \tag{E.12}$$

Working out the case $p > q + 1$ **(c)** yields even divergences for $z = 0$. Finally, the implementation should be commented: The basic structure of the code was written by M. Meinecke [63] for QCD resummation. At some points, a few simplifications were carried out as well as the QED modifications by the author of this work. The Gamma function had to be implemented approximately, using the Lanczos approximation:

$$\Gamma(z + 1) = \sqrt{2\pi}(z + g + 1/2)^{z+1/2} \exp(-z - g - 1/2)A_g(z) \tag{E.13}$$

with

$$A_g(z) = \frac{1}{2}p_0(g) + p_1(g)\frac{z}{z + 1} + p_2(g)\frac{z(z - 1)}{(z + 1)(z + 2)} + ... \tag{E.14}$$

containing an arbitrary constant g and

$$p_k(g) = \sum_{a=0}^{k} C(2k+1, 2a+1)\frac{\sqrt{2}}{\pi}(a-1/2)!(a+g+1/2)^{-(a+1/2)}\exp(a+g+1/2) \quad \text{(E.15)}$$

with $C(i,j)$ representing the Chebyshev polynomial coefficient matrix.

Following [65], an improvement of the convergence of our series was implemented:

$$\begin{aligned}
{}_4F_3(1,1,1,1;a,a,z;1) = &\frac{1}{a^2z(z-2)2-a))(a-z)^2} \\
&\times [a^2(z-1)^4_4F_3(1,1,1,1;a,a,z+1;1) \\
&+ a(a-1)^3z(3a+1-4z)_4F_3(1,1,1,1;a+1,a,z;1) \\
&+ (a-1)^4z(z-a)_4F_3(1,1,1,1;a+1,a+1,z;1)]
\end{aligned}$$

$$\begin{aligned}
{}_4F_3(1,1,1,1;a,b,z;1) = &\frac{1}{a+b+x-4}\left[\frac{(a-1)^4}{a(a-b)(a-z)}{}_4F_3(1,1,1,1;a+1,b,z;1)\right. \\
&+ \frac{(b-1)^4}{b(b-a)(b-z)}{}_4F_3(1,1,1,1;a,b+1,z;1) \\
&\left.\frac{(z-1)^4}{z(z-a)(z-b)}{}_4F_3(1,1,1,1;a,b,z+1;1)\right]
\end{aligned}$$

These results arise from the identity

$$\begin{aligned}
{}_4F_3(1,1,1,1;2,2,z;1) = \frac{1}{4z^2(2-z)^2}&[4(z-1)^4_4F_3(1,1,1,1;2,2,z+1;1) \\
&+ 2z(7-4z)_4F_3(1,1,1,1;3,2,z;1) \\
&x(x-2)_4F_3(1,1,1,1;3,3,x;1)]
\end{aligned}$$

F. Dipole Formulae for Real Corrections of Stau Annihilation

The integration over the gluon phase space in the diagrams of Fig. 7.3 led to the integral

$$\mathbf{I} = -\frac{C_F g_s^2}{8\pi^2}\frac{(4\pi)^\epsilon}{\Gamma(1-\epsilon)} \cdot \left[\left(\frac{\mu^2}{s_{12}}\right)^\epsilon \left(\mathcal{V}_q(s_{12}, m_q, m_q; \epsilon) - \frac{\pi^2}{3}\right) \right.$$
$$\left. + \frac{\Gamma_q(m_q, \epsilon)}{C_F} + \frac{3}{2}\ln\left(\frac{\mu^2}{s_{12}}\right) + 5 - \zeta(2)\right] \tag{F.1}$$

With the definitions $\beta = \sqrt{1-4\mu_q^2}$, $\mu_q = m_q/\sqrt{s}$ and $s_{12} = s - 2m_q^2$ we can express $\mathcal{V}_q$, decomposed into a singular and a regular part $\mathcal{V}^S + \mathcal{V}^{NS}$ as follows:

$$\mathcal{V}^S(s_{12}, m_q, m_q; \epsilon) = \frac{1+\beta^2}{2\beta}\left[\frac{1}{\epsilon}\ln\left(\frac{1-\beta}{1+\beta}\right) \right.$$
$$\left. -\frac{1}{2}\ln^2\left(\frac{1-\beta}{1+\beta}\right) - \zeta(2) + \ln\left(\frac{1-\beta}{1+\beta}\right)\cdot\ln\left(\frac{2}{1+\beta^2}\right)\right] \tag{F.2}$$

$$\mathcal{V}^{NS}(s_{12}, m_q, m_q; \epsilon) = \frac{3}{2}\ln\left(\frac{1+\beta^2}{2}\right) + \frac{1+\beta^2}{2}$$
$$\times \quad \left[2\ln\left(\frac{1-\beta}{1+\beta}\right)\cdot\ln\left(\frac{2(1+\beta^2)}{(1+\beta)^2}\right) + 2\mathrm{Li}_2\left(\frac{1-\beta}{1+\beta}\right)^2 \right.$$
$$\left. -2\mathrm{Li}_2\left(\frac{2\beta}{1+\beta}\right) - \zeta(2)\right] + \ln\left(1 - \frac{\sqrt{1-\beta^2}}{2}\right) \tag{F.3}$$
$$-2\ln(1-\sqrt{1-\beta^2}) - \frac{1-\beta^2}{1+\beta^2}\ln\left(\frac{\sqrt{1-\beta^2}}{2-\sqrt{1-\beta^2}}\right)$$
$$+3\zeta(2) - \frac{\sqrt{1-\beta^2}}{2-\sqrt{1-\beta^2}} + 2\frac{1-\beta^2-\sqrt{1-\beta^2}}{1+\beta^2}$$

It remains the definition of

$$\Gamma_q(m_q; \epsilon) = C_F\left[\frac{1}{\epsilon} + \frac{1}{2}\ln\left(\frac{m_q^2}{Q^2}\right)\right] \tag{F.4}$$

with the renormalisation scale Q. Furthermore, the dipole contributions from $|\mathcal{M}^{2\to 3}|^2 = \mathcal{D}_{31,2} + \mathcal{D}_{32,1}$ need an explicit expression. These elements are related via the interchange of k_1 and k_2. Hence, we only give

$$\begin{aligned}\mathcal{D}_{31,2} = C_F \frac{8\pi\alpha_s}{s} |\mathcal{M}_{tree}|^2 \cdot \frac{1}{1-x_2} \Bigg[\frac{2(1-2\mu_q^2)}{2-x_1-x_2} \\ - \frac{\beta}{\sqrt{x_2^2 - 4\mu_q^2}} \frac{x_2 - 2\mu_q^2}{1-2\mu_q^2} \left(2 + \frac{x_1 - 1}{x_2 - 2\mu_q^2} + \frac{2\mu_q^2}{1-x_2} \right) \Bigg]\end{aligned} \tag{F.5}$$

with the abbreviations $x_i = 2k_i.q/q^2$, $q^2 = (k_1 + k_2 + k_3)^2 = s$.

Bibliography

[1] ZWICKY, Fritz: Die Rotverschiebung von extragalaktischen Nebeln. In: *Helv. Phys. Acta* ***6*** (1933), S. 110-127

[2] RUBIN, Vera C. ; FORD JR., W. Kent: Rotation of the Andromeda nebula from a spectroscopic survey of emission regions. In *Astrophysical Journal* **159** (1970)

[3] *apod.nasa.gov/apod/ap060824.html* (17.03.2018)

[4] PECCEI, Roberto D. ; QUINN, Helen R.: CP conservation in the presence of pseudoparticles. In: *Phys. Rev. Lett.* **38**, p. 1440 (1977)

[5] DUFFY, Leanne ; VAN BIBBER, Karl: Axions as dark matter particles. In: *New Journal of Physics* **11** (2009)

[6] ESCH, Sonja: Dark Matter, Neutrino Masses and Lepton Flavour Violation in Radiative See-Saw Models. Dissertation, University of Münster (2018)

[7] CALIBBI, Lorenzo ; ZIEGLER, Robert ; ZUPAN, Jure: Minimal Models for Dark Matter and the Muon g-2 Anomaly. In: arxiv.org (1804.00009) (2018)

[8] MIURA, Makoto: Search for Proton Decay via $p \rightarrow e^{+}\pi^{0}$ in 0.31 megaton·years exposure of the Super-Kamiokande Water Cherenkov Detector. In: *Phys. Rev.* **90** (2017)

[9] HEBBEKER, Thomas: Can the S-Neutrino be the lightest supersymmetric Particle? In: Phys. Lett. **470B** (1999)

[10] BOYARSKI, Andrej et al.: Sterile neutrino dark matter. In: Prog. Part. Nucl. Phys. **104** (2019)

[11] MILGROM, Mordehai: A modification of the Newtonian dynamics as a possible alternative to the hidden mass hypothesis. In: *Astrophysical Journal* **270** (1983), S. 365-370

[12] BABICHEV, Eugeny et al.: Gravitational Origin of Dark Matter. In: arxiv.org (1604.08564) (2016).

[13] AALSETH, C.A. et al.: Search for an Annual Modulation in a P-type Point Contact Germanium Dark Matter Detector. In: *Phys. Rev. Lett.* **107** (2011)

[14] XENON100 Collaboration: The Xenon100 Dark Matter Experiment. In: *Astropart. Phys.* **35** (2012)

[15] TAN, A. et al.: Dark matter search results from the commissioning run of PandaX-II. In: 93.12,122009 (2019)

[16] ABDALLAH, Jalal et al.: Simplified Models for Dark Matter and Missing Energy Searches at the LHC. In: eprint - arXiv: 1409.2893 (2014

[17] The CMS Collaboration: Observation of a new boson at a mass of 125 GeV with the CMS experiment at the LHC. In: *Phys. Rev. Lett.*, eprint - arXiv: 1207.7235 (2012)

[18] POPPER, Karl R.: *Vermutungen und Widerlegungen. Wachstum der wissenschaftlichen Erkenntnis* (1963) Mohr Siebeck, Tübingen

[19] Planck Collaboration: Planck 2015 Results. XIII. Cosmological Parameters.

[20] *m.esa.int/spaceinimages* (18.03.2018)

[21] HOOPER, Dan: TASI Lectures on Dark Matter (2008)

[22] GONDOLO, Paolo: DarkSUSY: Computing supersymmetric dark matter properties numerically. In: JCAP **0407** 008 (2004)

[23] HERRMANN, Björn ; KLASEN, Michael: SUSY-QCD Corrections to Dark Matter Annihilation in the Higgs Funnel. In *Phys. Rev.* **D76**: 117704 (2007)

[24] HERRMANN, Björn ; KLASEN, Michael ; KOVAŘÍK, Karol: Neutralino Annihilation into Massive Quarks with SUSY-QCD Corrections. In *Phys. Rev.* **D79**: 061701 (2009)

[25] HERRMANN, Björn ; KLASEN, Michael ; KOVAŘÍK, Karol: SUSY-QCD effects on neutralino dark matter annihilation beyond scalar or gaugino mass unification. In *Phys. Rev.* **D80**: 085025 (2009)

[26] HERRMANN, Björn et. al.: One-loop corrections to gaugino co-annihilation into quarks in the MSSM. In *Phys. Rev.* **D89**: 114012 (2014)

[27] HERRMANN, Björn: Radiative corrections to neutralino annihilation: Recent developments. arXiv:1011.6550 (2014)

[28] HARZ, Julia et. al.: One-loop corrections to neutralino-stop coannihilation revisited. In *Phys. Rev.* **D91**: 034028 (2015)

[29] HARZ, Julia et. al.: SUSY-QCD corrections to stop annihilation into electroweak final states including Coulomb enhancement effects. In *Phys. Rev.* **D91**: 034012 (2015)

[30] BRANAHL, Johannes: Stau coannihilation into light and heavy quarks. Bachelor's Thesis, WWU Münster (2018).

[31] BRANAHL, Johannes ; HERRMANN, Björn ; KLASEN, Michael et al. : SUSY-QCD corrected and Sommerfeld enhanced stau annihilation into heavy quarks with scheme and scale uncertainties. In: Phys. Rev. D **100**, 115003 (2019)

[32] HARZ, Julia: Supersymmetric QCD Corrections and Phenomenological Studies in Relation to Coannihilation of Dark Matter. Dissertation, University of Hamburg (2013)

[33] ALLANACH, B.C.: SUSY Les Houches Accord 2. In: Comput. Phys. Comm. **180**, 8 (2009)

[34] SKANDS et al.: SUSY Les Houches accord: Interfacing SUSY spectrum calculators, decay packages, and event generators. In: JHEP **0407** , 036 (2004)

[35] POROD, Werner: SPheno, a program for calculating supersymmetric spectra, SUSY particle decays and SUSY particle production at e+ e- colliders. In: Comput. Phys. Comm. **153**, 275 (2003)

[36] POROD, Werner: SPheno 3.1: Extensions including flavour, CP-phases and models beyond the MSSM. In: Comput. Phys. Comm. **183**, 2458 (2012)

[37] PUKHOV, Alexander et al.: CalcHEP 2.3: MSSM, structure functions, event generation, batchs, and generation of matrix element for other packages. In: arxiv.org (0412191v2) (2009)

[38] BÉLANGER, G. et al.: micrOMEGAs: Version 1.3. In: *Computer Physics Communications* **174** (2006), S. 577 ff.

[39] JOYCE, James: *Finnegan's Wake*. Faber, London (1939).

[40] JONES, H.F.: *Groups, Representations and Physics*, Taylor and Francis, 1998

[41] PESKIN, Michael E. ; SCHROEDER, Daniel V.: An Introduction to Quantum Field Theory. Westview Press (1995)

[42] FADDEEV, Ludvig ; POPOV, Victor: Feynman diagrams for the Yang-Mills field. In: *Phys. Lett.* **B25**(1) (1967)

[43] MARTIN, Stephen P.: A Supersymmetry Primer. *Adv.Ser.Direct.High Energy Phys.* ***21**,* (2010)

[44] KALKA, Harald ; SOFF, Gerhard: *Supersymmetrie*, Teubner Studienbücher, 1997

[45] HAAG, Rudolf ; ŁOPUSZANSKI, Jan ; SOHNIUS, Martin: All possible generators of supersymmetries of the S-matrix. In: *Nuclear Physics B* ***88*** (1975), S.257 ff.

[46] COLEMAN, Sidney ; MANDULA, Jeffrey: All Possible Symmetries of the S Matrix. In: *Phys. Rev. D* ***159*** (1967), S. 1251 ff.

[47] WESS, Julius ; ZUMINO, Bruno: Supergauge transformations in four dimensions. In: *Nucl. Phys.* **B70** (1974).

[48] BERGER, C.F. ; Gainer, J.S. et al.: Supersymmetry without prejudice. In: *High En. Phys.* (2009)

[49] BARBIERI, Ricardo ; FERRARA, Sergio ; SAVOY, Carlos A.: Gauge Models with Spontaneously Broken Local Supersymmetry. In: *Physics Letters B* **119** (1982)

[50] HALL, Lawrence J. ; LYKKEN, Jospeh D, ; WEINBERG, Steven: Supergravity as the Messenger of Supersymmetry Breaking. In: *Physical Review D* **27** (1983)

[51] physics.stackexchange.com

[52] KINOSHITA, Toichiro: Mass Singularities of Feynman Amplitudes. In: *Journal of Mathematical Physics* **3** (1962), S. 650 ff.

[53] WICK, Gian C.: The evaluation of the collision matrix. In: Phys. Rev. **80** (1950)

[54] HUE, L.T. et al.: General formula for symmetry factors of Feynman diagrams. (unpublished, 2012)

[55] MARTIN, Stephen P. ; Younkin, James: Radiative corrections to stoponium annihilation decays. In: *Phys. Rev.* **D80**: 035026 (2009)

[56] CATANI, Stefano ; SEYMOUR, Michael: The Dipole formalism for the calculation of QCD jet cross-sections at next-to-leading order. In: Phys. Lett. B **378**, 287 (1996)

[57] CATANI, Stefano ; DITTMAIER, Stefan ; SEYMOUR, Michael ; TROCSANYI, Zoltan: The Dipole formalism for next-to-leading order QCD calculations with massive partons. In: Nucl. Phys. B **627**, 189 (2002)

[58] DITTMAIER, Stefan: A general approach to photon radiation off fermions. In: Nucl. Phys. B **565**, 69 (2000)

[59] BRYCHKOV, Yuri et al. : *Integrals and Series, Vol. 1*, Gordon and Breach Science Publishers (1966)

[60] DENNER, Ansgar: Techniques for the calculation of electroweak radiative corrections at the one-loop level and results for W-physics at LEP200.

[61] BETHE, Hans ; SALPETER, E.: A Relativistic Equation for Bound-State Problems. In: Phys. Rev. **84** (1951)

[62] HRYCZUK, Andrzey: The Sommerfeld enhancement for scalar particles and application to sfermion co-annihilation regions. In: Phys. Lett. **B699**, 271(2011)

[63] MEINECKE, Moritz: SUSY-QCD Corrections to the (Co-)Annihilation of Neutralino Dark Matter within the MSSM. Dissertation at the WWU Münster (2015)

[64] KAUTH, Matthias R. et al: Gluino Pair Production at the LHC: The Threshold. In: Nucl. Phys. **B831** (2010).

[65] BILLOIRE, Alain: How Heavy Must Be Quarks in Order to Build Coulombic q anti-q Bound States. In: Phys. Lett. **92B**, 343 (1980)

[66] HARZ, Julia ; PETRAKI, Kalliopi: Higgs Enhancement for the Dark Matter Relic Density. In: *Phys. Rev.* **D97**: 075041 (2018)

[67] HARZ, Julia ; PETRAKI, Kalliopi: Higgs-mediated bound states in dark-matter models. In: arxiv (1901.10030v2) (2019)

[68] CAHILL-RAWLEY, Matthew W. et al.: The New Look pMSSM with Neutralino and Gravitino LSPs. In: Eur. Phys. J. C **72**, 2156 (2012)

[69] HEISIG, Jan: Gravitino LSP and leptogenesis after the first LHC results. In: JCAP **1404** 023 (2014)

[70] BATTAGLIA, Marco et al.: LHC constraints on Gravitino Dark Matter. In: Phys. Rev. D **92** , no. 11, 115008 (2015)

[71] PRADLER, Josef ; STEFFEN, Frank: Thermal gravitino production and collider tests of leptogenesis. In: Phys. Rev. D **75**, 023509 (2007)

[72] RYCHKOV, Vyacheslav ; STRUMIA, Alessandro: Thermal production of gravitinos. In: Phys. Rev. D **75**, 075011 (2007)

[73] KOFMAN, Lev ; LINDE, Andrei ; STAROBINSKY, Alexei: Reheating after inflation. In: Phys. Rev. Lett. **73**, 3195 (1994)

[74] POSPELOV, Maxim ; PRADLER, Josef ; STEFFEN, Frank: Constraints on Supersymmetric Models from Catalytic Primordial Nucleosynthesis of Beryllium. In: JCAP **0811**, 020 (2008)

[75] FUKS, Benjamin ; HERRMANN, Björn ; KLASEN, Michael: Flavour Violation in Gauge-Mediated Supersymmetry Breaking Models: Experimental Constraints and Phenomenology at the LHC. In: Nucl. Phys. B **810**, 266 (2009)

[76] DERYA, Vera: Colour factors in QCD (2008), seminar thesis at LPSC, Grenoble

[77] HABER, Howard: Useful relations involving the generators of SU(N). (Notes on QCD lecture, 2016)

[78] BORODULIN, V.I. et al.: *Compendium of Relations.* Institute for High Energy Physics, Moscow (1995).

[79] EBERL, Helmut: Strahlungskorrekturen im minimalen supersymmetrischen Standardmodell. Dissertation, University of Vienna (1998)

[80] PASSARINO, Giampiero ; VELTMAN, Martinus: One Loop Corrections for e+ e- Annihilation Into mu+ mu- in the Weinberg Model. In: Nucl. Phys. B **160**, 151 (1979).

[81] KOVAŘÍK, Karol: *Hitchhiker's Guide to Renormalisation* (unpublished notes, version of 2017)

[82] DEUR, Alexandre ; BRODSKEY, Stanley ; DE TERAMOND, Guy: The QCD Running Coupling. In: *Prog. Part. Nuc. Phys.* **90** (2016)

[83] BENEKE, Martin et al.: Soft radiation in heavy-particle pair production: all-order colour structure and two-loop anomalous dimension
*Nucl.Phys. B**828**,69-101* (2010)

[84] ELLIS, R. Keith et al.: One-loop calculations in quantum field theory: from Feynman diagrams to unitarity cuts. *High Energy Physics* **10** (2012)

[85] DANEDO, Flip: Defense Against the Dark Arts. Notes on dark matter and particle physics. (2011) *Cornell University, Ithaca* (unpublished)

[86] DREES, Manuel ; GODBOLE, Rohini M. ; ROY, Probir:
Theory and Phenomenology of Sparticles. World Scientific, 2005.

[87] LEE, Tsung-Dao ; NAUENBERG, Michael: Degenerate Systems and Mass Singularities

[88] SCHWARTZ, Matthew D.: *Quantum Field Theory and the Standard Model*
Cambridge University Press, 2014

[89] GONZALEZ, Anthony H. et al.: A direct empirical proof of the existence of dark matter. In: *Astrophysical Journal* **648** (2006)

[90] DEUR, Alexandre ; BRODSKEY, Stanley ; DE TERAMOND, Guy: The QCD Running Coupling. In: *Prog. Part. Nuc. Phys.* **90** (2016)

[91] SCHMIEMANN, Saskia et. al.: Squark-pair annihilation into quarks at next-to-leading order. In *Phys. Rev.* **D99**: 095015 (2019)

[92] GELMINI, Graciela ; GONDOLO, Paolo: Cosmic abundances of stable particles: Improved analysis. In: Nucl. Phys. **B360**, 145 (1991)

[93] EDSJÖ, Joakim ; GONDOLO, Paolo: Neutralino relic density including coannihilations. In: Phys. Rev. D **56**, 1879 (1997)

[94] HUNTER, J. D.: Matplotlib: A 2D graphics environment. In: Comput. Sci. Eng. **9** (2007) 90.

[95] BINOSI, D. et al.: JaxoDraw: A Graphical user interface for drawing Feynman diagrams. In: Comput. Phys. Commun. **191**, 76 (2004)

Danksagung

Zu allererst gilt mein Dank *Prof. Dr. Michael Klasen* für die Möglichkeit, in seiner Arbeitsgruppe das spannende wie fordernde Thema zu bearbeiten und dabei eine Menge über quantenfeldtheoretische Berechnungen erlernen zu können. Sehr geehrt gefühlt habe ich mich ob der Nominierung zum Lindau Nobel Laureate Meeting. Darüber hinaus war mir die Teilnahme am Annual Retreat des Graduiertenkollegs, die ich nicht als selbstverständlich ansehe, eine Freude.

PD Dr. Karol Kovařík! Dir möchte ich für deine stets offene Tür für Fragen und tiefergehende Diskussionen danken, die die Arbeit aus mancher Sackgasse manövriert haben. Mit deiner Hilfsbereitschaft, deinem Wissen und deinem Humor bist du ein unverzichtbarer Teil der AG!

Meine Bürokollegen *Dr. Saskia Schmiemann* und *Sybrand Zeinstra* haben mir stets eine angenehme Arbeitsatmosphäre beschert. Insbesondere danke Saskia, dass du mir in den Anfängen immer mit Rat und Tat zur Seite standest. Die Zusammenarbeit mit unseren SUSY-Experten und Kollaborationsmitgliedern von extern - *Dr. Julia Harz* und *Dr. Björn Herrmann* - war sehr lehrreich für mich. Herzlichen Dank für die Zeit, die ihr euch genommen habt! *Florian Fabry* - mit dir habe ich gemeinsam viele Probleme in der Quantenfeldtheorie gelöst und schlussendlich haben wir unser jeweiliges Master-Projekt vollendet. Verrückte Ideen zu diskutieren und eine Menge über Teilchen und Felder zu lernen hat mir immer viel Spaß gemacht.

Meinen Eltern danke ich für die vielen Wochenenden, an denen ich in Aerzen Kraft für die nächste Woche tanken und die Supersymmetrie hinter mir lassen konnte. Und zuletzt danke ich dir, *Sonja*, die du die Höhen und Tiefen der Anfertigung dieser Arbeit stets miterleben musstest und dennoch immer ein offenes Ohr für mich hattest.

Plots and Feynman diagrams presented in this thesis have been created using Matplotlib [94] and JaxoDraw [95].